Czech Technical University in Prague

Faculty of Electrical Engineering
Department of Physics

ANALYSIS OF BROADBAND ELECTRIC AND MAGNETIC SIGNALS RADIATED FROM LIGHTNING DISCHARGES

Doctoral Thesis

Ing. Ivana Kolmašová

Prague, October 2013

Ph.D. Programme: Electrical Engineering and Information Technology
Branch of study: Plasma Physics

Supervisor: Prof. RNDr. Pavel Kubeš, CSc.
Supervisor-Specialist: Doc. RNDr. Ondřej Santolík, Dr.

DECLARATION

I declare that this doctoral thesis has not been submitted as an exercise for a degree at this or any other university, and that it is entirely my own work.

Prague, October 2013 Ivana Kolmašová

ACKNOWLEDGEMENTS

I would like to thank my adviser Pavel Kubeš for supporting me during these past three years. I am very grateful for his scientific advice. I would like to thank my adviser-specialist Ondřej Santolík, who as a good friend was always willing to help me. He provided the encouragement and advice necessary for me to go through the PhD program and to complete my thesis. The joy and enthusiasm they both have for their research were contagious and motivational for me. I could not have imagined having a better guidance for my PhD study.

I would like to thank my colleagues from the Institute of Atmospherics Physics for their technical assistance and friendship. It has meant much to me.

I would like to thank my whole family, my parents and my children, for all their love and encouragement. My children Jan, Jana and Petra always believed that I was able to complete my study.

I wish to thank my father. His love for physics, his wisdom, and knowledge inspired me. I like our discussions about physics. Thank you.

ABSTRACT

This thesis is aimed at broadband electric and magnetic signals radiated by lightning discharges. In spite of more than 250 years of research it is still not known what triggers the lightning discharge. It is not yet fully understood how a thundercloud gets charged. The mystery of lightning initiation is hidden inside the thundercloud. In-situ and optical measurements of in-cloud processes are difficult and sometimes impossible. However in-cloud discharges which are believed to signalize initiation of the lightning strokes, radiate electromagnetic signals. Analysis of remote measurements of signals radiated by in-cloud lightning processes can therefore serve as a useful tool for their investigation.

In the frame of this thesis, electromagnetic manifestations of particular lightning processes were measured using a newly developed broad-band analyzer with a sampling interval of 12.5 ns. We concentrate our attention on the microsecond- and submicrosecond-scale variations of electromagnetic fields generated by the in-cloud currents. These variations have a direct link to the propagation of in-cloud discharges in the complicated charge structure inside the thunderclouds.

The main result of the thesis is a successful experimental determination of properties of inter-stroke pulse trains. This result is based on a systematic analysis of variations of inter-pulse intervals and peak amplitudes which has been done for the first time. We propose a possible generation mechanism involving interactions of in-cloud leaders with periodical charge structures. This hypothesis can explain the observed evolution of peak amplitudes and inter-pulse intervals and also the observed asymmetry in the shapes of pulses.

List of symbols

B	horizontal component of the magnetic induction vector
Bp_F	dominant peak amplitude of the horizontal component of the magnetic induction vector of the first stroke
Bp_{SX}	dominant peak amplitude of the horizontal component of the magnetic induction vector of the x-th subsequent stroke
c	speed of light
C_T	capacitance of the "tube cable"
dB/dt	time derivative of the horizontal component of the magnetic induction vector
E	the vertical component of the electric field intensity vector
f_r	resonant frequency
I	current
I_F	peak current of the first stroke
I_{SX}	peak current of the x-th subsequent stroke
L_L	inductance of the loop
L_C	inductance of the cable
μ_0	permeability of the free space
ρ_t	effective current reflection coefficients at the top of the channel
ρ_b	effective current reflection coefficients at the bottom of the channel
v	velocity
TR_F	rise time of dB/dt of the first stroke
TR_{SX}	rise time of dB/dt of the x-th subsequent stroke

Note, that throughout the text, we use the term "magnetic field" instead of "horizontal component of the magnetic induction vector", following the conventions usual in the literature. Analogously we use the term "electric field" for "vertical component of the electric field intensity vector".

List of abbreviations

The following table describes the meanings of various abbreviations and acronyms used throughout the thesis.

Abbreviation	Meaning
ACF	Altered Channel Flash
ADC	Analog-to-Digital Converter
BFB	Bolt-From-the-Blue
BJ	Blue Jet
CEA	Commissariat à l'énergie atomique et aux énergies alternatives
CELDN	Central European Lightning Detection Network
CG-	negative Cloud-to-Ground discharge
CG+	positive Cloud-to-Ground discharge
CID	Compact Intra-Cloud Discharge
CNES	Centre National d'Etudes Spatiales
ELF	Extra Low Frequency
EW	Event Waveform
FB	Filter Bank
FPGA	Field-Programmable Gate Array
FWHM	Full With at Half Maximum
GJ	Gigantic Jet
GPS	Global Positioning System
HF	High Frequency
HyMeX	HYdrological cycle in Mediterranean EXperiment
IC	Intra-Cloud discharge
IME-HF	Instrument Mesure Electrique – Haute Frequence
LC filter	passive filter composed of inductors and capacitors
LF	Low Frequency
LMA	Lightning Mapping Array
LSBB	Laboratoire Souterrain a Bas-Bruit
NCF	New Channel Flash

Abbreviation	Meaning
NBE	Narrow Bipolar Event
NBP	Narrow Bipolar Pulse
PB	Preliminary Breakdown
PBFA	Position By Fast Antenna
PCB	Printed Circuit Board
PROM	Programmable Read-Only Memory
RF	Radio Frequency
RMS	Root Mean Square
RS	Return Stroke
SDRAM	Synchronous Dynamic Random Access Memory
SEE	Single Event Effect
SLAVIA	Shielded Loop Antenna with a Versatile Integrated Amplifier
SPDT switch	Single Pole Double Throw switch
TARANIS	Tool for the Analysis of Radiations from Lightning and Sprites
TCSM	Travelling Current Source Model
TGF	Terrestrial Gamma ray Flashes
TLM	Transmission Line Model
VHF	Very High Frequency
VLF	Very Low Frequency

List of figures

List of tables

1. MOTIVATION

Lightning… a phenomenon which is so common and at the same time so mysterious. It accompanies us since time immemorial; sometimes it is closer than we would have wished. We are fascinated by its variability, we like its spectacular shapes, we are afraid of its power. We have known more than one quarter of a millennium that lightning is a natural electrical discharge between a thundercloud and the Earth.

But do we understand it? What do we know about its initiation? Yes, many of the questions have been answered. Regarding the initiation of lightning we have not gotten much further than Franklin.

It is unbelievable, but we still don't understand what causes lightning flashes. It is not clear how a lightning discharge is born. It's not yet fully understood how a thundercloud gets charged. We don't know what triggers the lightning discharge. We don't know how the spark needed for the initiation of discharges is formed in the thundercloud. The electric field measured in thunderclouds is about 10 times smaller than what is needed to initiate a discharge. Are discharges initiated by collisions between ice particles in thunderclouds? Are high-energy particles from cosmic rays responsible for the triggering of discharges? From a practical point of view, will we ever be able to predict when and where lightning will strike?

The solution of these puzzles is probably hidden inside the thundercloud. But can we look inside thundercloud? In-situ measurements of in-cloud processes are incredibly difficult. Optical measurements are possible only if the observed processes occur very close to the cloud edge.

But we know that the in-cloud discharges radiate electromagnetic signals. Thus the analysis of the remote measurements of signals radiated by in-cloud lightning processes can serve as a useful tool for their investigation.

2. REVIEW OF PREVIOUS RESULTS

2.1 Historical overview

Lightning and thunder has been fascinating people for thousands of years mainly due to their impressive luminous and acoustic manifestations. Due to the unbelievable power of lightning and its enormous destructive effects, lightning and thunder have for ages been attributed to gods. This was changed one stormy day in June 1752, when Benjamin Franklin carried out his famous experiment with a kite, a rope and a Leyden jar which proved his idea that lightning was an electrical current in nature. Franklin also showed that lightning flashes originated in clouds. Until the late nineteenth century, only photography and spectroscopy were available as tools for lightning research. First recordings of the lightning current came from the middle of the twentieth century.

Various lightning processes radiate electromagnetic signals. Their frequencies differ according to the speed of associated lightning processes. The first measurements of electromagnetic signals radiated by close and distant lightning discharges were performed in the thirties and the forties of the last century. The first measurements of magnetic and electric signals radiated by lightning flashes in microsecond and submicrosecond scales were done in the seventies of the last century and began the modern era of the electromagnetic measurements related to lightning [*Rakov and Uman, 2003*].

2.2 Lightning terminology

The whole phenomenon is usually termed the “lightning flash”. The lightning flash can be composed of one or more “lightning strokes”. Each stroke involves a leader and a return stroke. Some strokes may involve also a “continuing current” that follows immediately the return stroke in the existing lightning channel. The transient processes occurring in the period of continuing current are named M-component. The first strokes in the flash are initiated by “stepped” leader; subsequent strokes are preceded by “dart” or by “dart-stepped” leaders. Discharges transporting the cloud charge to the ground are

named cloud-to-ground (CG) discharges. According to the polarity of the transferred charge and to the direction of the propagation of the discharge we divide the CG discharges into four categories: most common downward negative lightning (~ 90%), upward negative lightning, downward positive lightning and upward positive lightning. The majority of discharges (~ 75%) don't reach the ground. These cloud discharges are divided into three categories: cloud-to air, inter-cloud and intra-cloud (IC) discharges.

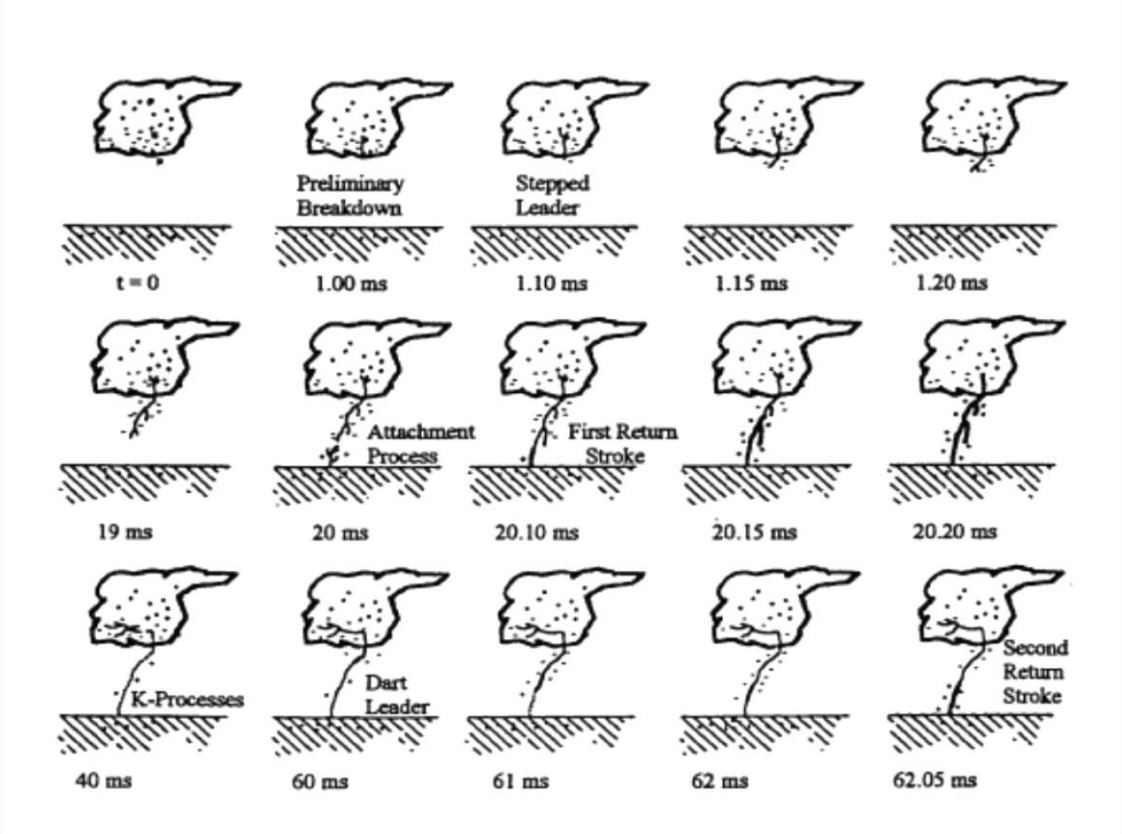

Fig. 1 Typical time development and typical components of the negative cloud-to-ground discharge [*Rakov and Uman*, 2003]

The time sequence showing the typical development and the typical components of the negative cloud-to-ground discharge is shown in Fig. 1. The source of the lightning discharge is a thundercloud – cumulonimbus. The process of the distribution of the charge inside the cloud will be discussed in section 2.3. The in-cloud process called preliminary breakdown lasts from a few milliseconds to several tens of milliseconds and generates the condition for the formation of the stepped leader. During this initial in-cloud process a single channel or a sequence of channels is formed. In the latter case,

these channels extend in different directions from the cloud charge source. Finally one of these channels evolves into the downward moving stepped leader which bridges the cloud charge source and the ground. The preliminary breakdown process sometimes produces a train of relatively large microsecond-scale pulses, called as characteristic or preliminary breakdown pulses. These pulses are thought to indicate the end of the preliminary breakdown process. The properties of the trains of preliminary breakdown pulses will be described in section 2.6.1. The occurrence of these trains also apparently indicates the moment when the downward moving leader quits the cloud base. The electromagnetic signals radiated by stepped leaders will be discussed in section 2.6.2. The stepped leader forms the conductive path between the cloud and the ground. The duration of the stepped leader is typically several tens of milliseconds and the average leader current is a few hundreds of amperes. When the leader approaches ground, one or more upward connecting leaders are initiated. The connection between the downward and upward moving leaders is called the attachment process and occurs usually several tens of meters above the ground. The attachment process is in fact the first stage of the return stroke. The return stroke transports the charge stored in the leader channel to the ground. The typical speed of the return stroke is between one-third and one-half of the speed of light. The peak current can exceed one hundred thousands of amperes. The high return stroke current heats the channel to the temperature of close to 30 000 K and creates a channel pressure of 10^6 Pa or more. The resulting channel expansion is accompanied by an intense optical radiation and by a sound wave – thunder. The electromagnetic signals radiated by the return strokes will be described in sections 2.6.3 and 2.6.4. The magnetic signals radiated by the return stroke can be computed if the spatial and temporal properties of the current in the return stroke lightning channel are known. *Uman and McLain* [1969] introduced transition line model for the return stroke current which will be described in section 2.6.6 and used in section 5.4 for the estimation of the relations between the peak values of magnetic induction, current in the lightning channel and velocity of the movement of the current wave. The subsequent strokes within the same flash are triggered by dart leaders. Between the end of the first return stroke and the initiation of the dart leader, J- processes and K-changes occur in the cloud. The redistribution of the charge inside the cloud runs during the J-process. K-changes could be seen as the transients occurring during the slow J-process. Both the J-processes and the K-changes serve to transport of additional charge into the existing channel. The K-changes could be also considered as "attempted" dart leaders. The field

variations connected with K-changes will be discussed in section 2.6.7. The discharge continues with the dart leader that moves to the ground with the average speed of 10^7 m/s and usually ignores the first stroke branches. When the dart leader approaches ground, similar attachment process starts the subsequent return stroke [*Rakov and Uman,* 2003]. The multiplicity of the strokes and the differences between the first and subsequent return stroke field waveforms will be discussed in section 2.6.5.

2.3 Charge structure of the thundercloud

The cumulonimbus cloud type also known as thundercloud is the primary source of lightning. The mechanism of the electrification of the thundercloud involves two main processes: 1) small-scale process of the charging of individual hydrometeors (various liquid or frozen water particles in the atmosphere), and 2) the process that spatially separates these particles by their polarity and thus creates the charges regions in the cloud.

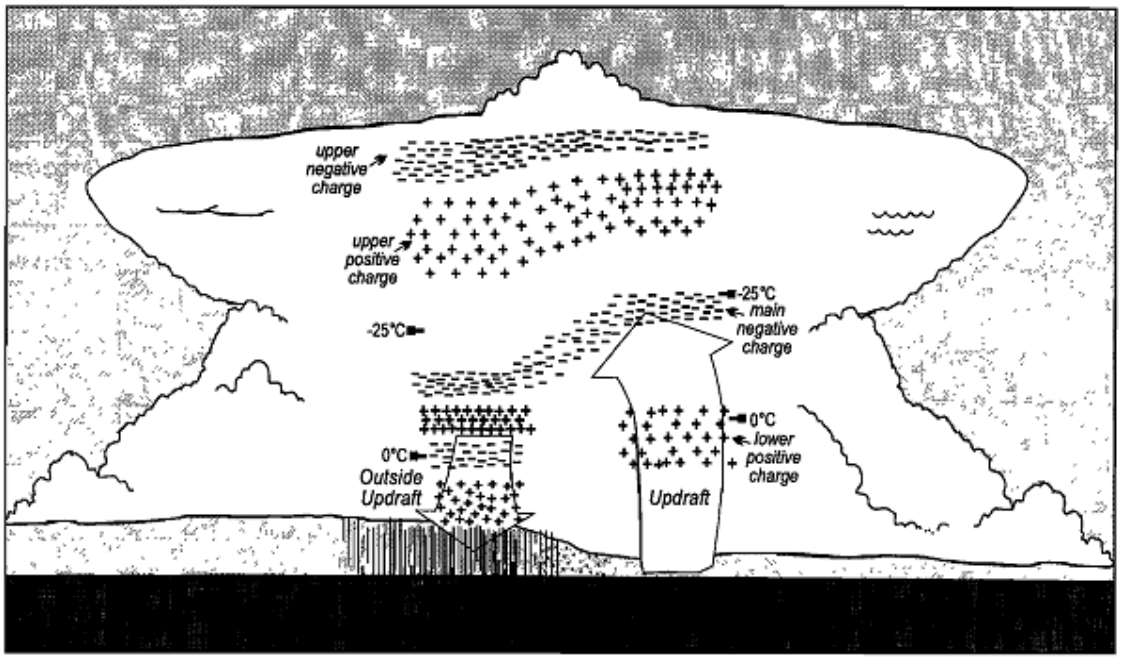

Fig. 2 Schematic of the basic charge structure in the convective region of a thunderstorm [*Stolzenburg et al.,* 1998]

This mechanism is still not completely clear. The generally accepted charging mechanism is non-inductive collisional charging. According to this mechanism, the electric charges are produced by collisions between precipitated particles (graupel) and cloud particles (small ice crystals) at certain temperature and in the presence of liquid water [*Rakov and Uman*, 2003]. Most measurements of the charging of the hydrometeors were carried out under laboratory conditions. The first complex in situ measurement of the charge, size and shape of hydrometeors in an electrified cloud were reported by *Weinheimer et al.*[1991]. An induction cylinder together with optical array probe placed on a sailplane was used for the measurement. The measured charges agreed in both sign and range of magnitudes with the expectations based on the laboratory results and supported the non-inductive collision mechanism for the charging of hydrometeors. The simplest representation of the thundercloud electrical structure is a dipole. This dipole is composed of an upper positive charge region and a lower negative charge region. The normal negative CG lightning transfers negative charge from the lower negative charge region to the ground. However, the dipole model is too simple to explain wide variety of observations; for example the dipole model isn't consistent with the occurrence of positive CG lightning discharges. *Williams* [1989] summarized in his review the evidences for the tripole structure of the electrified clouds. The tripole model consists of a dominant region of a negative charge, upper positive charge region and smaller and a more localized lower positive charge region. According to this review the lower positive charge region plays the essential role in the CG lightning initiation.

Ten years later *Stolzenburg et al.* [1998] reported, based on balloon observations, that a typical thundercloud couldn't be described as a simple dipole or tripole. The charge structure of the thunderclouds is more complex and contains many charge regions. Within convective updrafts the basic charge structure has four charge regions, outside updrafts of convection there are typically at least six charge regions (Fig. 2).

Stolzenburg and Marshall [1998] presented "maps" of the charge regions in the thunderclouds based on the simultaneous measurement of the vector of electric field along a mainly vertical path of a balloon-born sensor and the measurement of the charge of individual precipitation particles. The measurement was performed during two storms occurring in central New Mexico in 1979 and 1984. They were able to measure a charge of individual precipitation particle as a hail, a raindrop or a graupel, if it was

larger than 10 pC. The charge densities in the thundercloud obtained from the balloon sounding in 1984 are shown in Figure 3.

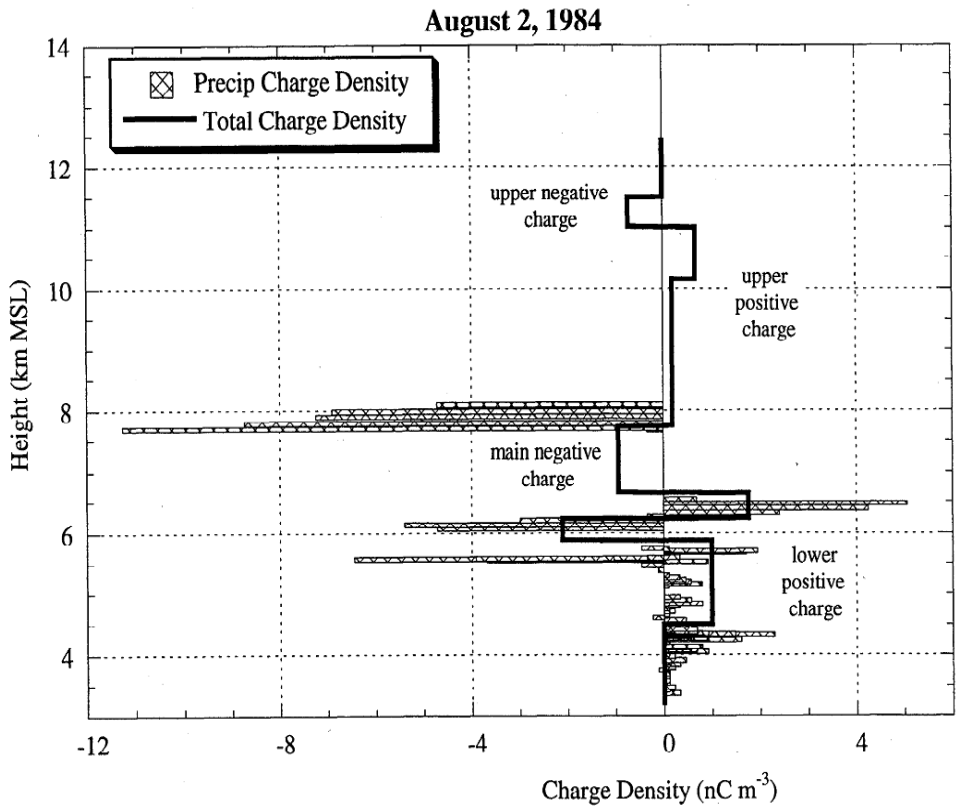

Fig. 3 Charge densities measured inside a thundercloud in August 1984 in central New Mexico [*Stolzenburg and Marshall*, 1998]

The existence of the two "extra" charge regions (between the lower positive and the main negative charge regions) derived from the sounding of electric field has been confirmed by an independent detection of the charge of individual precipitation particles. They also found that the charge is arranged in relatively shallow layers (a few hundred meters). The balloon sounding from *Coleman et al.* [2007] reported extensive horizontal intra-cloud branching and charge movement not only in IC flashes but also (surprisingly) in CG flashes as a result of a complex charge structure in the thundercloud in the horizontal direction. Interesting results of the in situ measurement of the charge and size of precipitation particles in two different mesoscale convective systems in Oklahoma were reported by *Bateman et al.* [1995]. The precipitation charge from 4 to 400 pC and the equivalent diameters from 0.8 to 8 mm were measured using

an instrument placed on a balloon. They found that the measured particles were not the major charge carrier and hypothesized that smaller particles were responsible for the measured electric fields. The relation between the polarity of the charge and the size of the precipitation particles is plotted in Figure 4 and surprisingly doesn't clearly confirm the generally accepted assignment of a negative charge to larger particles.

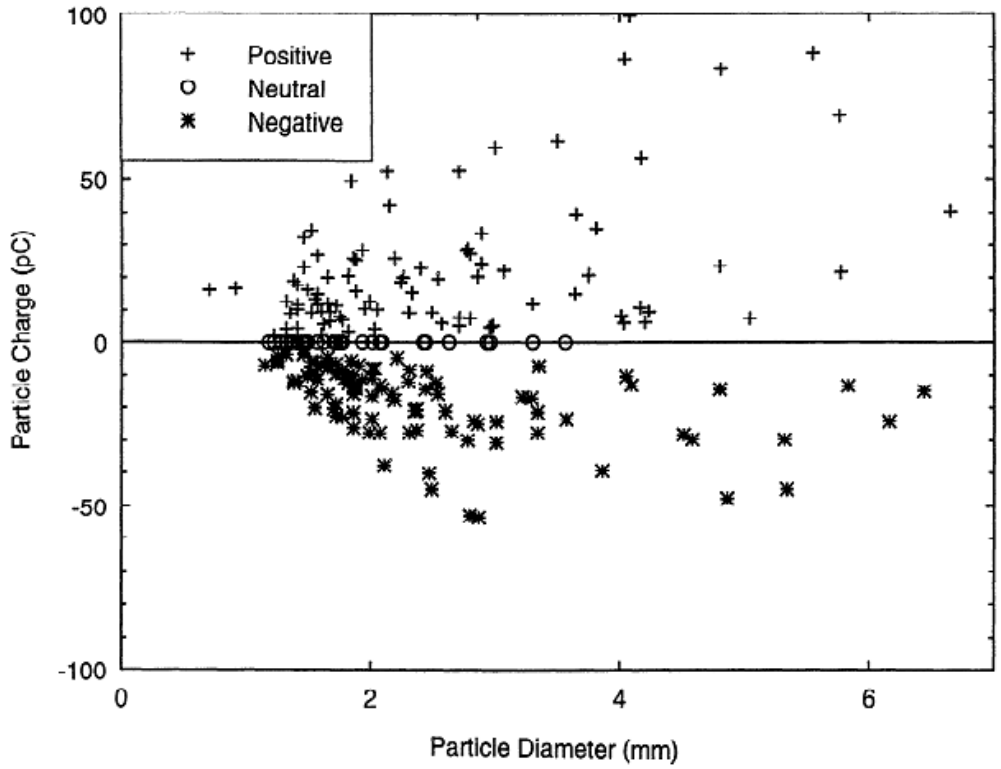

Fig. 4 Scatter diagram of particle charge versus particle size [from *Bateman et al.*, 1995]

Byrne et al. [1983] described the balloon born corona probes designed for the measurement of vertical electrical fields. These probes were used for the in-situ measurement of the electric structure of four thunderclouds. The authors found that the negative charge region is generally thinner that the positive charge region. The negative region had a vertical extent of less than 1 km, the observed thickness of the positive charge region was approximately 1.5 km.

In summary, the recent in-situ measurements confirmed that more than one charge region should be added to the classical tripolar charge structure. There is a consensus on the dominant mechanism for the initial stages of the cloud electrification. The collisions between graupel and small ice crystals in the presence of water droplets result in charging of ice particles. The large-scale separation of these charged particles

is caused by gravity forces. There is no consensus on the details of this charging process. Studies of the charging mechanism includes three areas; in-situ measurements, remote measurements of signals radiated by in-cloud discharges and numerical simulations of the evolution of the thundercloud.

2.4 Thunderstorms and the global electrical circuit

Up to ~2000 thunderstorms are active over Earth's surface at any given time. From 40 to 100 lightning discharges occur every second. These lightning discharges radiate intense electromagnetic pulses, which heat the partly ionized layers of the upper atmosphere [*Neubert*, 2003]. The thunderstorms represent huge electric batteries in the global electrical circuit, which was described by *Rycroft* et al.[2000, 2007, 2012], *Williams* [2009] and others. The schematic diagram showing the principles of the global electrical circuit is given in Figure 5.

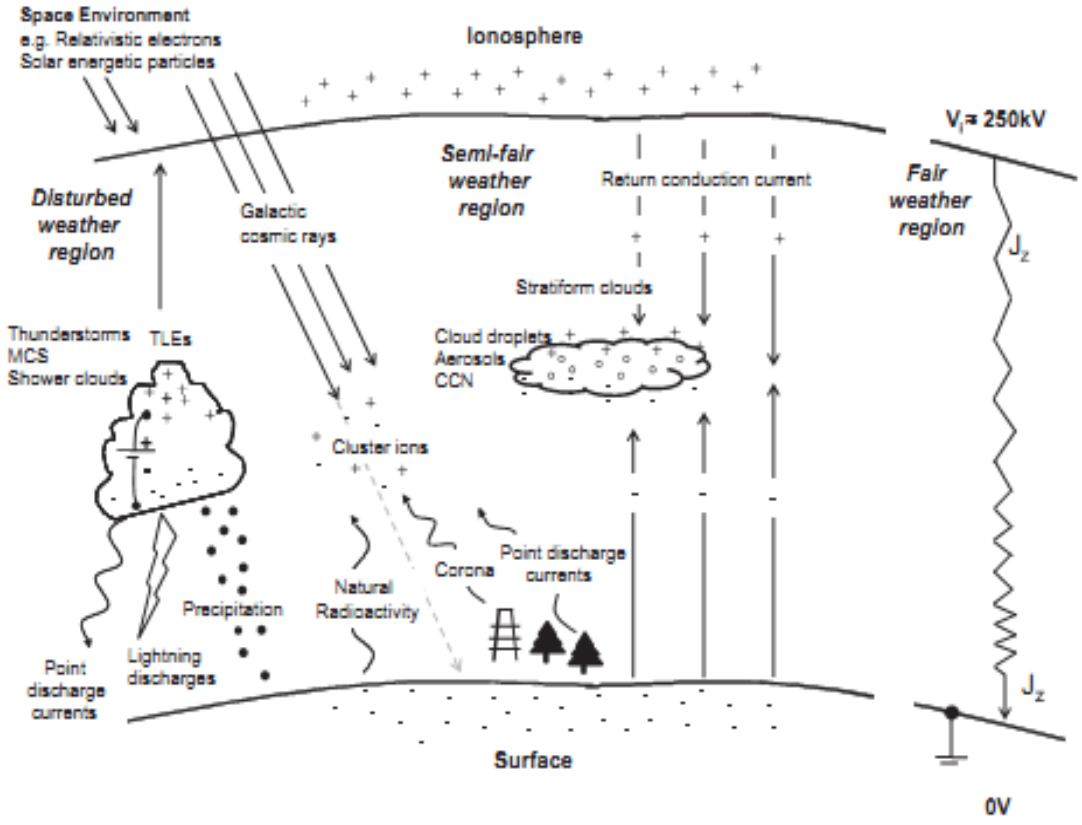

Fig. 5 Schematic diagram of the global electrical circuit [*Rycroft et al.*, 2012]

The thunderstorm batteries are distributed over the globe mainly in the thunderstorm regions of the Americas, Africa, and Asia. The thunderstorm batteries charge the ionosphere positive with respect to the ground. As both the ionosphere and the ground are good electric conductors, the charge is redistributed globally. The strength of the maintained fair weather electric field then reaches 200 V/m to 300 V/m at the ground level. This potential difference drives a vertical electric conduction current downward from the ionosphere to the ground in all fair-weather regions of the globe. The fair-weather current density is about 10^{-12} A/m^2 [*Rycroft et al.,* 2012]. Thunderstorms also directly couple the atmosphere to the magnetosphere, as the electromagnetic radiation from lightning causes the precipitation of the energetic electrons from the radiation belts into the atmosphere [*Neubert,* 2003].

2.5 Transient Luminous Events (TLEs)

Transient luminous events are large-scale optical emissions directly related to the thunderstorms and occurring between the top of the thunderclouds and the lower ionospheric altitudes. The first image of a TLE was captured in 1989 during the test of an auroral imaging camera during one dark night in the middle of the Minnesota prairie [*Franz et al.,* 1990]. Since 1989, several different types of TLEs were documented and classified [*Neubert,* 2003*; Pasko,* 2010, *and references herein*]. An overview of different types of TLEs is shown in Figure 6. Sprites are luminous flashes which may extend more than 40 km horizontally. The largest sprites develop at the base of the ionosphere at an altitude of about 90 km altitude and extend rapidly downwards almost to the thundercloud tops. Different types of red sprites got their special names according to their shape: "Carrot" sprites, "columnifor" sprites or "jellyfish" sprites are the most frequently observed TLEs. The sprites last from a few milliseconds to a few hundreds of milliseconds. A sprite usually appears close to and soon after a conventional CG+ discharge with a large charge moment. In contrast to the fully ionized channels of conventional lightning flashes, the current channels of sprites are weakly ionized. Other general types of TLEs occur less frequently. Blue jets are fountains of blue light that propagate upward from the top of the thunderclouds to the altitude of 40 km. Elves are luminous rings producing significant ionization at the altitudes of about 90 km after

being generated by powerful lightning. They are centered over the corresponding return stroke and spread laterally with the speed of light. The upward moving gigantic jets are electric discharges shooting up from a thundercloud. They reach altitudes of about 90 km and create a direct electrical path between the top of the thundercloud and the lower ionosphere. The "halos" are glows, which sometimes accompany the sprites [*Neubert*, 2003*; Pasko*, 2010, *and references herein*].

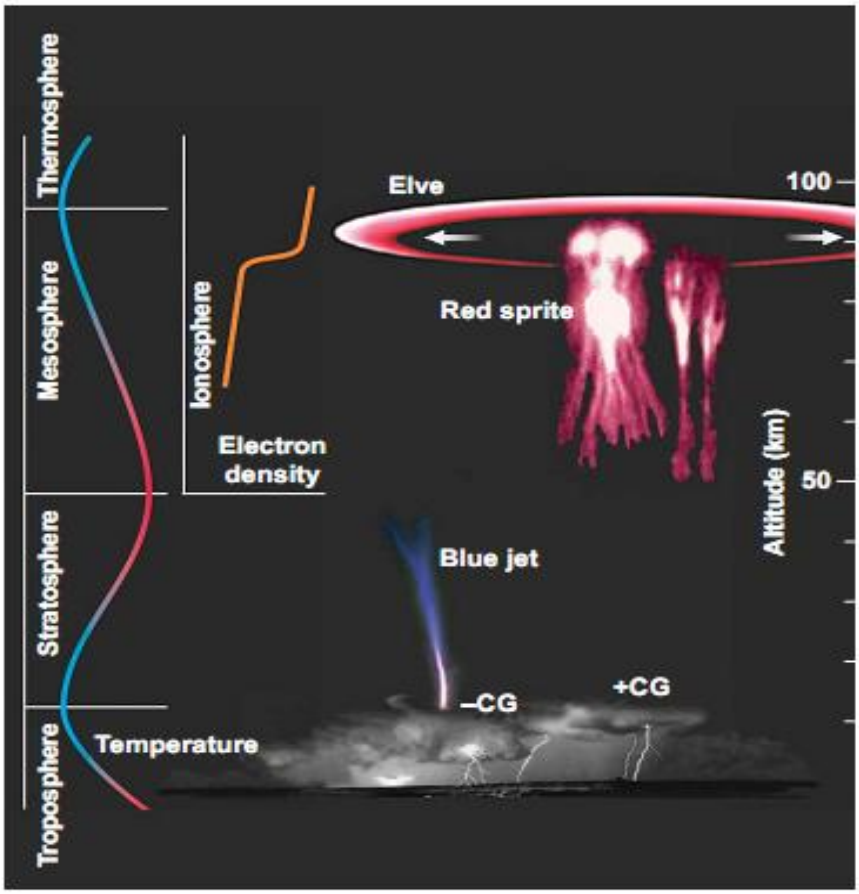

Fig. 6 Overview of transient luminous emissions [*Neubert*, 2003]

The time sequence of the carrot sprite evolution presented by *Cummer et al.* [2006], and shown in Figure 7, is well-resolved in both time and space. The sequence of images was captured at 5000 frames per second. This sprite was preceded by a positive CG lightning return stroke with a peak current of +166.3 kA, the charge moment 500 Ckm at a distance of 284 km from the camera. The sprite began to evolve 2.2 ms after the return stroke at an altitude of 73 km from the bottom of a relatively bright halo that began 1.4 ms earlier. Based on this sequence of frames the authors concluded that sprites can initiate from the brightening inhomogeneities at the bottom of a developing halo.

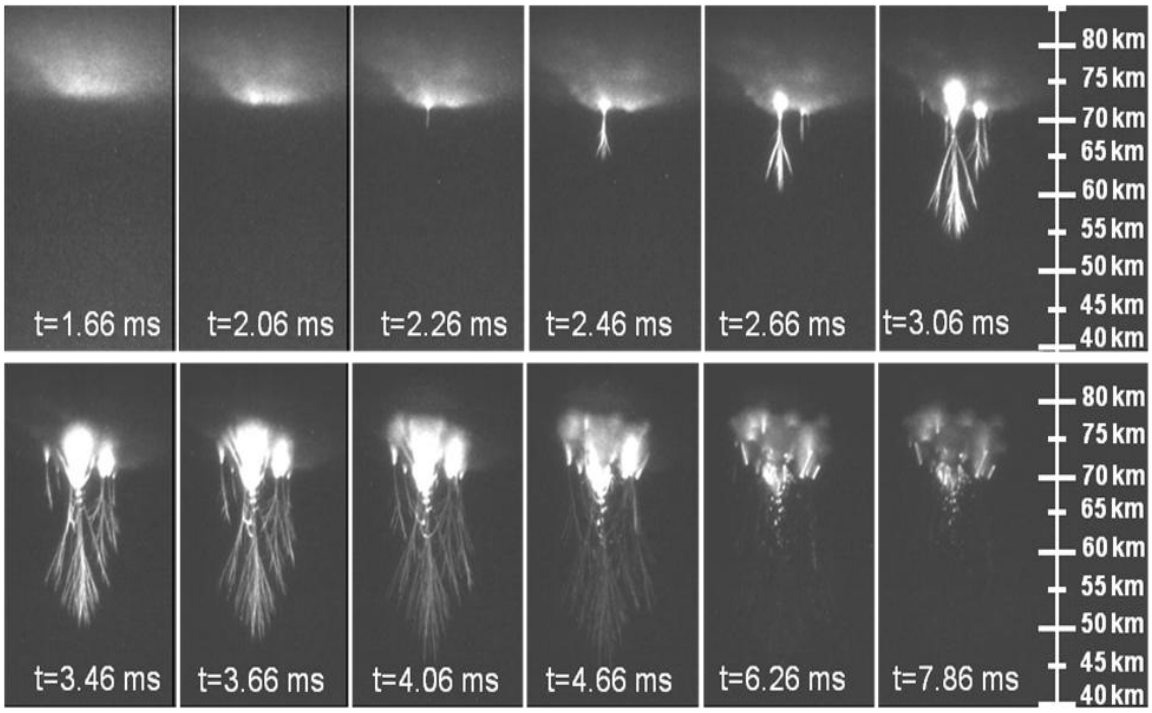

Fig. 7 High speed sprite images, each labeled with its time from the lightning return stroke initiation [*Cummer et al.*, 2006]

Soula et al. [2011] reported an observation and an analysis of five gigantic jets (GJ), which have been recorded with video and photo cameras above an isolated tropical storm close to the Reunion Island. The tops of the gigantic jets were located between 80 and 90 km. All these gigantic jets were accompanied by long, continuous cloud illumination. The CG flashes weren't simultaneously detected. The authors assumed that gigantic jets mainly originate in intracloud discharges. The lower parts of the gigantic jets at the altitude from of 20 to 40 km produced blue luminosity which decreased with altitude. Bright red luminous beads were observed in a surrounding zone of 40–65 km. Different stages of the development of the observed gigantic are shown in Figure 8: the end of the leading jet for GJ4, fully developed jets GJ2 and GJ3, and the beginning of the trailing jet for GJ1 and GJ5.

Krehbiel et al. [2008] considered charge imbalances in the thunderclouds as a fundamental condition, which allows the propagation of the leaders downwards as CG discharges or upwards as jet discharges. Based on the modeling, the authors presented two principal situations in which an upward discharge can be produced. Blue jets can

occur as a result of the electric breakdown between the upper charge region and the charge region attracted to the cloud top. Gigantic jets probably begin as normal intracloud discharges between the dominant negative charge region and the upper positive charge region and continue to propagate out of the top of the thundercloud. Simulated discharges illustrating different lightning types are shown in Figure 9.

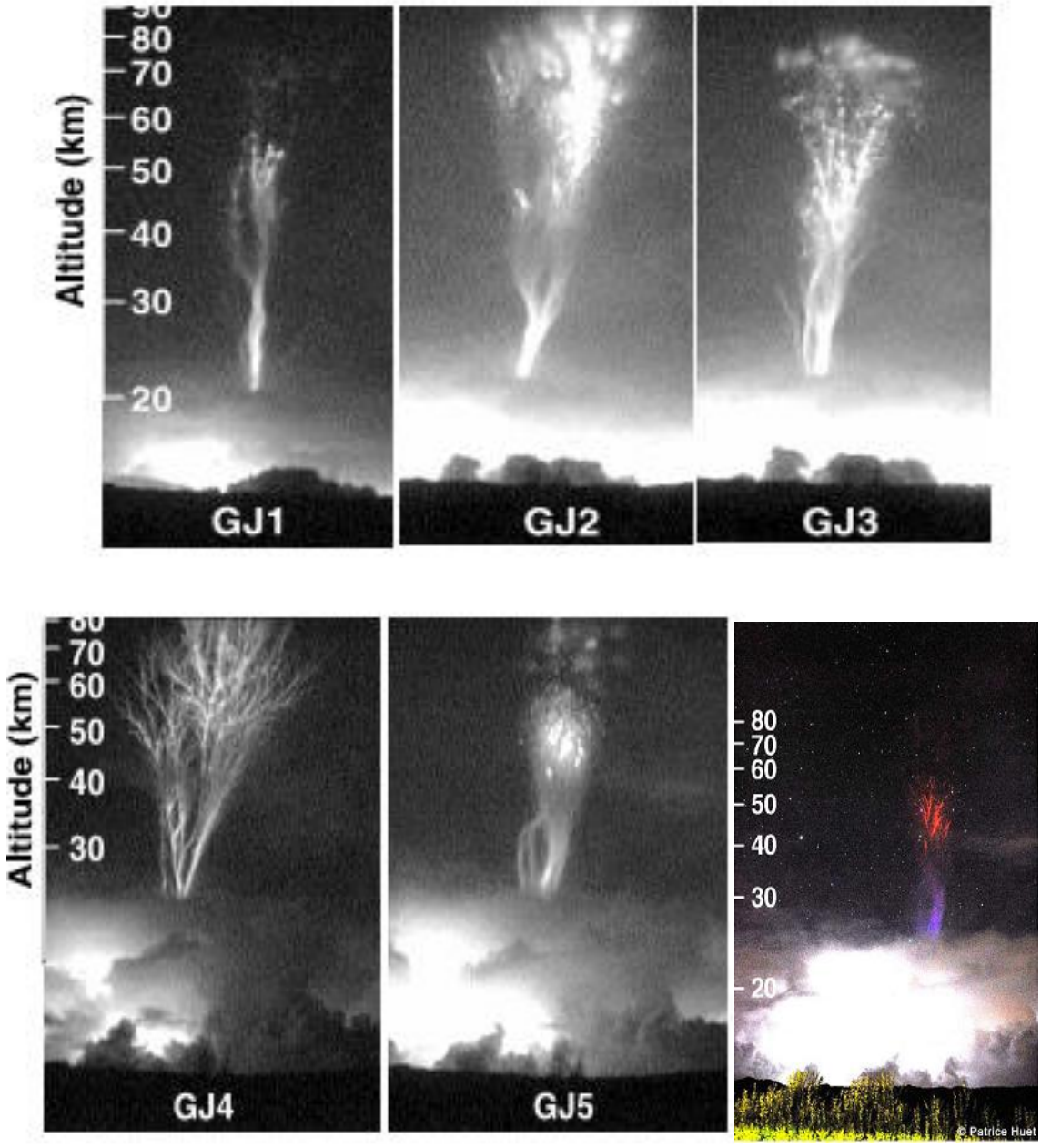

Fig. 8 Black-and-white images of the five GJs at different stages of their development and the color photograph of GJ5 [*Soula et al.*, 2011]

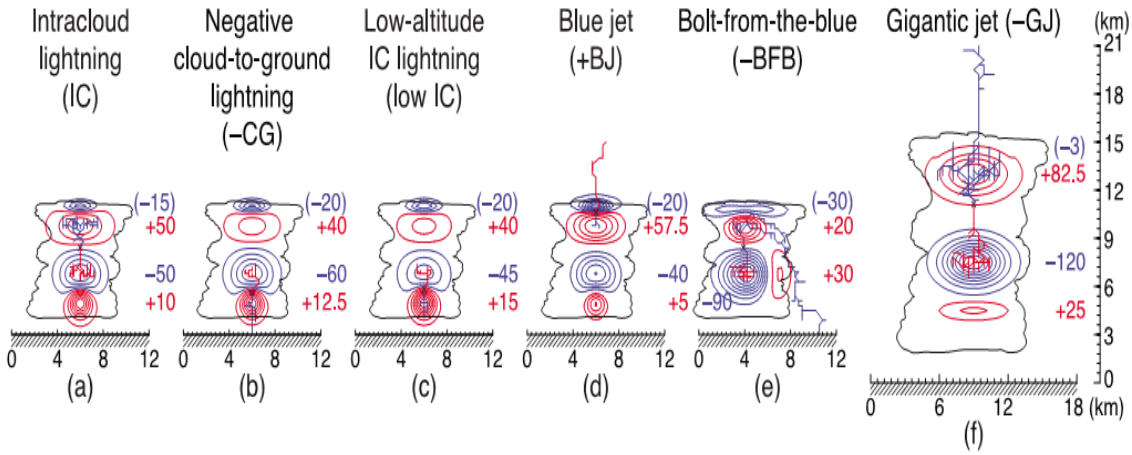

Fig. 9 Simulated charge distributions for different types of lightning discharges (blue and red colors indicate negative and positive charge regions) [*Krehbiel et al.*, 2008]

The transient luminous events are considered to be the most dramatic recent discovery in the solar-terrestrial physics. The possibility of the large-scale gas discharge events above the thunderclouds was first predicted in 1925 by the Nobel Prize winner C.T.R. Wilson [*Pasko*, 2010]. Transient luminous events have being intensively studied since their discovery in 1989. Their possible influence on the atmospheric chemistry and on the global electric circuit is widely discussed. The ground-based observations have been completed by observations from the balloons and from the space. For example the French microsatellite mission TARANIS (Tool for the Analysis of Radiations from Lightning and Sprites), will contribute to a better understanding of these lightning phenomena occurring above thunderclouds.

2.6 Properties of the signals radiated by particular lightning phenomena

2.6.1 Preliminary breakdown pulses

A sequence of pulses lasting from a few milliseconds to several tens of milliseconds is usually observed prior to the first return stroke. This sequence is composed of three parts. It begins with an initial larger pulse train which is believed to be connected with initial breakdown processes. The duration of the train is on the order of 1 ms. The preliminary breakdown pulses are followed by a relatively low and irregular pulse activity. The sequence ends with another pulse train. This latter pulse train has the duration of several tens of microseconds to several hundreds of microseconds. It is attributed to the last stages of the stepped leader. It is not understood yet how these initial pulses are generated. Several conductive channels are probably formed inside the cloud during the preliminary breakdown process. One of the channels evolves into the downward moving stepped leader. The train of preliminary breakdown pulses could then identify the beginning of the stepped leader development. The occurrence and the properties of the pulses may depend on the storm type, the stage of the storm life cycle, and on the geographical conditions [*Rakov and Uman*, 2003].

The percentage of the first return strokes, which are preceded by a preliminary breakdown pulse trains varied from 20% to 91% [*Nag and Rakov*, 2008*; Gomes et al.*, 1998*; Baharudin et al.*, 2010]. It is not clear whether the preliminary breakdown pulse train is missing in some cases or whether it is too small to be detected. The preliminary breakdown pulse activity is less observed in the tropical region and the probability of occurrence of this pulse activity increases with the latitude. *Gomes et al.* [1998] hypothesized that this effect can be caused by a weaker positive charge region at the cloud base in the tropics in comparison with the temperate regions. The largest pulses in the train are typically bipolar with the initial polarity identical to the polarity of the following first return stroke. However *Baharudin et al*. [2010] reported the opposite polarity of the largest preliminary breakdown pulse and of the dominant peak of the first return stroke in 9 % of flashes observed in Malaysia. The peak-to-peak amplitude of the largest preliminary breakdown pulses could be comparable with the amplitude of the

succeeding return stroke. *Gomes et al.* [1998] observed in Sweden a high percentage of flashes, where the amplitude of the largest preliminary breakdown pulse exceeds the amplitude of the following first return stroke. The preliminary breakdown pulses were recorded in Florida, in Malaysia, in Srí Lanka and in Sweden and their properties were reported by *Nag et al*. [2009]*; Baharudin et al*.[2010], *Cooray and Jayratne* [1994] and *Gomes et al.*[1998].

Stolzenburg et al. [2013] recently introduced a new hypothesis about the generation of the preliminary breakdown pulses based on the time-correlated high-speed video and electromagnetic field measurements. The authors found that the bursts of light recorded by the high-speed video (50 000 frames/s) are coincident with largest preliminary breakdown pulses in E-field data. *Stolzenburg et al*. [2013] therefore hypothesized that they observed the light coming from the initiation location of a flash. They assumed that the bursts of light and the coincident electromagnetic pulses were caused by the same physical event. They observed that the bursts of light were propagating downwards, that all bursts started at the same location, that each new burst is longer than the previous one, and that each new burst illuminated the whole path of the previous one. Based on these optical observations *Stolzenburg et al*. [2013] concluded that each burst of light is a visible manifestation of an in-cloud leader initiation. All leaders began at the same location, propagated downwards along the same path as previous leaders, and each leader extended the conductive path downwards. The visible steps in the progression of the in-cloud leaders were about 300 – 1500 m long. Summarizing the results, *Stolzenburg et al*. [2013] hypothesized that each large preliminary breakdown pulse which is accompanied by a visible light pulse can be caused by a current surge that is hundreds of meters long.

The same team of authors tried to locate the preliminary breakdown pulses using a network of ten E-change sensors at Kennedy Space Center in Florida. They developed a time-of-arrival technique called Position By Fast Antenna (PBFA). Each E-change sensor has a bandwidth up to 2.6 MHz and a sampling interval of 0.1 or 0.2 μs. The network covered a horizontal area of approximately 70 km x 100 km. The measurements of electric field changes were completed by optical observation and by the data from the LMA (Lightning Mapping Array) network. The results were reported by *Karunarathne et al.* [2013]. The authors tested that the PBFA technique correctly located preliminary breakdown pulses. They concluded that the observed vertical motion of pulses was caused by the vertical motion of negative charges in the cloud.

The downward motion was observed for negative CG flashes and the upward motion was observed for IC flashes. Similar motion was also detected by the LMA lightning mapping system in some cases. *Karunarathne et al.* [2013] stated that the LMA system didn't show one-to-one connection between the VHF sources and the breakdown pulses and that only a few percents of pulses were detected by the LMA lightning mapping system. The authors concluded that the newly developed PBFA technique provides an important new tool for understanding of the lightning initiation.

2.6.2 Stepped leader and dart-stepped leader

The leader is a path of ionized air which propagates downward from a thunderstorm cloud during the initial stages of a lightning strike. The tip of the leader is usually moving to the ground in a series of discrete steps. Measured photographically, a typical step near the ground has a length of about 20 m and the average speed of the leader tip is near 2 x 10^5 m/s [*Schonland et al.,* 1935]. Finally the tip of the leader approaches the ground and makes a contact with one or more upward propagating leaders. The velocity of the propagation of the stepped leader is considered to be a significant parameter of the electrical breakdown process. *Heavner et al.* [2002] summarized the previous observations of the speeds of the leader propagation and stated that this velocity could be dependent on the composition of the precipitation mix in a thundercloud. The authors found that higher portion of ice crystals in the thundercloud can produce extremely strong fields. A large region of the stronger field probably produces faster leaders. The authors hypothesized that the higher corona threshold of ice crystals in comparison with water droplets is responsible for this situation. This idea was confirmed by simultaneous ground and satellite observations of the radiation of the leaders during the winter storms. *Heavner et al.* [2002] reported the existence of unusually fast vertical leaders which propagated at the speeds on the order of 10^6 m/s in the winter storms.

The waveforms of electric or magnetic fields radiated by the leaders contain small pulses corresponding to the leader steps. The shapes of the pulses produced by the normal step and by the dart step are very similar. The step waveform usually consists of a fast initial pulse followed by small and slowly varying overshoot. The unipolar pulses in the inter-stroke pulse trains, which will be discussed in section 2.6.8, have also the

same shape. *Krider et al.* [1977] described properties of the electric field pulses produced by stepped and dart-stepped leaders in both maritime (Florida) and continental (Arizona) conditions. The authors investigated the 200 μs long electric-field waveforms just before the return stroke in the discharges to the ground. The mean time interval between the steps in the stepped leaders was about 16 μs in Florida and about 25 μs in Arizona. According to the authors this difference resulted probably in the larger number of very small and hardly recognizable pulses in the records of stepped leaders from Arizona. The mean interval between the dart steps was about 6 μs in Florida and about 8 μs in Arizona. These intervals were quite similar for both localities. The amplitudes of the pulses increased with upcoming return stroke and the amplitude of the largest pulse was about 10% of the amplitude of the corresponding return stroke peak. The authors found that the ratio between the largest leader pulse and corresponding first return stroke peak and the ratio between the largest dart step pulse and the corresponding subsequent return stroke peak were similar and that they were the same in both Arizona and Florida. The mean time interval between the last leader step and the following return stroke peak was measured only in Florida and was about 11 μs.

According to the study of electric fields of return strokes [*Uman et al.*, 1976], the shape and the amplitude of the pulses propagating over the Earth's surface may have been distorted owing to the propagation effects. The degree of distortion is dependent on the propagation distance and on the nature of the surface. Therefore *Krider et al.* [1977] measured the time interval between 10 and 90 % of the peak amplitude of individual pulses and the full with at half maximum (FWHM) only at close strokes in Florida, where the radiated electromagnetic wave propagated mainly over the seawater with good conductivity. The mean time interval between the 10 and 90 % of the peak amplitude of individual pulses was about 0.3 μs and the FWHM was about 0.4 - 0.5 μs. The authors stated that these results represented the upper limits of the corresponding values in fact, because they were close to the accuracy of their antenna system.

Similar measurements of the electric and magnetic fields radiated by stepped leaders were made at Korean seaside and reported by *Lee et al.* [2006]. The mean time intervals between the peak of the last leader pulse and the peak of the return stroke were 16.2 μs and 14.8 μs for the positive and negative polarities of leader pulses, respectively. In this study the time intervals between the stepped-leader pulses were widely distributed over the range of 5 – 70 μs, and the mean was about of 16 μs. The mean FWHM of the stepped-leader pulses was 1.3 μs. These numbers are not

completely consistent with the observation made by *Krider et al*. [1977]. *Lee et al.* [2006] proposed that these differences were probably caused by shorter (100 μs) records prior to the corresponding return strokes in comparison with previous studies.

Qie et al. [2002] investigated the electric field radiated by stepped and dart-stepped leaders in the time interval of 200 μs before the return stroke. The measurements were run in the Southeastern China. They found that the time interval between successive stepped leader pulses is 1.7 times larger than the time interval between successive dart-stepped leader pulses. This is not consistent with the observations of *Krider et al*. [1977], who reported that that the time interval between successive stepped leader pulses is about three times larger than the time interval between successive dart-stepped leader pulses for both Arizona and Florida measurements. *Qie et al.* [2002] proposed the following explanation for this difference: The authors divided the stepped leaders in three categories according to the shape of the waveform of the radiated electric field. The first type of stepped leaders (42 % of the recorded cases) is characterized by a small pulse superimposed on the rising edge of the dominant peak of the return stroke pulse. Second type (33 % of the recorded cases) exhibited relatively smooth electric field changes between the last leader step and the following return stroke. The third type of stepped leader (25 % of the recorded cases) is characterized by several small pulses between the last leader step and the following return stroke. *Qie et al.* [2002] hypothesized that different manifestations of the stepped leader movement in their records of radiated electric field are based on the different geometries of the lightning channels and that *Krider et al*. [1977] considered only the first type of stepped leaders in their comparison with the inter-pulse intervals of dart-stepped leaders.

Stolzenberg et al. (2013b) reported occurrence of stepped-to-dart leaders preceding a subsequent lightning return stroke. A leader propagating in steps via virgin air breakdown is probably attracted by the previous still ionized path and follows this path to the ground. This behavior was observed in ~ 1 % of leaders of recorded subsequent return strokes. A high speed video observation of the step-to-dart changes was confirmed by time-correlated electromagnetic measurements.

As the shapes of the electric fields produced by normal and dart steps and also by intra-cloud discharges are very similar, the processes producing these pulses might be similar as well. *Krider et al.* [1977] hypothesized that the fast current pulse produced by the formation of a new step might propagate backwards along the conductive leader

channel and dissipate during several microseconds or more. If the peak current and the propagation velocity of this fast current pulse remain constant during the first 1 or 2 μs, then the radiated electric field can have the observed stepped shape proportional to the current step.

2.6.3 Return stroke

The channel of ionized air between the cloud and the ground is established, when the leader tip joins the upward moving discharge. This conductive path allows for a much greater current to propagate from the Earth back into the cloud. This most luminous and noticeable part of the lightning discharge is called the return stroke. The experimental data on the return strokes could be grouped in four categories: 1) parameters derived from current measurements, 2) luminosity variations along the channel, 3) electric- and magnetic-field changes and 4) temperature, pressure and electron density of the lightning channel.

Vertical electric field and horizontal magnetic fields are usually measured. The electric-field records of very close return strokes (at the distance of several kilometers) contain also an electrostatic component and the magnetic-field records of close return strokes contain an inductive component. The magnetic and electric fields produced by distant return strokes contain only the radiation component and have essentially the same wave shapes. The fields radiated by return strokes depend primarily on the order of the stroke in the flash. The shapes of the first return stroke peaks and of subsequent return strokes peaks are similar, but with different temporal properties. *Weidman et al.* [1978] measured the fine structure of different lightning return stroke waveforms. According to their study, the first return stroke begins with a front which rises slowly for about 2-8 μs to about half of the peak amplitude. The initial front of the subsequent stroke peak lasts only about of 0.5-1 μs. After this front both first and subsequent strokes rise suddenly to the peak with the 10-90% rise times of about 0.2 μs. These measurements of *Weidman et al.* [1978] were limited by their recording system with the limit of 150ns and therefore many of the fast transition rise times were equal to this limit. *Weidman et al.* [1980] reported repeated measurements of the rise times in return stroke fields using improved instrumentation with the response time of 40 ns for the measurement of the electric field and of 10 ns for the measurement of the electric-field

time derivative. The vehicle with the instrumentation was located about 10 m from a sea wall. The recorded fields were produced by return strokes in lightning discharges that struck above the sea and propagated entirely over sea water to the recording site. Thus the distortion of the shape of the waveform caused by propagation over the land was minimized. The mean rise time of the fast part of the return stroke peaks was about 90 ns, less than the measurement published by *Weidman et al.* [1978] because of the improved response time of their recording system and because of their event selection. *Weidman et al.* [1980] also reported in their study the mean rise time of the return strokes which struck the sea water and propagated over about 3 km of a land surface. The mean rise time of these return stroke peaks was increased to about 200 ns, which was consistent with the study of the propagation effects of return strokes published by *Uman et al.* [1976]. All waveforms of the first return strokes contained the subsidiary peaks which are produced by the effect of branches.

2.6.4 Positive lightning

Positive downward lightning cloud-to-ground discharges (CG+) account only for about 10% of all cloud-to-ground discharges. This type of discharge was less studied due to its low occurrence but, ten years ago, it begun to attract attention because of its relation to sprites. In addition, damages to various objects caused by CG+ discharges are substantially more severe than the damages caused by CG- discharges [*Rakov and Uman*, 2003]. *Nag and Rakov* [2012] presented the conceptual cloud charge configuration leading to production of CG+ discharge. Possible in-cloud charge distributions are shown in Figure 10.

Titled dipole configuration (10a) was observed during winter-storms in Japan. The positive charge centre is exposed to the ground due to a horizontal displacement caused by strong winds. Positive monopole configuration (10b) was also observed in Japan. This configuration is dominant in Japanese winter storms. *Kitagawa and Michimoto* [1994] reported that the clouds have a dipole structure at their developing stage and a tripole structure at their mature stage. As the lower positive and negative charges in the tripole charge structure are carried mainly by heavy graupels, which fall off rapidly from the cloud, the positive charge predominates in the cloud for the relatively long period. This monopole configuration leads to the production of positive

cloud-to-ground lightning discharges.

The properties of positive cloud-to-ground discharges occurring in Florida were investigated by *Nag and Rakov* [2012]. The trains of preliminary breakdown pulses were observed in 15% of recorded positive flashes. These pulses may be viewed as a manifestation of an interaction of the downward moving positive leader with the negative charge centre. In contrast to negative CG flashes the electric field waveforms of positive CG discharges contained the stepped leader pulses only in 27% of cases.

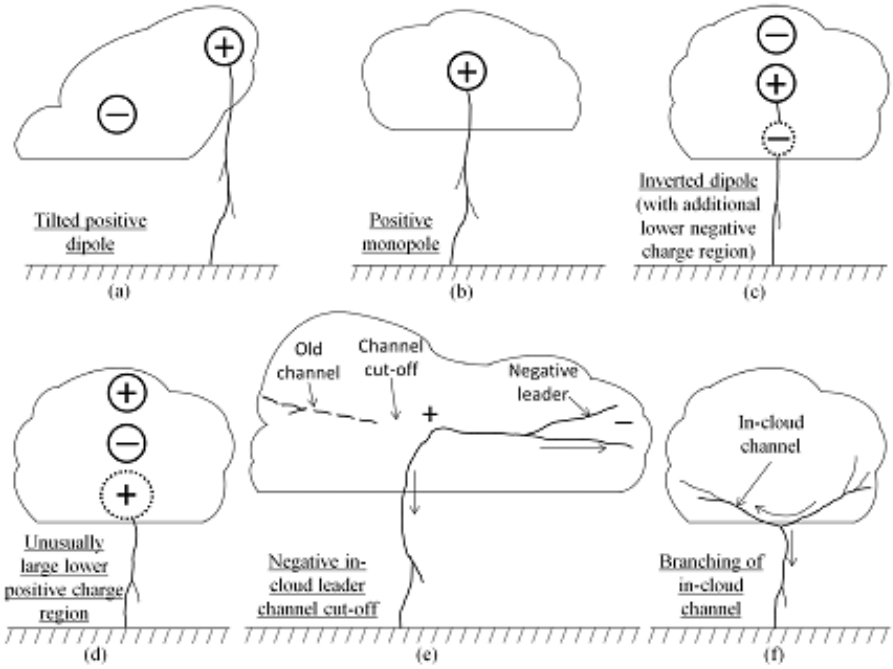

Fig. 10 Charge configuration and scenarios leading to production of CG+

2.6.5 Multiplicity of return strokes

The overall shapes of the subsequent stroke fields were often very similar within the same flash. Sometimes the subsequent strokes partly or completely create a new lightning channel. In that case the shapes of these subsequent stroke waveforms differ from the waveform of the corresponding first stroke. The subsequent stroke creating a new channel is usually preceded by a dart-stepped leader; the subsequent stroke copying the same channel is preceded by a dart leader. The waveforms of the

subsequent strokes belonging to one flash show sometimes slight differences corresponding probably to the temporal changes of the lightning channel geometry during the development of the flash. The peak amplitudes of the subsequent strokes are usually smaller that the peak amplitude of the first stroke and tend to decrease within the given flash.

Rakov et al. [1990] presented properties of negative cloud-to-ground flashes as a function of the stroke order. The data used for their analysis were derived from simultaneous electric-field and TV records. The stroke order and the new termination on ground were defined optically. The first strokes in multiple-stroke flashes exhibited significantly higher mean values of the electric field peak compared to the peaks observed in single-stroke flashes. Several step-like field changes separated by tens of milliseconds have been found in the electric-field records after the single return strokes. These changes were probably related to the leaders that tried to reach the ground unsuccessfully. Sometimes the subsequent stroke creates a new termination on the ground. The percentage of strokes forming the new termination on the ground decreased from 37 % for the second stroke to zero for strokes of order 5 and higher. The tendency to create the new termination to ground increased with the inter-stroke interval. Only 10 % of second strokes following the same channel as the first stroke were preceded by inter-stroke interval longer than 100 ms. *Thottappillil et al.* [1992] presented detailed data on subsequent strokes whose initial electric field peaks were greater than the first stroke peak in the same flash. The measurement of electric field was completed by the TV camera network records to obtain the information about the position of the corresponding lightning channel. The authors stated that surprisingly more than 33 % of the observed multiple flashes contained subsequent stroke with a larger field peak than the first stroke. Subsequent strokes with the larger field peaks were observed both in the previous formed channel and in the newly created channel. The subsequent strokes with a larger field peak following the same channel were preceded by 3 times shorter leader in comparison with all other smaller leaders traversing previously formed channel. Finally the larger subsequent strokes were preceded by longer inter-stroke interval with the mean value of 130 ms. Similar study of relative magnitudes of electric-field peaks of the first and subsequent return strokes measured in Florida, Austria, Brazil and Sweden was presented by *Nag et al.* [2008]. According to their observations, the electric field peak of the first strokes was roughly 2 times larger than the field peak of the subsequent strokes in all the investigated localities. On the contrary, the occurrence of the

subsequent stroke field peaks larger than the first stroke peak varied for different storms and different localities. About 30 % of flashes in Florida, Brazil and Sweden contained at least one subsequent stroke field peak greater than the first return stroke peak. About one half of flashes in Austria manifested this behavior. This discrepancy wasn't explained in the study; however in Florida, Brazil and Sweden the fields were measured very close to the sea and the difference in the lightning properties measured in maritime and continental condition was reported several times in the lightning literature [*Krider et al.,* 1975, *Cooray et al.,* 1994].

Cooray et al.[1994] compared inter-stroke intervals in the ground flashes measured by recording the electric field at microsecond resolution in Sri Lanka, Sweden and Florida. The authors concluded that the similarity of lightning characteristics for the three different geographical locations were rather remarkable. However, the geometric-mean inter-stroke intervals for the maritime and continental region differ in their study. They measured identical values for both the maritime regions and about 20% smaller number for the continental region. Since the inter-stroke interval is strongly dependent on the intra-cloud processes, this slight difference in the inter-stroke intervals may support the idea of the differences in the charge structure of the thunderstorm clouds in the different locations.

Interesting statistics of cloud-to-ground lightning with multiple grounds contact were reported by *Valine et al.* [2002] who recorded lightning flashes on a videotape in Arizona. The authors used the categorization of the flashes with multiple ground contacts defined by *Rakov et al.* [1994]; 1) the flashes which exhibited separate channels between the cloud base and the ground and 2) flashes which shared a common channel at higher altitudes and then forked and struck the ground in two or more places. The development of both types of flashes is plotted in Fig. 11.

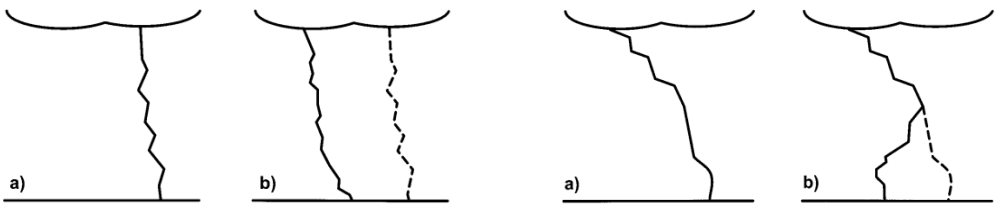

Fig. 11 The development of typical "new channel flash" (NCF - left plot) and of typical "altered channel flash" (ACF - right plot) [*Valine et al.,* 2002]

A generally accepted definition of the multiple stroke flash is as follows: the time difference between two following strokes should be less than 500 ms and the distance between the ground contacts should be less than 10 km. In case of close NCF in time and location it isn't possible to distinguish if the different channels contacting ground were preceded by two different stepped leaders propagating downwards and created in fact two single-stroke flashes, or if the strokes belonged to the same flash. The average number of the lightning strike points was 1.45 per CG flash, which is consistent with the average value found in other geographical locations. A large branch in the first return stroke contributed sometimes to the forming of an ACF. According to the study, 21% of ACF seemed to follow the large visible branch from the first stroke. They admitted that a part of NCFs could be in fact ACFs that forked above the cloud base. The authors presented also other interesting results: 67% of the new strike points were produced by the second stroke in the channel, the chance of forming a new or an altered channel rapidly decreased with the stroke order and the presence of a long continuing current also lowered the probability of producing a new lightning channel.

Much lower multiplicity of the strokes was reported for positive lightning flashes. Positive flashes usually have a single stroke. *Nag and Rakov* [2012] reported the average number of the strokes per flash of 1.2. The subsequent strokes mainly created a new termination on the ground.

2.6.6 Transmission line model of the lightning current channel

Transmission line model (TLM) is a simple model of the lightning channel which is widely used for modelling of the channel of a stepped leader or return stroke. The model was presented by *Uman and McLain* [1969, 1970].

The current wave is injected at the base of the channel and propagates at a constant speed without attenuation or dispersion. Figure 12 shows the geometrical factors used for the calculation of the magnetic field of the stepped leader (a) or of the return stroke (b). The channel of the return stroke or stepped leader is idealized as a straight vertical line perpendicular to the perfectly conducting ground.

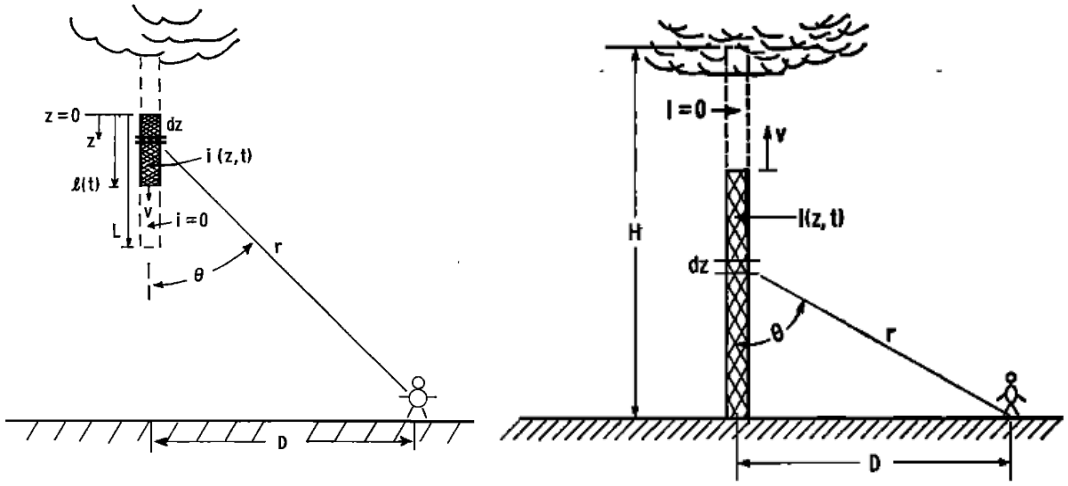

Fig. 12 Drawing defining the geometrical factors used in computations of the magnetic field of (a) the stepped leader and (b) the return stroke [*Uman and McLain*, 1969, 1970]

Uman and McLain [1969, 1970] define the magnetic field *B* on the ground surface at a distance *D* from the lightning channel produced by the stepped leader current *I (z, t)* by

$$B_{\varphi}(D,t) = \frac{\mu_0}{2\pi} \int_0^{\mathrm{L}} \frac{\sin\theta}{r} \left[\frac{I(z,t')}{r} + \frac{1}{c} \frac{\partial I(z,t')}{\partial t'} \right] \mathrm{d}z \qquad (1)$$

Magnetic field *B* on the ground surface at a distance *D* from the lightning channel produced by the return stroke current *I (z, t)*.Then reads:

$$B_{\varphi}(D,t) = \frac{\mu_0}{2\pi} \int_0^{H} \frac{\sin\theta}{r} \left[\frac{I(z,t')}{r} + \frac{1}{c} \frac{\partial I(z,t')}{\partial t'} \right] \mathrm{d}z \qquad (2)$$

In equations (1) and (2), t' is the retarded time $t' = t - r/c$, *c* is the speed of light, μ_0 is the permeability of the free space. The first term on the right-hand side of the equations is the induction field; the second term is the radiation field. The induction field can be neglected for the distances *D*>>*L* or *D*>>*H*. The current wave propagates along the channel at a velocity *v(t)*, as it would propagate along a transmission line. The

current at the propagating wave front grows linearly from zero to an appropriate value $I(l(t), t)$, where $l(t) = \int_0^t v(t)dt$. With these assumptions, equations (1) and (2) can be rewritten as

$$B_\varphi = \frac{\mu_0 \sin\theta}{2\pi r c} v\, I(t) \qquad \text{for } t < \tau_v \qquad (3)$$

$$B_\varphi = \frac{\mu_0 \sin\theta}{2\pi r c} v\, [I(t) - I(t - \tau_v)] \qquad \text{for } t > \tau_v\,, \qquad (4)$$

where $\tau_v = L/v$ (or $\tau_v = H/v$ respectively) is time, during which the current front traverses a channel of the stepped leader (or a channel of a return stroke, respectively). If the current is written $I = I_0 f(t)$, where I_0 is the peak current, equations (3) and (4) can be rewritten as

$$B_\varphi = \frac{\mu_0 \sin\theta}{2\pi r c} v\, I_0\, f(t) \qquad (5)$$

Variations of the magnetic field radiated by the return stroke or by the stepped leader therefore approximately follow the variations of the current in the channel.

Schoene et al. [2003] compared the model-predicted electric and magnetic field waveforms with the measured waveforms from triggered lightning. The authors tested (1) the simple transmission line model, (2) a modified transmission line model with a linear current decay as a function of height and (3) a modified transmission line model with an exponential current decay as a function of height. They also tested another widely used model - travelling current source model (TCSM). In the TCSM the current source travels upward at the constant speed and injects the current wave in the channel. This current wave propagates downwards and is absorbed at the ground without reflection.

Schoene et al. [2003] found that if the return stroke speed was chosen to be ~ 10^8 m/s, the simple TLM works well in reproducing the electric and magnetic fields radiated by the return stroke during the first microseconds. The authors didn't find any significant difference in the results obtained from the simple TLM and from both modified versions of TLM. They found that the TCSM underestimates the measured

electric fields for higher return stroke speeds (~ $2 \cdot 10^8$ m/s). The TCSM also produces narrow spikes in the predicted electric and magnetic fields which were not observed in the measurements.

2.6.7 K-changes and M-component

The redistribution of the charge in the thundercloud during the inter-stroke period manifests itself as the change in the electric and magnetic fields between the cloud and the ground. This relatively slow "junction" process (J-change) is accompanied by the rapid small field variations called "K-changes". The K in the term "K-change" stands either for klein (the German expression for small) or for N. Kitagawa and M. Kobayashi, who studied this lightning process in detail for the first time in 1960. K-changes in both ground and cloud flashes appear as a step-like or ramp-like electric field change [*Rakov et al.,* 1992]. The term "M-component" is used for the electric field change which refers to the temporary increase of the luminosity of the lightning channel observed after some ground return strokes. M-component has usually the characteristic hook-like shape in the records of the vertical component of the electric field [*Rakov and Uman,* 2003].

The time properties of the K-change and M-component sequences are reported by *Thottappillil et al.* [1990]. According to their measurements of close ground flashes the geometric-mean interval between following K-changes or M-components were dissimilar: 12.5 ms for K-changes (Fig.13) and 2.1 ms for M-component intervals. Also the position of the K-change and of the M-component within the overall flash record was different. K-changes occurred quite regularly between the strokes and M-components could be found only several milliseconds after the stroke in the period of continuing current. In their discussion the authors stated that one half of their inter-stroke intervals showed no K-changes and that average number of K-changes per inter-stroke interval containing K-changes was about four. They speculated that a more sensitive instrument would detect about 20 K-changes per inter-stroke interval.

Shao et al. [1996] studied spatial and temporal development of intra-cloud lightning. Based on their VHF observation the authors described the details of the particular stages of an intra-cloud discharge. They found slow vertical K-streamers in the active stage of the flash and fast horizontal K-streamers in the final stage of the

flash. According to their study the K-streamers were identical to dart leaders observed during the inter-stroke intervals of CG flashes. They also observed the bursts of VHF radiation accompanying the fast step electric field change indicative for a sudden current increase along the channel.

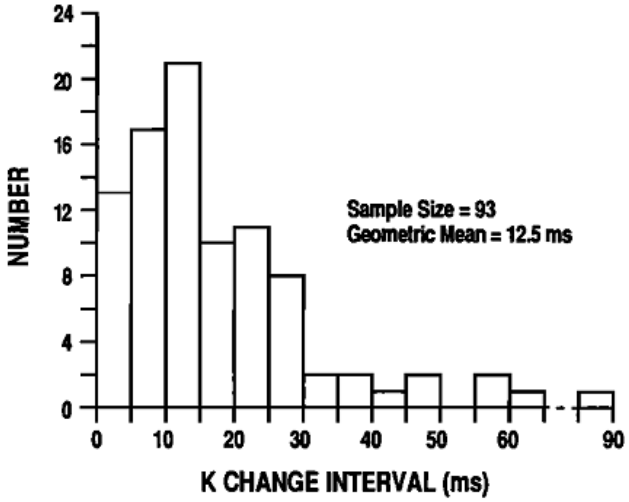

Fig. 13 Frequency distribution of time intervals between successive K changes measured in Florida [*Thottappillil et al.*,1990]

2.6.8 Inter-stroke pulse trains

Some subsequent leaders (dart-stepped leaders) exhibit stepwise movement to the ground. Their optically detected speed was about of 10^6 m/s. It means that it was the intermediate value between the speeds of the stepped and the dart leaders. The steps in the dart-stepped leader are believed to be accompanied by the bursts of regular unipolar microsecond-scale pulses [*Davis*, 1999].

These bursts occurring in the cloud flashes were first studied by *Krider et al.* [1975]. In this study the authors compared the time interval between neighboring pulses in the observed bursts and the interval between the bright steps in the dart-stepped leader photographed and reported by *Schonland* [1956]. Based on the similarity of these time intervals *Krider et al.* [1975] suggested that the dart-like K-change developing in the stepped manner could produce the observed uniform pulses. The analogous bursts in

the electric-field waveforms of the cloud-to-ground and in the intra-cloud lightning discharged were observed and reported by *Rakov et al.* [1992, 1996]. According to these studies, the movement of the charge in the existing intra-cloud lightning channel between the strokes can give rise to the microsecond-scale electromagnetic pulses. *Rakov et al.* [1992] found that 24% of the recorded K-changes and 53% of the recorded M-components were accompanied by the microsecond-scale pulse activity. The pulses occurring during the K-step and M-hook field changes differed in terms of amplitudes, regularity and intervals between the neighboring pulse trains. If we multiply the occurrence of K-changes in inter-stroke interval reported by *Thottappillil et al.* [1990] and the occurrence of microsecond-scale pulse activity associated with K-changes [*Rakov et al.*, 1992], we obtain relatively small probability of about 12% that an inter-stroke interval contains trains of pulses.

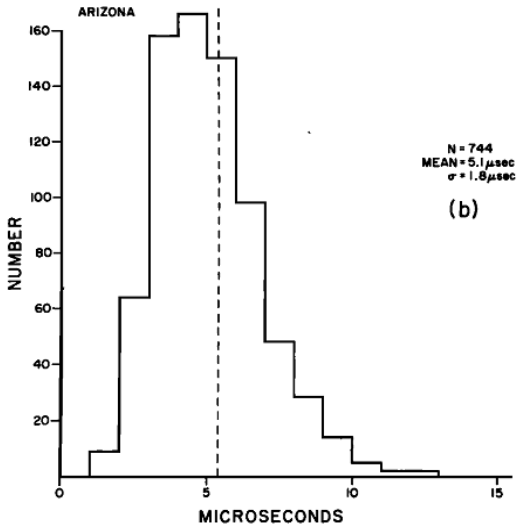

Fig. 14 Time intervals between successive pulses measured in bursts in Arizona [*Krider et al.*, 1975]

Davis [1999] measured the time derivative of the electric field generated by dart-stepped leaders, by the leaders preceding a new ground termination, and by the IC leaders. Thanks to the multipoint measurement (five stations) he was able to estimate the location and the speed of the movement of the leaders. He noticed the presence of trains of pulses in his records and compared the properties of the pulse trains connected with different types of leaders. Due to the insufficient length of the waveform records (205 μs only) he limited his study to the comparison of the inter-pulse interval. The

inter-pulse interval was 2.8 μs, 7.6 μs, and 5.1 μs for trains in the dart-stepped leaders, in the leaders preceding new ground termination, and for the trains in IC discharges, respectively. The author found that the inter-pulse intervals were increasing and the speed of the leader movement was decreasing with time in a given train for all types of leaders. He concluded that the length of the steps in the propagation of the leaders remained unchanged, which is consistent with the optical observations.

Krider et al. [1975] measured the time interval between successive pulses in both maritime (Florida) and continental (Arizona) conditions (Fig. 14). The mean values of both inter-pulse interval measurements were similar: 6.1 μs for the seaside and 5.1 μs for the inland. The distribution of the inter-pulse distance for the continental conditions is narrower than for the maritime conditions. The differences in the distributions of inter-pulse intervals for the seaside and inland conditions probably result from the differences in the charge structure of the maritime and continental thunderstorm clouds.

The amplitude of the pulses and the spacing between successive pulses are changing with time within a given train. *Rakov et al.* [1992, 1996] reported that the amplitudes of the pulses and the pulse repetition rates tended to decrease with time within the observed bursts. *Wang et al.* [2010] classified four types of the bursts according to the evolution of the inter-pulse interval and the polarity of the pulses. According to this classification a "normal" burst exhibits an increasing inter-pulse interval and decreasing pulse amplitude within a given burst, a "back" burst exhibits a reverse behavior. The wave form of a "symmetry" burst is composed of a "normal" burst followed immediately with the "back" burst. In a "reversal" burst there is the polarity of pulses inverted during the development of the burst. The authors assigned different evolution patterns to different lightning phenomena. *Wang et al.* [2010] speculated that the „normal " burst can be seen as a small intra-cloud return stroke, the "back" burst as a leader of the small return stroke, the "symmetrical" burst as a combination of both and the "reversal" burst can be connected with CG+ discharge.

The pulses belonging to one train usually have the same polarity. *Rakov et al.* [1996] reported the equal occurrence of the trains with the negative and positive pulses. They also noted the reversal of the polarity of pulses within some of the observed trains. With their single-station measurement the relation of the polarity to the orientation to the source could not be determined. *Davis* [1999] recorded the intra-cloud trains associated with different polarity of the pulses simultaneously in different stations and also the polarity reversal at the single station. They found that for 66% of pulses the

polarity of the pulses was consistent with the current flowing in the channel between two consecutive source locations. The reversal in the polarity was attributed to the change of the channel geometry and to the possible development of the branches.

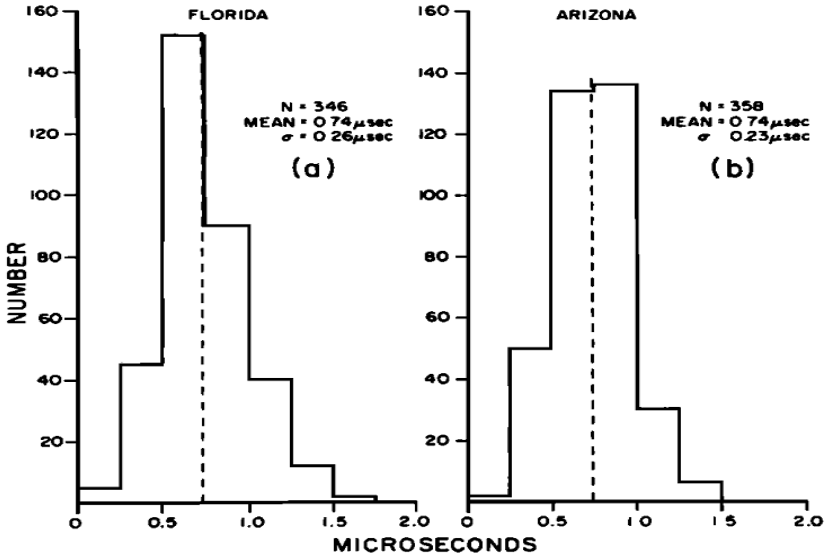

Fig. 15 Full width at half maximum measured for individual pulses in (a) Florida and (b) Arizona [*Krider et al.*, 1975]

The measurement of the FWHM of individual pulses was done by *Krider et al* [1975]. In their study the FWHM was measured for several hundreds of pulses recorded in Florida and Arizona (Fig. 15). The shape of the pulses and the average FWHM (0.74 μs) were identical for both locations.

2.6.9 Compact intracloud discharges (CIDs) and bouncing wave type discharges

A compact intracloud discharge is one of the least understood lightning phenomena. The CID usually produces an isolated bipolar pulse. The CIDs have recently attracted attention because they are considered to be the strongest natural source of HF and VHF radiation. The relation of the CIDs to the terrestrial gamma ray flashes (TGF) is also intensively discussed. About 73 % of CIDs occur in isolation,

about 24 % occur close to the cloud-to-ground or "normal" intracloud flash. 4 % of CIDs occur in pairs separated by less than 200 ms. A spatial extent of the compact intracloud discharges is quite small, 300 m - 1000 m. The observed CIDs occurred typically at high altitudes above 10 km. *Nag et al.* [2010] reported that the total electric field pulse duration for 157 CIDs observed in Florida varied from 10 μs to 30 μs with the geometric mean of 23 μs. This type of discharge was originally called NBE (Narrow Bipolar Event) or NBP (Narrow Bipolar Pulse) because of its manifestation in electromagnetic measurements [*Nag and Rakov*, 2009].

.

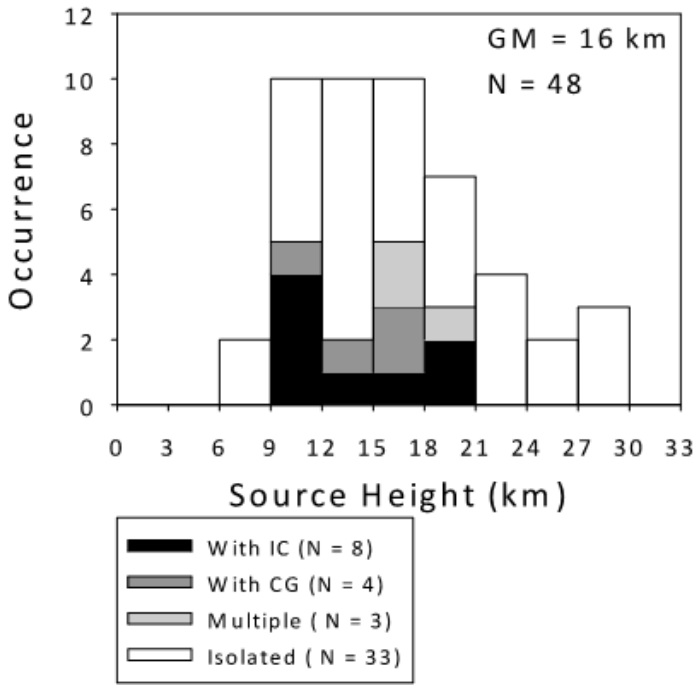

Fig.16 Histogram of radiation source heights for 48 CIDs [*Nag et al., 2010*]

Jacobson and Heavner [2005] examined the relation of CIDs to "ordinary" negative CG lightning discharges using the same ground detection system in Florida. Their data set covered four years of observation and consisted of more than three million of lightning events. One third of these events were completed with the infrared images of the top-cloud temperatures done by the satellite GOES-East IR. The authors didn't find any thunderstorms in which only CIDs would occur without presence of other types of lightning. Most CIDs occurred at altitudes within the upper troposphere. They didn't find any difference in the cloud-top-temperature distributions for CIDs and

for "ordinary" CG- discharges. The distributions of cloud-top temperatures for both types of discharges have a peak within –50°C and –60 °C. Both types of discharges were almost never observed in the cloud systems for which the cloud-top temperature was higher than –40°C.

Nag et al. [2010] examined the height of radiation source for 48 CIDs observed in Florida. The histogram of the obtained heights is plotted in Figure 16. *Sharma et al.* [2008] and *Ahmad et al*. [2010] measured the properties of the CIDs in tropical regions of Sri Lanka and of Malaysia. Both authors showed that the characteristics of the tropical CIDs are comparable with the properties of the CIDs from Florida reported by *Nag et al*. [2010a]. This indicates that the occurrence and the characteristics of CIDs are probably independent of the geographical location

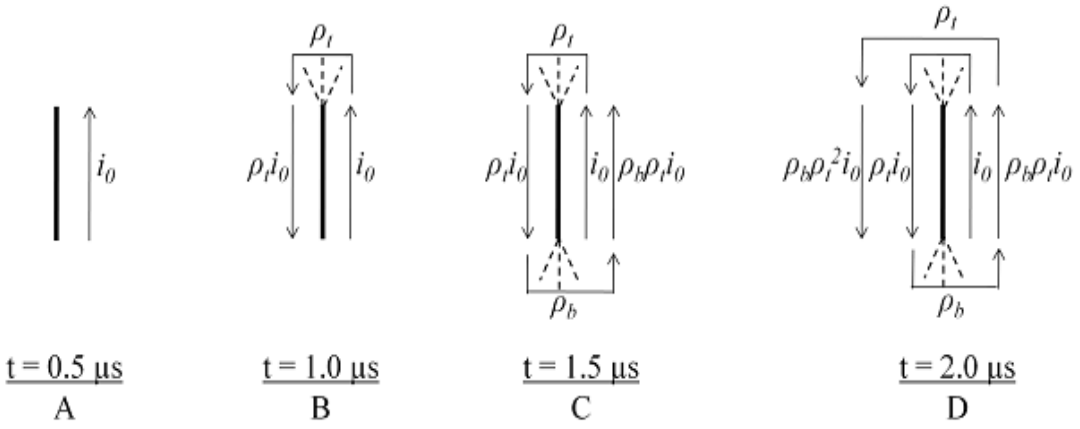

Fig. 17 Schematic representation of the bouncing wave mechanism of CID [*Nag and Rakov,* 2010a]

Hamlin et al. [2007] found secondary peaks after the initial peak in the electric field waveforms for 12 % of their CIDs. They interpreted these secondary peaks as signatures of reflections of inter-channel current pulses. The authors examined why the reflection signatures were only found in small percentage of the observed CIDs. The presence of the reflection signatures in the waveforms of the observed CIDs didn't appear to be the dependent on the day time, on the average source height, or on the type of the storm. *Hamlin et al.* [2007] hypothesized that only cases with short channels were detected, where the current pulse probably had sufficient amplitude to show a detectable radiation at the reflection points. The authors also hypothesized that a current pulse propagating in a less conductive current channel is attenuated faster and doesn't exhibit

detectable reflection signatures. *Nag and Rakov* [2010a and 2010b] proposed the bouncing wave mechanism for the generation of the secondary peaks in the waveforms of the CIDs. The current pulse is injected at one end of a relatively short conductive channel, is reflected successively multiple times, until it is absorbed or attenuated. The schematic representation of the bouncing wave mechanism of a CID with the channel length Δh = 100 m and the propagation speed $v = 2 \cdot 10^8$ m/s is plotted in Figure 17.

Nag and Rakov [2010a] used a transmission line model with the impedance mismatch at the ends of the channel for their modeling of the vertical channel of the CIDs. They assumed that the line is uniform and that there are no losses along the line. All losses are included in the reflection coefficients at the ends of the line. The effective current reflection coefficients are assumed to be constant. The current at any place in the channel can be expressed as a sum of upward and downward propagating current waves. The sum of upward propagating current waves can be written as

$$i_u(h_1, t) = \sum_{n=1,3,5,\ldots}^{\infty} \rho_t^{\frac{n-1}{2}} \rho_b^{\frac{n-1}{2}} i_0 \left(h_1, t - \frac{(n-1)\,\Delta h}{v}\right), \qquad (6)$$

and for the sum of the downward propagating current waves we have

$$i_d(h_2, t) = \sum_{n=2,4,6,\ldots}^{\infty} \rho_t^{\frac{n}{2}} \rho_b^{\frac{n-1}{2}} i_0 \left(h_2, t - \frac{(n-1)\,\Delta h}{v}\right), \qquad (7)$$

where i_0 is the incident current, Δh is the channel length, v is the current wave speed, ρ_t and ρ_b are effective current reflection coefficients at the top and at the bottom of the channel. The length of the current channel can be therefore deduced from the period of the oscillations.

3. AIMS OF THE THESIS

The aim of this doctoral thesis is to analyze electromagnetic signals radiated by in-cloud processes and consequently to contribute to the understanding of charge distribution in thunderclouds that is directly linked to lightning initiation. The electromagnetic manifestations of particular lightning processes need to be investigated in detail. Special attention should be paid to the electromagnetic pulses generated by the in-cloud currents and to the comparison of obtained results with results of previously published studies. The specific questions to be answered by this thesis work are as follows:

(1) What are the properties of trains of regular unipolar microsecond-scale electromagnetic pulses produced by intra-cloud lightning discharges between the return strokes? What is the generation mechanism of these pulse trains?

(2) What are the typical characteristics of the pulse sequences occurring prior to the first return stroke?

(3) What are the fine properties of the dominant peaks of the return strokes? Can we use measurements of these properties as a tool for estimation of the stroke multiplicity?

(4) Is there any link between a bouncing wave type discharge and other lightning phenomena?

4. DATA

4.1 Instrumentation

For our measurements we use a magnetic-field antenna coupled with a ground-based version of a broadband high-frequency analyzer IME-HF (Instrument Mesure Electrique – Haute Frequence) which is being developed in the Institute of Atmospheric Physics for the TARANIS spacecraft. The TARANIS mission (Tool for the Analysis of Radiations from lightNIng and Sprites) is a French microsatellite mission, which will carry the unique set of instruments dedicated for observing of transient luminous events and terrestrial gamma ray flashes from space. The satellite is scheduled to be launched in the end of 2015. The description of the payload, of the orbit and of the scientific aim of the mission will be given in section 4.1.1.

The design of the instrument which is dedicated for the measurements in space is specific in terms of the choice of components, materials, and also manufacturing processes. The reliability and availability of the instrument has to be guaranteed over the lifetime of the mission. This leads to the usage of specific parts, materials and processes which are space qualified. In case of the usage of non qualified or new parts, processes or materials, additional tests have to be performed. The instrument also has to be also compliant with the space environment specifications. The vibrations and shocks during the launch, the vacuum with wide temperature ranges and the space radiation predicted for the orbit need to be considered. Low power consumption is also one of the crucial parameters when selecting the components.

Verification of the ability of the instrument to fulfill the scientific specification of a space mission is complicated procedure which is difficult to perform in laboratory conditions. As our analyzer is designed to measure electromagnetic manifestations of lightning discharges in space, we can take advantage of the similarity of these manifestations in space and on the ground and use the nature itself as a variable, unpredictable and gorgeous laboratory. The design of the analyzer, the results of the prototype tests, and the data structure are described in sections 4.1.2, 4.1.3 and 4.1.4. The design and the results of the calibration of the antennas are presented in sections 4.1.5 and 5.7.1. Both our ground based receiving stations are introduced in section 4.1.6.

4.1.1 The TARANIS mission

TARANIS is a scientific micro-satellite of the French space agency CNES. Its launch on a Sun synchronous quasi-polar orbit at 700 km altitude is planned for the end of 2015. The anticipated lifetime will be 2-3 years. The general objective of the TARANIS mission is to study magnetosphere-ionosphere-atmosphere coupling via transient processes. Radiation from lightning and optical phenomena TLE (Transient Luminous Events) (blue jets, red sprites, halos, elves) will be observed above stormy regions at altitudes between 20 and 100 km. The detection and the study of the gamma-ray and X-ray flashes called TGFs (Terrestrial Gamma Flashes), are also part of the mission objectives. TARANIS will carry a unique complex payload of seven scientific instruments detecting electromagnetic radiation from very low frequencies up to 37 MHz, optical radiation, gamma rays and X rays, and energetic electrons.

Four main objectives of TARANIS mission are:
- to estimate the rate of occurrence of TLEs, TGFs and their associated emissions and to highlight triggering factors
- to characterize TGFs and runaway electrons that are accelerated upwards from the atmosphere to the magnetosphere
- to identify the effects of TLEs and TGFs on coupling between the ionosphere and the magnetosphere
- to specify the role of precipitated electrons in coupling between the magnetosphere and the atmosphere

The system is designed to observe stormy regions and to detect TLEs and TGFs as the satellite travels above the phenomena at around 700 km of altitude. A trigger is then sent to each of the payload instruments so that they can acquire the maximum amount of data during the event. The capacity of the onboard storage memory and telemetry system will make possible to accumulate a large amount of data for each event and for a large number of events per day. Statistical analysis and correlations of different parameters will be therefore possible. *(http://smsc.cnes.fr/TARANIS)*

The payload includes the following instruments (Figs. 18 and 19):

MCP, optical cameras and photometers

XGRE, gamma-rays detector

IDEE, energetic electron detector (70 KeV - 4 MeV)

IME-BF, analyzer of electric and magnetic fields and ion thermal plasma (0 - 3 MHz)

IMM, three-axis search coil magnetometer

SI, Ion probe

IME-HF, HF electric field analyzer (100 kHz - 36 MHz)

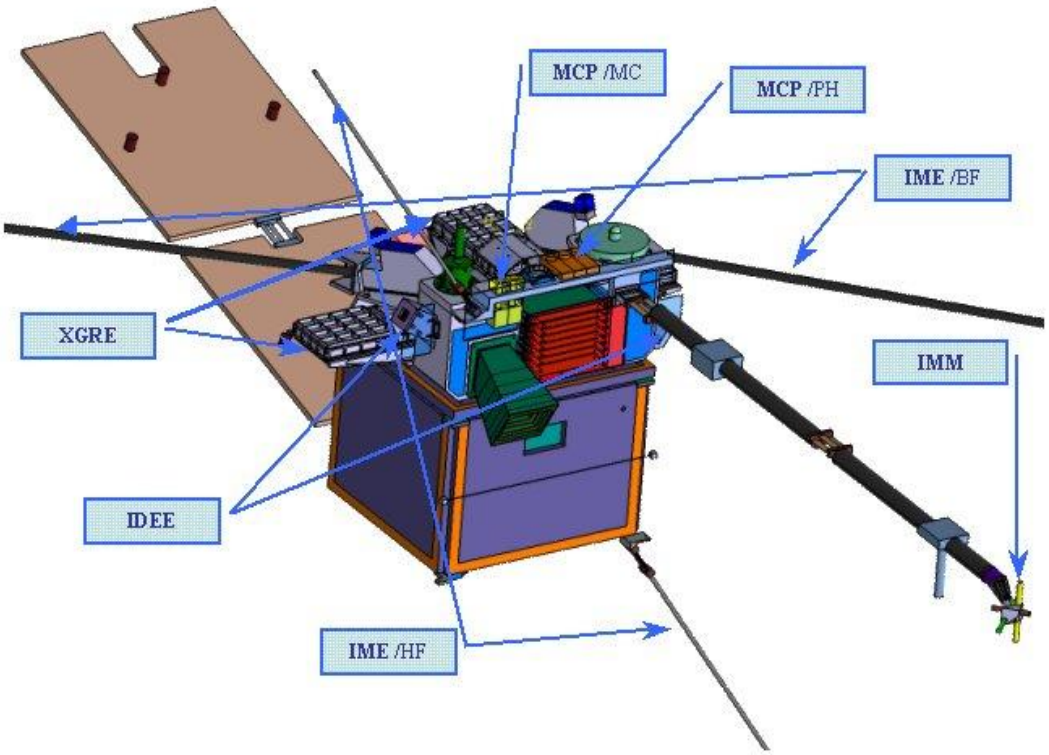

Fig. 18 Scientific payload of the TARANIS mission (the sensors related to particular instruments are marked by blue arrows)

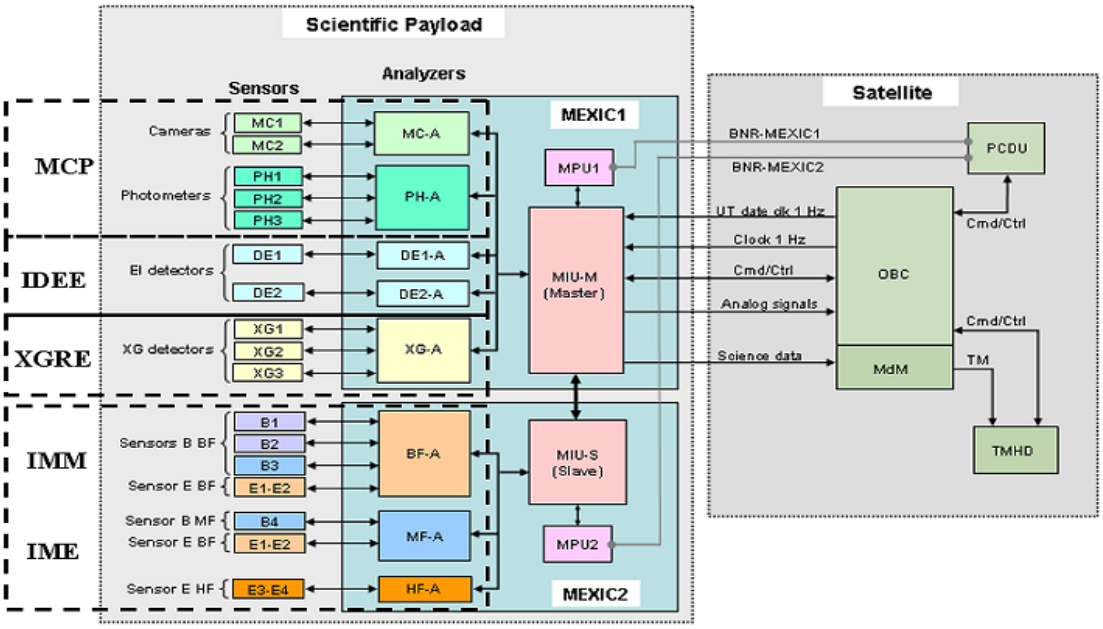

Fig. 19 Block diagram showing the connection of the scientific payload and the satellite

The main goals of the IME-HF analyzer can be summarized in five points:

- Identification of possible wave signatures associated with transient luminous phenomena during storms
- Characterization of lightning flashes from their HF electromagnetic signatures
- Identification of possible HF electromagnetic or/and electrostatic signatures of precipitated and accelerated particles
- Determination of characteristic frequencies of the medium using natural wave properties
- Global mapping of the natural and artificial waves in the HF frequency range, with an emphasis on the transient events *(http://babeta.ufa.cas.cz/TARANIS)*

4.1.2 Broadband analyzer design

The block diagram of the analyzer is shown in Figure 20 and the assembled analyzer is shown in Figure 21. The schematic drawings and the PCB design of the analyzer are shown in Appendix B1. The analog part of the analyzer includes two fully differential amplifiers AD8132, two anti-aliasing filters and a set of twelve band-pass filters with amplifiers AD8014 and RMS detectors AD8310. The signals from these detectors are used as input data for a flexible event detection algorithm, which will be described later.

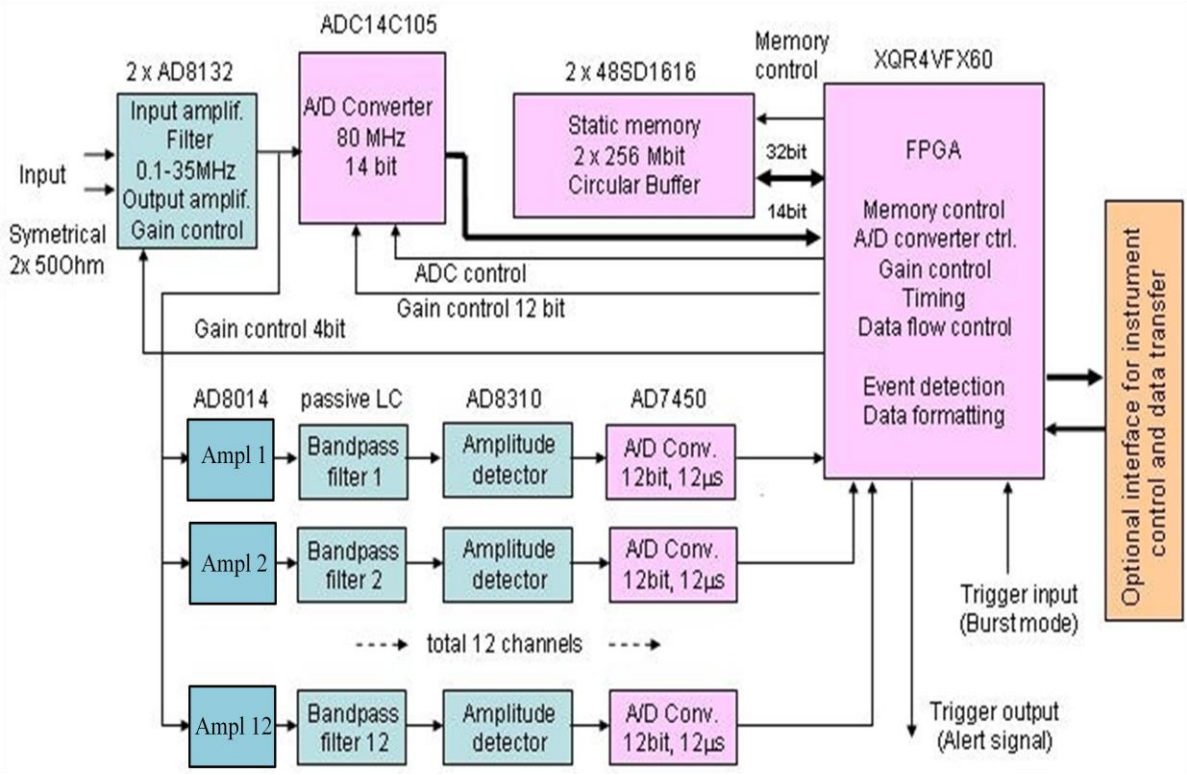

Fig. 20 Block diagram of the broadband analyzer IME-HF

Two antialiasing filters and 12 band-pass filters are placed on separate PCBs. These PCBs, each of them containing one filter, are mounted on the main PCB and placed in the shielded box as shown in Figure 22. Two antialiasing filters are placed in a separate part of the shielded box. The antialiasing filter is a passive LC low-pass filter of 11-th order; the cut-off frequency is set to 36 MHz. Each band-pass filter is a serial combination of two (low-pass and high-pass) passive LC filters of 9-th order. The central frequencies of filters are as follows (in MHz): 1.5, 4.5, 7.5, 10.5, 13.5, 16.5, 19.5, 22.5, 25.5, 28.5, 31.5, 34.5 . The attenuations at the central frequency of a neighboring channel are about ~15 dB. The gains of both AD8132 amplifiers are separately set by switching the feedback resistors with the dual SPDT analog switches DG636 controlled by the FPGA. The digital part of the analyzer includes radiation hardened Virtex4 FPGA (XQR4VFX60), two radiation hardened 16 Mbit configuration PROMs (XQR17V16) and two radiation hardened 256 Mbit SDRAMs (48SD1616). The radiation hardened components were replaced by corresponding parts in a lower quality grades (FPGA - XC4VFX60, PROM - XCF16PVOG48, SDRAM - MT48LC32M16A2) in the ground-based prototype. The main clock frequency of

80 MHz is generated by a custom cut crystal oscillator HXO6106 optimized for the anticipated working temperature range between 30 and 40 °C. The 80 MHz signal from the oscillator is conditioned by three single buffer gates SN74LVC1G125 and used for both FPGA and ADC. The signal is digitized by 14-bit ADC (ADC14C105) at a frequency of 80 MHz. The possibility to select 12 bits from the total 14 bits works as a digital gain control. The parts of the waveforms are recorded in the circular buffer in the SDRAMs. The twelve RMS voltages obtained from the filter bank paths are digitized by 12-bit ADCs (AD7540). The same ADCs are used for the digitizing of voltages obtained from three temperature sensors. The analyzed frequency band goes from 5 kHz to 37 MHz.

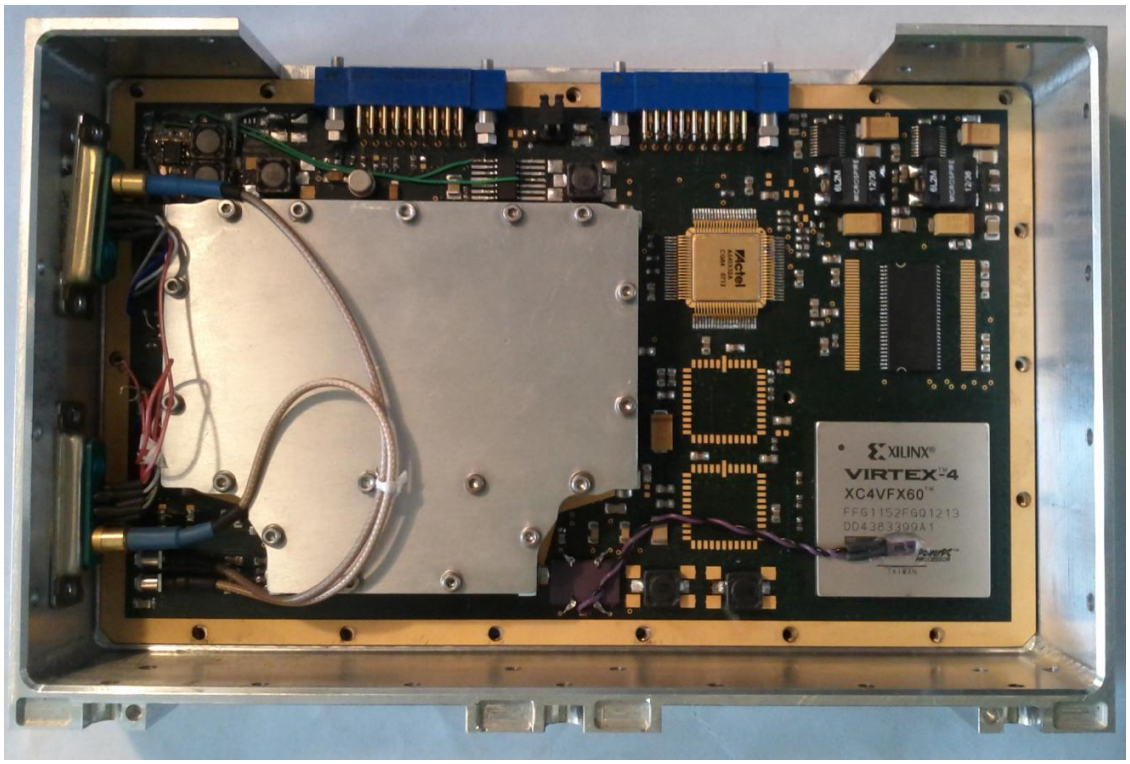

Fig. 21 The assembled analyzer in its frame

The latch-up protection of IME-HF instrument was implemented in order to minimize the influence of SEE (Single Event Effects caused by the radiation) on the IME-HF and to prevent possible damages. For the latch-up protection reasons the main power supply line 3.3V is divided into analog and digital power supply lines. Both lines are separately protected against the over-current (1.2 A) using the P-channel switches with thermal shutdown (MAX890). Other digital power supply voltages (1.2 V, 2.5 V)

are produced from the main power supply voltage 3.3 V by switching convertors (TPS54312, TPS54315). The negative power supply voltage -3.3 V is produced by three 60 mA charge pump voltage inverters TPS60403 connected in parallel to have a sufficient power for feeding the analog part of the analyzer. The analyzer controls the power supply +5 V and -5 V for the preamplifiers. This power supply voltage is switched on/off separately for each preamplifier. The negative power supply voltage - 5 V for the preamplifiers is made by two 60mA charge pump voltage inverters TPS60403. Two P-channel switches with thermal shutdown (MAX890) are used for the switch on/off of the 5 V power lines. This arrangement secures the proper switching-on sequence of the power supply voltages and at the same time protect the preamplifiers against the over-current. In the case of malfunction of one of the preamplifiers, this arrangement can also be used to separately switch off its power supply, and thus to conserve a limited performance of the IME -HF instrument.

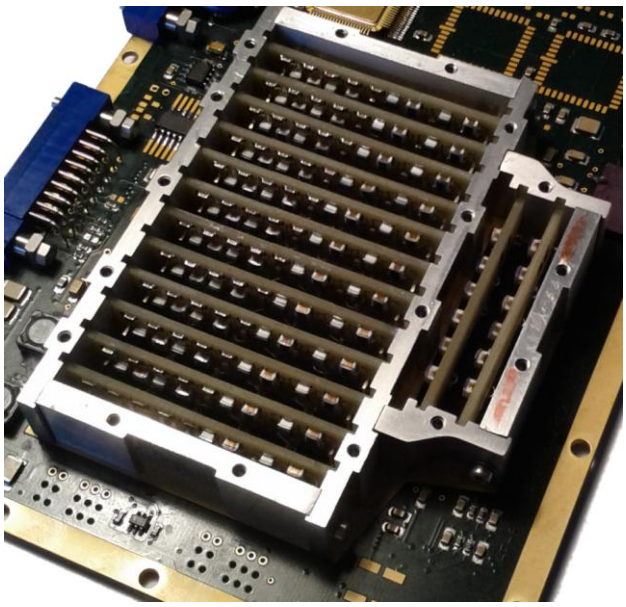

Fig. 22 The accommodation of the PCBs of individual filters in the shielding box

Two types of selection of the interesting parts of the recorded waveform are implemented in the design of the analyzer. The first detection algorithm for transient signals based on filter bank channels is dedicated for the detection of interesting events during the flight. The second detection algorithm for transient signals is based on the waveform and is used for the observation on the ground. The rank for the first detection

algorithm is calculated as

$$R = \sum_i w_i \ \mathrm{nneg}(m_i - a_i)$$

where the sum goes over the 12 filter bank channels (RMS values), i =1…12. R is calculated using weights w_i, running average amplitudes a_i (calculated onboard using a parameter M, see below), and the maximum amplitudes m_i (calculated onboard using a parameter N, see below). The parameters M, N, and weights w_i are preset. The function nneg(x) is defined as nneg(x) $= x$ for $x > 0$, and nneg(x) = 0 for $x \leq 0$. The running average amplitudes a_i are calculated for each channel i separately as

$$a_i = 1/M \sum_j f_{ij}$$

where j is an index to a continuously measured series of past (~12 μs) samples for the given channel i. j runs from $I - M + 1$ to I. After starting the detection algorithm, I starts by a value of $M/8$ samples, then it increments by $M/8$ samples. The running averages a_i are always calculated from M samples. The maximum amplitudes m_i are always found in the series of N samples (usually $N \ll M$, the default value is M = 220 corresponding to a time interval of ~12.583 s, and N =16 corresponding to ~192 μs),

$$m_i = \max_j(f_{ij})$$

where j runs from $k - N + 1$ to k. After starting the algorithm, k starts by a value of N samples, and then it increments by $N/2$ samples. The successive intervals over which the maxima m_i are found, are therefore always overlaid by 50%, with the step between these intervals being $N/2$ samples. This is also the step of updates of R which defines the time resolution of the detection algorithm. If $N \leq M/8$ then the first value of R is calculated ~12 μs * $M/8$ after starting the algorithm else the first value of R is calculated ~12 μs * N after starting the algorithm. The value of R then continues to be updated with a regular time step of ~12 μs * $N/2$, always using the most recent set of a_i values. This update is done 24 cycles of the 10 MHz clock (~2.4 μs) after the last filter bank sample, over which the rank R is calculated. To generate the event detection alert, we use a criterion of having R larger than a predefined threshold P. The alert is then

generated immediately when *R* is updated to a value exceeding *P*.

The alternative detection algorithm based on the waveform is based on a simplified rank

$$R = w_i \,\mathrm{nneg}(m_i - a_i)$$

$$a_i = 1/M \sum_j f_j$$

$$m_i = \max_j(f_j)$$

where the maximum *m* is found as previously over a series of *N* samples, and *j* is an index to a continuously measured series of past (~12 μs) samples for a single time series *f*. This time series is obtained from the measured ~80 MHz waveform. From 960 consecutive 12-bit samples g_k absolute values (11 bits) are calculated, summed up into one new (~12 μs, 21 bits) sample, left-shifted by preset parameter (Trig_WF-1) and from 12 most significant bits we obtain f_j

$$f_j = 2^{(\mathrm{Trig\_WF}-1)} \sum_{k=1}^{960} \mathrm{abs}\,(g_k)$$

The parameters *M, N* are preset; the function nneg(*x*) is defined as previously, the function abs(x) is defined abs(x) = -x for x < 0, and abs(x) = x for x ≥ 0. Otherwise the detection algorithm works as in the previous case.

4.1.3 Results of the prototype tests

The performance of the prototype was tested in the thermal chamber in the wide temperature range from -20°C to +75°C. The noise of the analyzer itself, the power consumption, the harmonic distortion and the frequency response of the analyzer were measured and analyzed. Based on the results we can state that the performance of the analyzer with exception of the power consumption doesn't depend on the temperature. Following set of graphs (Figs. 23 – 28) shows the main results of the tests performed at the room temperature. Comment on Figure 28: the analyzer was switched on at ambient temperature +75°C and switched off when ambient temperature reached -20°C. Ambient temperature was thermostatically controlled. The internal temperature probe

was attached to the FPGA.

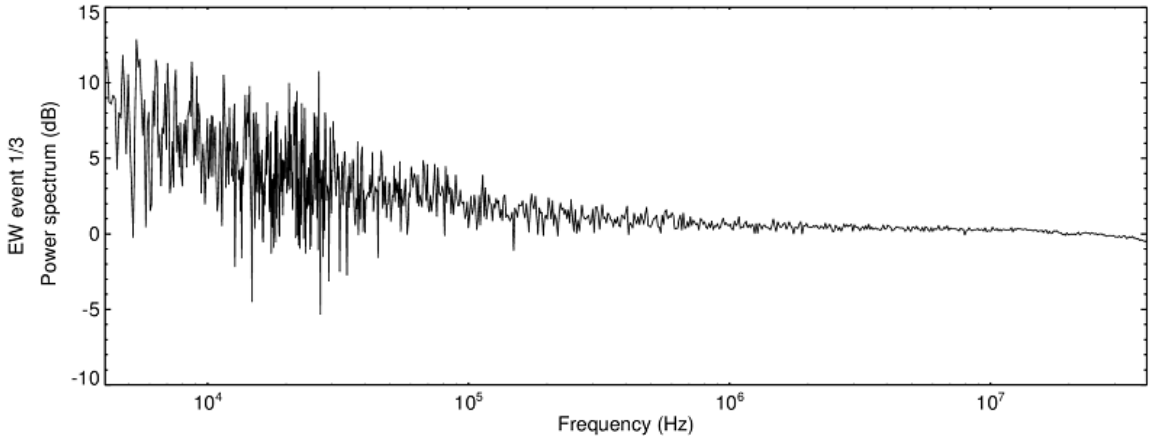

Fig. 23 Noise vs. frequency for unity gain (antenna inputs terminated by 50 Ω terminators)

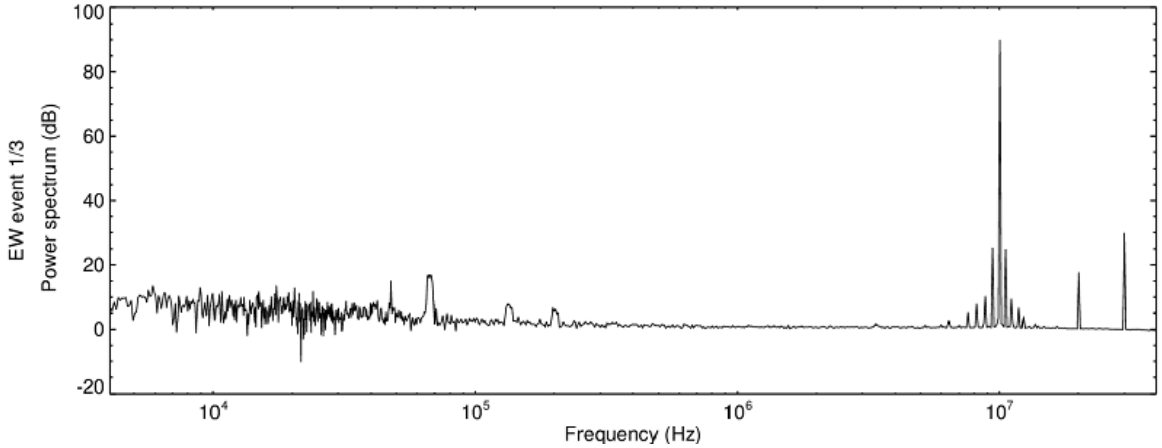

Fig. 24 Harmonic distortion at 10 MHz, differential signal 2.05 V_{pp} to each antenna input

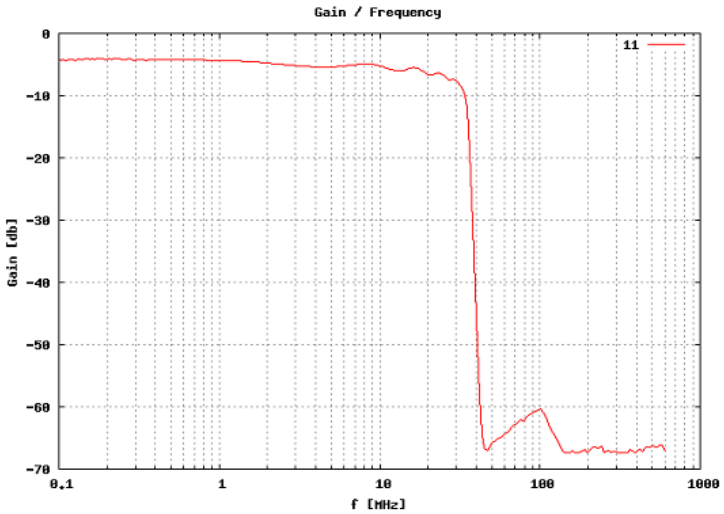

Fig. 25 Gain vs. frequency from 100 kHz to 600 MHz, single input signal 1.12 V_{pp}

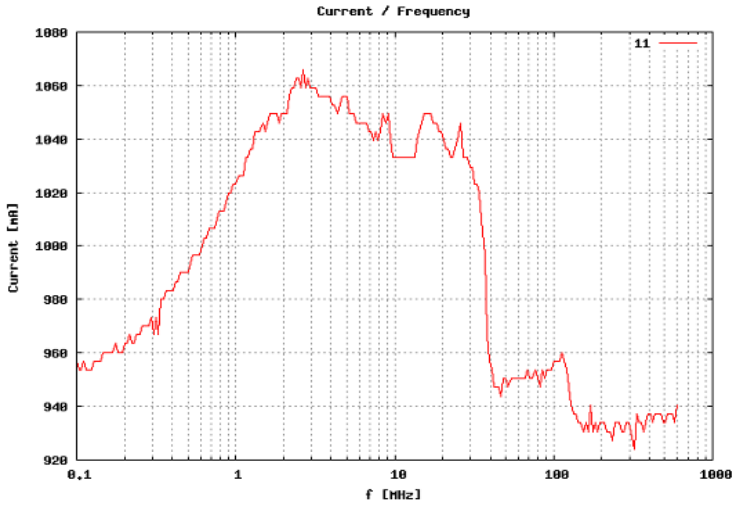

Fig. 26 Supply current vs. frequency from 100 kHz to 600 MHz, single input signal 1.12 V_{pp}

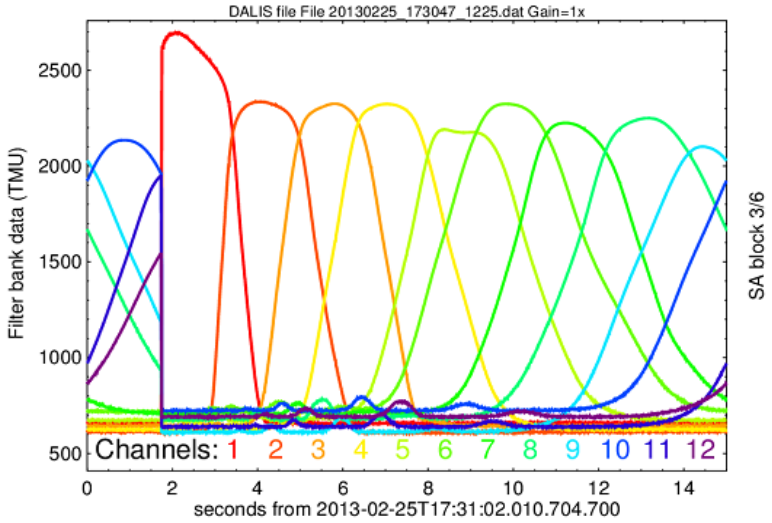

Fig. 27 Filter bank test, 2.05 Vpp differential signal, frequency sweep 1 kHz to 30 MHz, 15s sweep period

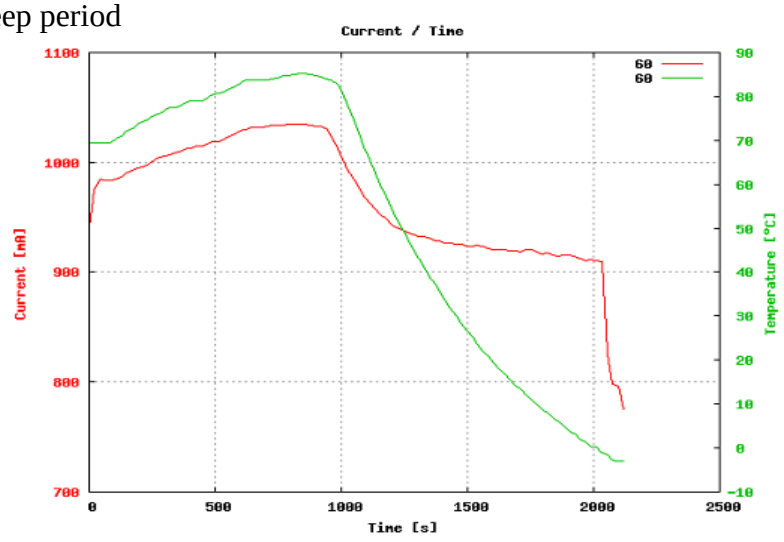

Fig. 28 Supply current vs. temperature

4.1.4 Data structure

The data structure of the analyzer depends on the working mode. The analyzer has several working modes:

a) Waiting modes - Standby mode - analyzer is ON and initialized but doesn't acquire any data
b) Test mode - used during test activities
c) Operational modes - Science mode

There are two working modes (Survey mode and Event mode) and two working configurations and in the Science Mode. For those two configurations there are two types of scientific data:
- Averaged values of the 12 signals issued from the filter bank (FB) sampled at 12μs
- Waveform sampled at 80MHz on 14 bits but only 12 bits are recorded. The selection of 12 bits is adjustable.

There are 3 different types of data (SA, SL and SR) in the Survey mode. Each telemetry block contains 2 times 18 packets.

SA: averaged signal from the filter bank on continuous mode. 615 samples are averaged, therefore, the length of time interval over which is averaged is 12 μs*615 =7.38 ms.

SR: Regular snapshots of short waveform. Each packet contains one snapshot. 18 snapshots, forming one SR package, are regularly distributed inside the 15.01092 s interval of one block. Thus, the time interval between the subsequent snapshots of waveform is 15.01092/18=0.83394 s. 1360 samples at 12 bit representation can fit into one block of 2040 bytes, thus, the length of one snapshot is 1360/80 MHz=17 μs. The frequency resolution is ~1/17 μs = 58.824 kHz. This type of data is suitable for monitoring the plasma frequency.

SL: longer waveform that fits into 18 packets. The time interval is selected by a detection algorithm. Similarly to SR, in each block 1360 samples are transmitted. The length of the waveform is 18*1360/ 80 MHz=306 μs at the 12 bit representation.

The storage of event mode data **EW** is initiated by an alert signal. The recorded data can be shifted in time with respect to the beginning of the alert signal. The pre-trigger time is adjustable. Each waveform sample has a length of 12 bits represented as

a signed integer number in the two's complement representation. 1360 samples are transmitted in each TARANIS packet: 1360 values *12bits/8bits = 2040 bytes are used. The EW data are sampled 8 times per one 10MHz clock which corresponds to ~80 MHz sampling rate. The EW data are divided into pages in the internal memory. One EW page takes 4 439 040 bits, containing 277 440 waveform samples (measured during 277 440 / 8 = 34 680 cycles of the 10MHz counter, ~3.468 ms), as well as time stamps. Each page is then always stored into 277440 / 1360 = 204 packets. The EW mode builds up one, two or three events, each of them containing a predefined number of pages according to the IME-HF configuration. The number of pages in each EW event (as well as in each EB event) is adjustable. The size of the circular buffer for the EW data expressed as a number of EW pages is also adjustable. The maximum number of alerts that are processed is 24. The triggering event signal can be received from an internal procedure based on the IME-HF event detection algorithm or as an external event signal generated from the satellite. Additional possibility for initiation of a triggering signal to record an EW event is its start at a predefined time, as time triggered. The time assignment for the ground based measurements is done by a GPS receiver connected to the analyzer.

4.1.5 A simple magnetic loop antenna

We were using a magnetic loop for our measurement of magnetic field. The antenna loop is formed by a single loop of a 50-Ω coaxial cable with a loop diameter of 1m (a similar antenna system was used by *Krider and Noggle* [1974]). The shape of the antenna is shown in Figure 29a.

We used a small circular transmitting antenna for the measurement of the frequency response of the receiving antenna. The shape of the transmitting antenna is shown in Figure 29b,c. The diameter of the transmitting antenna is 10 cm; the inductance is ~ 40 nH. The current flowing through the antenna wire and the serial resistance 51 Ω determines the amplitude of the excited magnetic field, which is almost independent on the frequency.

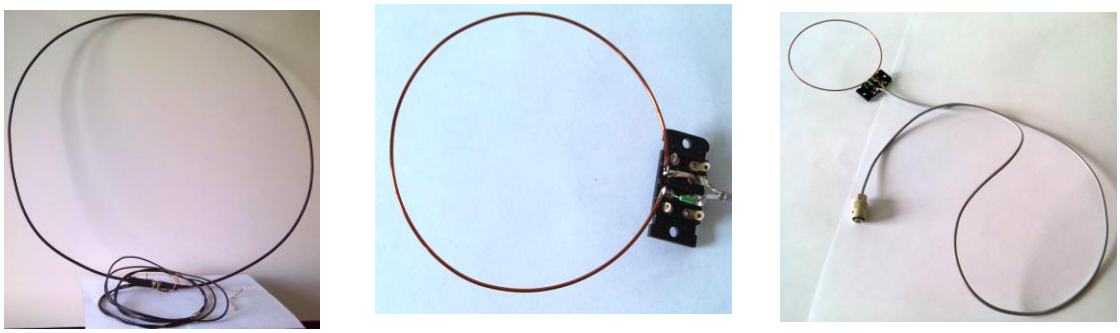

(a) **(b)** **(c)**

Fig. 29 (a) Antenna loop (type CABLE), (b, c) Transmitting antenna for the measurement of the frequency response of receiving antennas

First, we calculate the capacitance, the inductance and the resonant frequency of the simple passive receiving antenna (referred to as "type CABLE" in the following text). A circular loop of a 50-Ω coaxial cable with a radius r = 0.5 m is completed by connecting cables; each of them has a length of 0.75 m. The capacitance of the coaxial cable is 100 pF /m, thus the capacitance C of the antenna is ~ 300 pF. The inductance of the cable L_C can be calculated from the impedance of the cable $Z = 50\,\Omega = \sqrt{L_C/C}$, thus the inductance of the cable is 0.25 μH/m. We use the formula (8) for the calculation of the inductance of the loop L_L,

$$L_L = \mu_0\, r \left(\ln\frac{8r}{a}\right) - \frac{7}{4} \qquad (8)$$

where r is the radius of the antenna and a is the length of the cable. The inductance of the loop is 3.8 μH. The formula (9) is used for the calculation of the resonant frequency of the antenna.

$$f_r = \frac{1}{2\pi\sqrt{(L_C + L_L)C/2}} \qquad (9)$$

The calculated resonant frequency for the antenna type CABLE is 5.6 MHz. Calculated parameters are used for the simulation of the antenna by a model with distributed

parameters shown in Figure 30. We use the free online tool CircuitLab for the simulation of the behaviour of the antenna. (*www.circuitlab.com*)

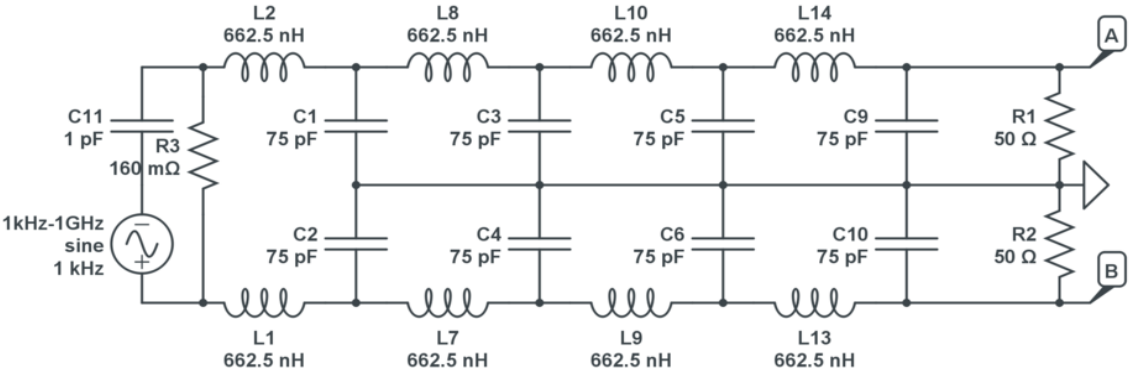

Fig. 30 Model of the antenna loop (type CABLE)

Now we can compare the frequency response of the model with the measurement of the frequency response of the real antenna loop (Figs. 31 and 32). We found that the properties of the model correspond quite well to the properties of the loop. The antenna works well under its resonant frequency; above 6 MHz it starts to integrate the signal. The shapes of very fast changes of magnetic field can be therefore partly distorted.

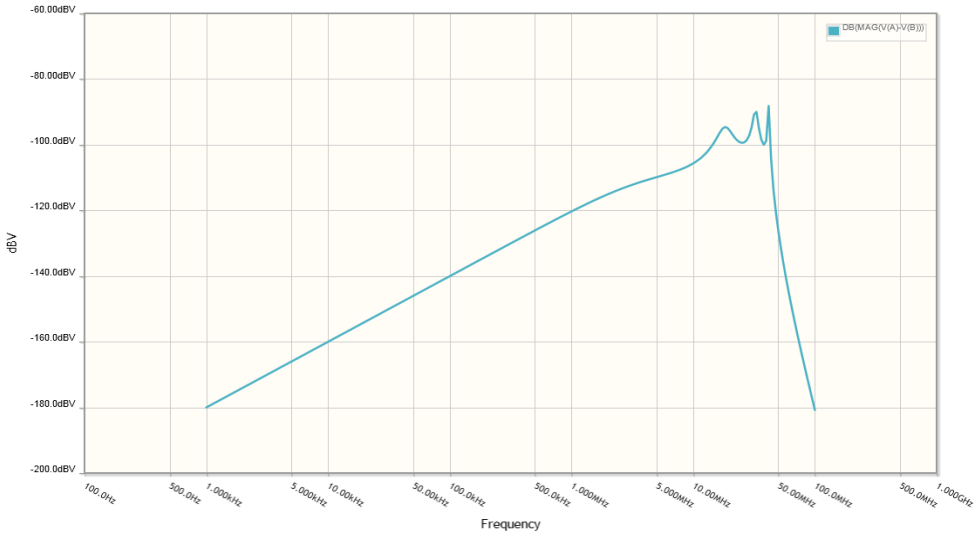

Fig. 31 The frequency response of the antenna model (type CABLE) with distributed parameters

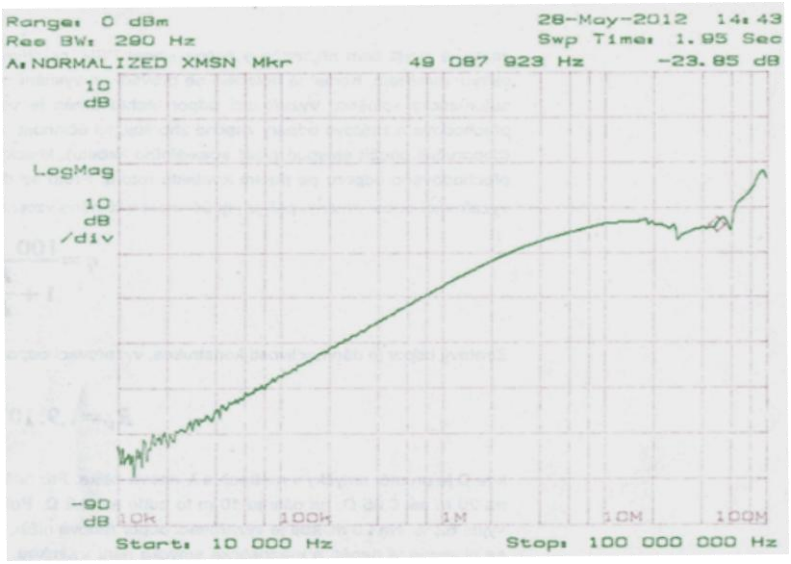

Fig. 32 The frequency response of the antenna loop (type CABLE)

4.1.6 Locations of the receiving stations

We started to measure the signals generated by lightning discharges in the laboratory of the Institute of Atmospheric Physics in Prague, Czech Republic (320m, 50.0411N, 14.4774E) in 2011. We also continuously monitor the thunderstorm activity in collaboration with LSBB (Laboratoire Souterrain a Bas-Bruit) in Rustrel, Southern France since 2012. We placed the analyzer together with the antenna system in a favorable electromagnetic environment on the summit of La Grande Montagne (1028 m, 43.9410N, 5.4836E), Plateau d'Albion. Thus we have the opportunity to compare the manifestation of different lightning phenomena in the inland of the Central Europe and in the higher altitude close to the Mediterranean. The dependency of the properties of lightning discharges on the geographical and climatic conditions was reported many times in the lightning literature [C*orray et al.,* 1994*; Kigitawa et al.,* 1994*; Gomes et al.,* 1998*; Sharme et al.,* 2008*, and others*]. However, measurements of signals radiated by lightning discharges weren't yet performed in locations having the same or similar climatic conditions as Prague or Rustrel. Our measurements can therefore contribute to a better understanding of properties of lightning discharges observed from different altitudes and geographical positions.

4.2 Data analysis method

We described the design of the analyzer in details in sections 3.1.2 and 3.1.3. The data structure is described in section 3.1.4. The properties of antenna system are presented in section 3.1.5. We performed the absolute calibration of the antenna in order to properly interpret the measured data. We used a Helmholtz pair of two identical circular magnetic coils placed symmetrically one on each side of the area, where the measured antenna was placed. Thus we obtained a quite uniform magnetic field suitable for the absolute calibration of the antennas. We found that we can approximate the magnetic-field time derivative *dB/dt* in the direction perpendicular to the loop by quotient of the voltage induced in the antenna loop and the loop area. Then we numerically integrated the waveform records to estimate the *B* component in this direction. The integrated noise of the analyzer is about 0.14 nT in the frequency range from 1 MHz to 37 MHz.

We were looking for the signatures of different lightning phenomena in the integrated waveform records. The strongest recorded signals were radiated by the return strokes and were compared them with the return stroke data obtained from CELDN (Central European Lightning Detection Network) and from METEORAGE (French meteorological service). Both services provide us with the information about the time, the location, the peak current and the type of the particular return stroke. Having the information about the timing of return strokes, we were able to concentrate on the time interval before the first return stroke or on the time interval between the strokes. The results of an analysis of the properties of different signals radiated by lightning flashes are presented in section 5.

5. EXPERIMENTAL RESULTS

5.1 Properties of unipolar magnetic field inter-stroke pulse trains

In this section we analyze properties of the trains of regular unipolar microsecond-scale magnetic-field pulses produced by intra-cloud lightning phenomena in continental conditions (Prague, Czech Republic). A review of the literature related to the inter-stroke pulse trains was given in section 2.6.8. We use a broad-band analyzer with a sampling interval of 12.5 ns, which we described in section 4.1. Our time resolution is by more than one order of magnitude better than the limit of measuring systems used in studies of *Krider* [1975] and *Rakov* [1996]. Our time resolution is also four times better than the resolution of *Davis* [1999] and the length of our recordings is about three orders of magnitude larger than in his data. Our measurements are therefore suitable for a clear identification of individual microsecond-scale pulses in the trains and, at the same time, for long recordings of multiple trains in a sequence. We estimated the time intervals between the trains, their durations, the number of pulses in the individual trains, and the inter-pulse time intervals.

5.1.1 Measurements

Our original data set consisted of 1409 regular pulses in 33 trains recorded during two thunderstorms in summer 2011 in Prague, Czech Republic. We do not have reliable information about the distances to the lightning phenomena that generated the recorded pulses. However, based on the most distant return strokes recorded by the Central European Lightning Detection Network (P. Novák, private communication, 2011), and observed during the same campaign we can estimate that the distances to the sources of the observed high-frequency signals were probably less than 20 km.

The amplitudes of all the pulses and the times of their peak values were estimated from the integrated *B* waveforms. To record a pulse we have chosen a threshold of 1 nT for the peak amplitude. This threshold is several times larger than the noise level of the analyzer. Each individual pulse is considered to be unipolar, if the

immediately following overshoot of the opposite polarity doesn't exceed one half of the peak amplitude of the original pulse. A group of pulses is considered to form an individual train when the time interval between the last pulse of a train and the first pulse of the next train exceeds 80 μs. This threshold has been chosen to be more than one order of magnitude higher than the expected inter-pulse interval (several microseconds). Examples of waveforms of individual pulses and trains with positive and negative pulse polarities are shown in Fig. 33a and Fig. 33b, respectively.

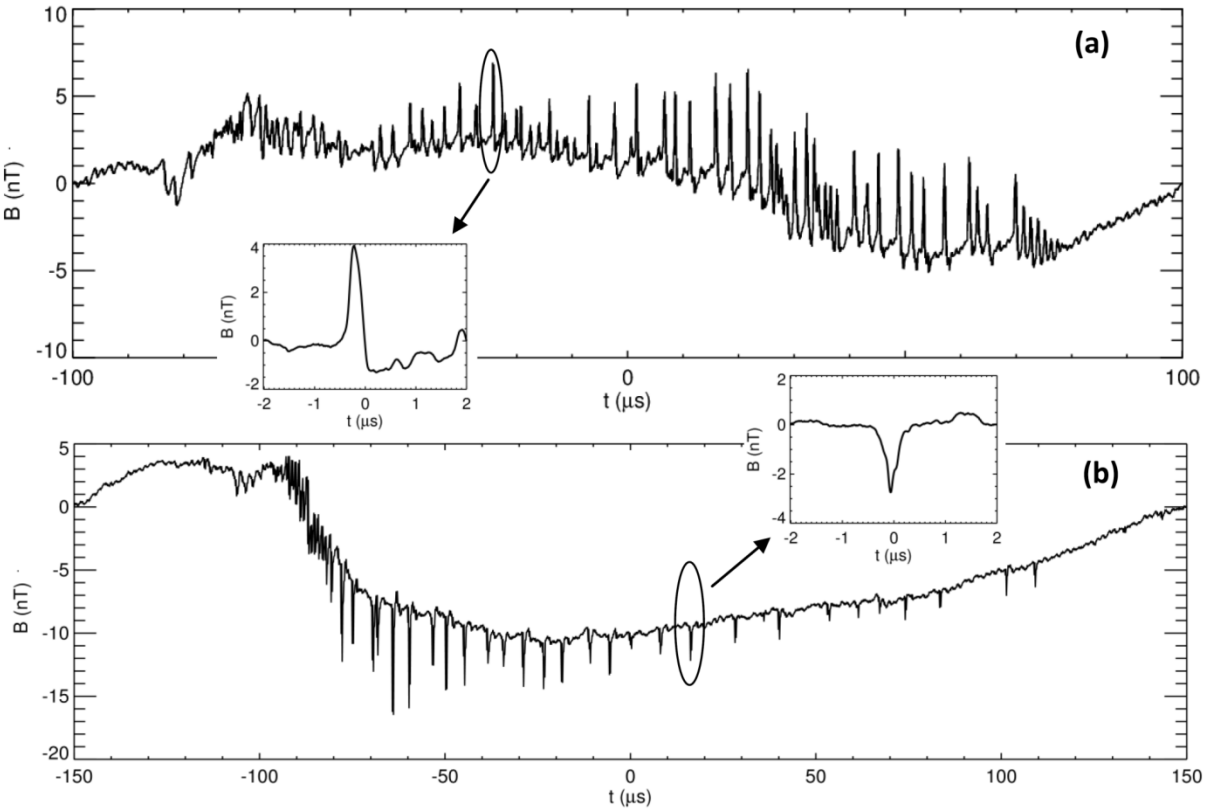

Fig. 33 Examples of the trains with (a) positive and (b) negative pulse polarities. Detailed examples of individual pulses are shown in the inlets.

Out of the original data set of 33 trains, we have observed 2 isolated trains, each in a separate 120-ms long recording, and 31 trains grouped in three separate sequences (with respectively 12, 13 and 6 trains). We have measured the time interval between the beginnings (times of the first pulses) of the neighboring trains in these sequences. The histogram of these time intervals is plotted in Fig. 34a. The distribution clearly has a "heavy tail" and is far from being normal. The geometrical average of the obtained values is 5.6 ms. The last train in the shortest sequence has a significantly longer time delay (68 ms).

As the next step of our analysis, all trains which contained bipolar pulses, and trains with both pulse polarities have been excluded from our statistics. Out of the 25 remaining trains, 8 trains contain pulses with positive polarities, and 17 trains have negative pulse polarities, corresponding to relations between directions of distant source currents and their unknown positions with respect to the orientation and position of the antenna. This analyzed data set contains the total number of 967 individual pulses. Duration of the individual trains varies from 48 μs to 448 μs with a mean value of 176 μs (Fig. 34b). This is more than 30 times shorter than the typical time intervals between the trains. The total number of pulses in a train varies from 12 to 109 with a mean value of 39 (Fig. 34c). The time interval between neighboring pulses within the trains ranges between 0.7 μs and 28 μs with a mean value of 4.7 μs (Fig. 34d). The ratio between the smallest and the largest amplitude of pulses in each individual train varies from 0.1 to 0.4 with a mean value of about 0.2 (Fig. 34e). The pulse amplitudes follow a wide distribution (Fig. 34f) but on average they reach approximately 0.5 of their maximum in a given train.

5.1.2 Discussion

In this study we attempt to improve our experimental knowledge of the properties of the trains of unipolar pulses. The resolution of our instrumentation is about by more than one order of magnitude better than the limit of a measuring systems used in previously published studies [*Krider et al.,* 1975 *and Rakov et al.,* 1996], allowing us to fully resolve individual pulses and to measure also long sequences of pulse trains.

To discuss our results, we can start by comparing the interval between the trains in our data set with the time properties of the K-change and M-component sequences reported by *Thottappillil et al.* [1990]. According to their measurements of close lightning flashes the geometric-mean interval between neighboring K-changes or M-components respectively were 12.5 ms or 2.1 ms. The geometric-mean time interval between neighboring trains in our records is about 6 ms, which is two times shorter than the time interval between K-changes and three times longer than the time interval between M-components reported by *Thottappillil et al.* [1990]. However, our histogram of time intervals between neighboring trains (Fig. 34a) is much closer to the histogram

for K-change intervals plotted by *Thottappillil et al.* [1990] and shown in Figure 13.

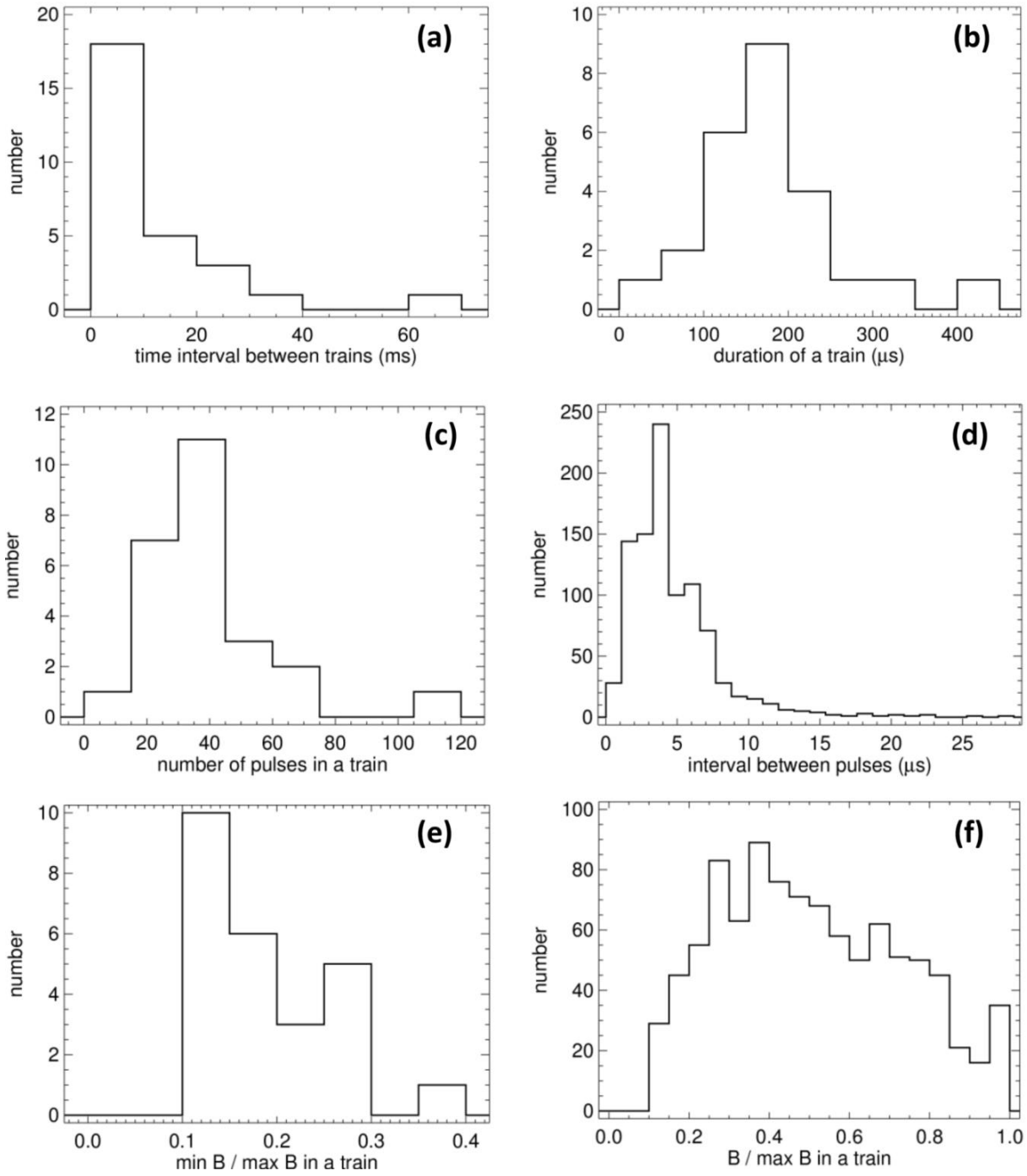

Fig. 34 (a)Time interval between the neighboring trains, (b) Duration of the trains, (c) Number of pulses in the trains, (d) Time interval between neighboring pulses in each train, (e) Ratio of the largest to the smallest amplitude of pulses in each individual train, (f) Pulse amplitudes normalized by their maximum in each individual train.

Shao et al. [1995] reported that K-changes are indistinguishable from dart leaders and attempted leaders in their radio-interferometric observation. They concluded

that, above the bottom of the thundercloud, these three lightning phenomena are identical. We can therefore also compare the time interval between neighboring trains in our records with the inter-step intervals of dart-stepped leaders. *Krider et al*. [1977] reported that the mean interval between dart steps was 6–8 μs, which is in a good agreement with our observations. The mean value of the inter-pulse interval in our data set is about 4 μs, which is consistent with the observations of *Krider et al.* [1975], who reported the mean value of 5.1μs for the time interval between successive pulses measured in Arizona. The histogram plotted in Fig. 34d is also very close to the histogram of *Krider et al.* [1975] shown in Figure 14.

We can therefore conclude that we have measured the same phenomenon as *Krider et al.* [1975] and *Rakov et al.* [1992, 1996] and that the observed pulse trains are most probably connected with K-changes and dart-stepped leaders. Combining the occurrence rate (50%) of K-changes in inter-stroke intervals reported by *Thottappillil et al.* [1990] with the 24% fraction of K-changes accompanied by the microsecond-scale activity [*Rakov et al.*, 1992], we obtain a relatively small probability of about 12% that a latter part of an inter-stroke interval contains K-related trains of pulses. Similar result can be obtained by combining the probability of occurrence of the dart-stepped leaders in the inter-stroke intervals [*Rakov and Uman*, 2003] with the probabilities of multiple stroke lightning.

5.2 Evolution of the pulse amplitude and of the inter-pulse interval within trains

5.2.1 Measurements

Fig. 35a and Fig. 35b respectively show an example of evolution of the inter-pulse interval and the pulse amplitude normalized by its maximum within the train from Fig. 33b. The fluctuations of obtained results are significant but the general trend is that the inter-pulse interval is increasing and the pulse amplitude is decreasing within this train. To roughly characterize the evolution of the inter-pulse intervals and normalized pulse amplitudes, we have estimated linear trends in all trains. We have calculated coefficients of a linear least-squares regression as a function of time. An example of the regression line is overplotted in figures Fig. 35a and Fig. 35b. The histograms of the growth/decay rates in the separate pulse trains are plotted in Fig. 35c and Fig. 35d, respectively, for the inter-pulse interval and the amplitude. The inter-pulse interval rises on average by 4.1 μs during the train duration, and, during the same time, the amplitude drops on average by 15% of its maximum. However, the spread of the obtained values is very large (from a decrease by 70% up to an increase by 37%) in the case of the normalized amplitudes.

Although the approximation by a linear function is very crude, it suggests that the inter-pulse interval is typically increasing in our data set. To verify this result, we have calculated the rank correlation coefficients between time and inter-pulse intervals and the corresponding probabilities of random occurrence of a positive or negative correlation. We have further selected only those trains where this probability is less than 5%, reducing the data set down to 16 trains. Out of these, 15 trains have a significantly positive correlation coefficient with an average value of 0.61, and only one train has a negative correlation coefficient of -0.51. For the normalized amplitude the situation is less clear, with 6 significantly positive and 11 significantly negative correlation coefficients (average values of 0.42, and -0.66, respectively). This analysis therefore shows that the typical evolution pattern is represented by growing inter-pulse intervals and decreasing normalized amplitudes. However, cases with increasing amplitudes or uncertain evolution trends also occur.

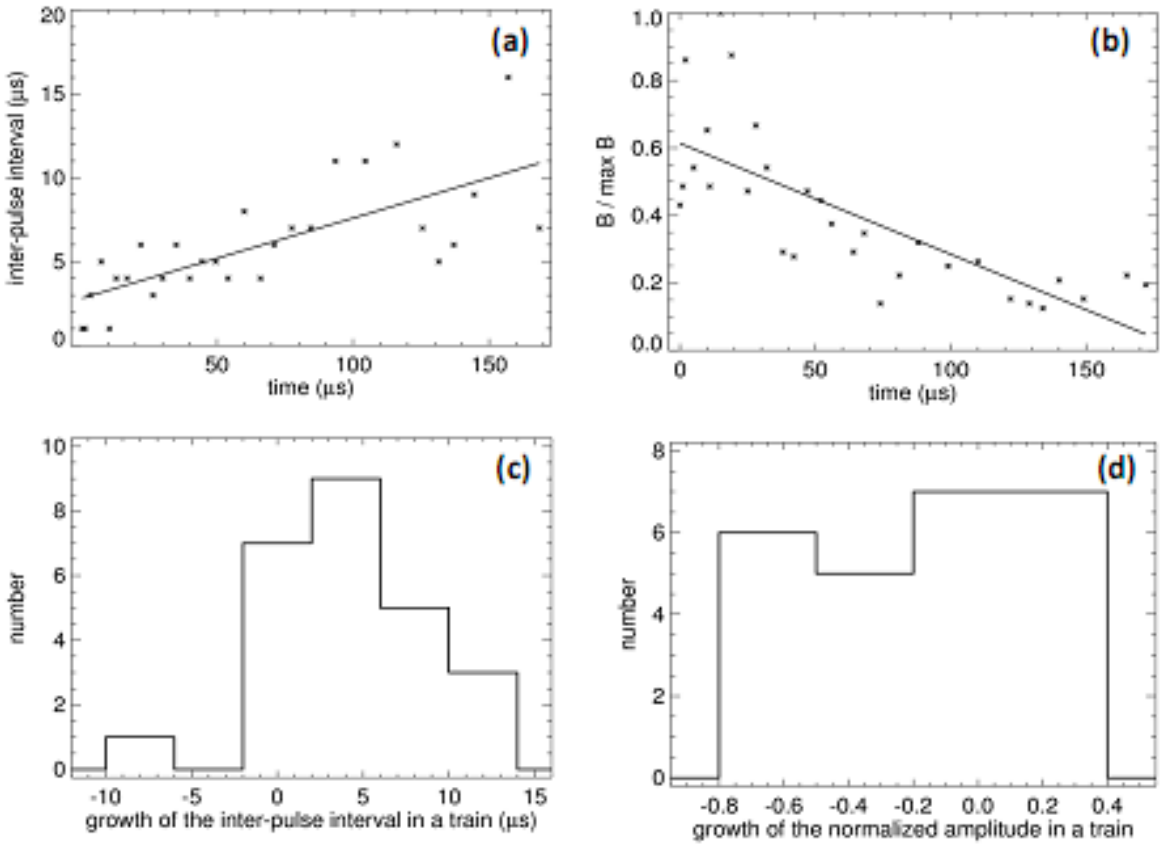

Fig. 35 Evolution of (a) the inter-pulse interval and (b) of the pulse amplitude normalized by its maximum value in a train from Fig. 1b, solid lines show linear fits. Histograms of linear trends for all analyzed trains: (c) the growth of inter-pulse interval within each individual train; (d) amplitude growth related to the maximum pulse amplitude in each train.

5.2.2 Discussion

In spite of this relatively low occurrence, observations of the pulse trains can bring new information about the charge structure in the thunderclouds, based on the temporal evolution of pulse properties. According to our measurements we can confirm that the most frequent evolution pattern of pulse train is characterized by an increasing inter-pulse interval and a decreasing pulse amplitude within an observed train, but we have less frequently observed all combinations of the evolution of the pulse amplitude and inter-pulse interval. These different evolution patterns also occurred during a single

120-ms long record and probably belonged to the same type of lightning process. Our results therefore disagree with the assignment of different evolution patterns to particular lightning phenomena proposed by *Wang et al*. [2000]. Our measurements rather indicate that evolution patterns of the peak amplitudes and inter-pulse intervals reflect the movement of a dart-stepped leader inside the cloud.

The observed variations of the pulse amplitudes can also be tentatively explained by the influence of a changing relative angle between the direction toward the source and the direction perpendicular to the antenna loop. Taking into account the typical speeds of dart stepped leaders on the order of 10^6 m/s [*Rakov and Uman*, 2003], and the typical duration of the pulse trains (~200 μs), the spatial dimension of the underlying lightning phenomena is on the order of a few hundreds of meters. This is by at least one order of magnitude lower than the typical distances between the antenna and the thundercloud, which correspond to possible amplitude variations of less than a few per cent within a given train, i.e., significantly lower than the observed variations.

Assuming that the speed of the movement of the dart leader was decreasing with time we can explain the observed increasing time interval between the neighboring pulses (96% trains in our dataset) on the condition that the distance between the neighboring charge pockets in the thundercloud is nearly constant, forming a hypothetical periodic charge structure at spatial scales on the order of 10 m. We are then also able to explain the sequential decrease of the amplitude of the pulses by the decrease of the speed of the leader propagation, because the radiated magnetic field is proportional to the speed of the leader movement [*Uman and McLain*, 1970]. Different distances between neighboring charge pockets and/or an increase of the speed of the leader propagation could probably also explain the observed untypical evolution patterns of the trains of the pulses.

Direct balloon measurements have shown that the charge distribution in the thunderclouds is rather complex at larger scales [*Stolzenburg and Marshall*, 1998]. Extended dataset of trains recorded in different conditions is needed to verify the above mentioned link of temporal properties of the trains to the small-scale properties of the charge structure.

5.3 Properties of individual pulses in the inter-stroke pulse trains

5.3.1 Measurements

Our high-resolution measurements with a sampling interval of 12.5 ns allow us to analyze the timing properties and the shapes of individual pulses in detail. We have limited the selection of the pulses for this analysis to a single record, most probably belonging to a single lightning flash, to exclude the influence of the differences in the propagation attenuation on the pulse shapes. The selected single 120-ms long record contained 12 pulse trains. We have excluded 2 trains containing bipolar pulses. The reduced dataset contains 327 negative and 54 positive unipolar pulses recorded in 9 negative and 1 positive pulse trains. The pulses were highly variable and sometimes irregular in shape. Only pulses with a clear shape have been included in the analysis of their fine properties. Typically, every isolated pulse is followed by a much smaller overshoot of the opposite polarity. We have manually estimated the full width at the half maximum (FWHM) and the durations of the rising and falling edges of individual pulses (Fig.36a).

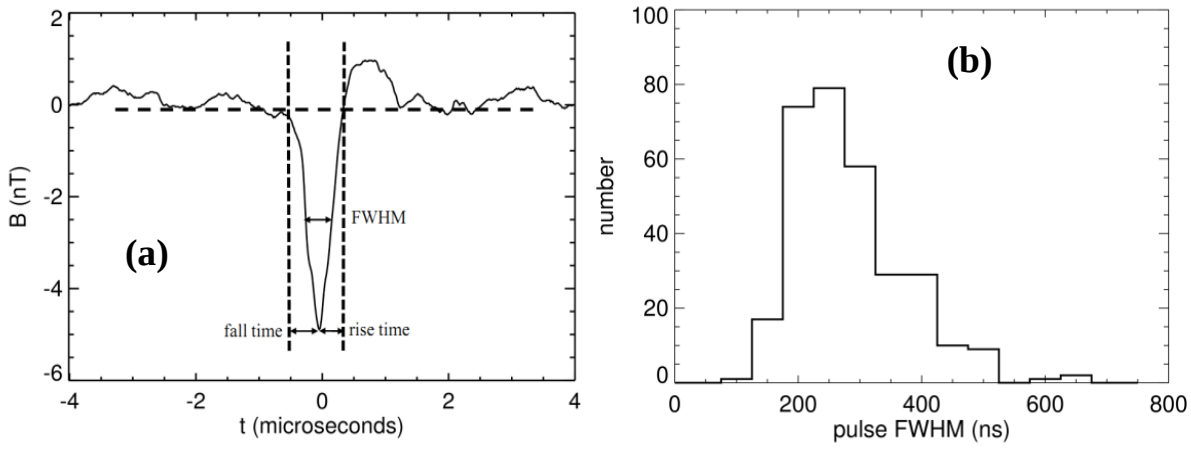

Fig. 36 (a) Method of the estimation of pulse characteristics, (b) Full Width at Half Maximum for individual pulses

The histogram of obtained values of FWHM is plotted in Figure 36b. The values vary from 131 ns to 653 ns with the mean value of about 287 ns. The results of manually estimated durations of rising and falling edges for pulses of both polarities are

summarized in Table 1. The histograms of obtained values are plotted in Figure 37.

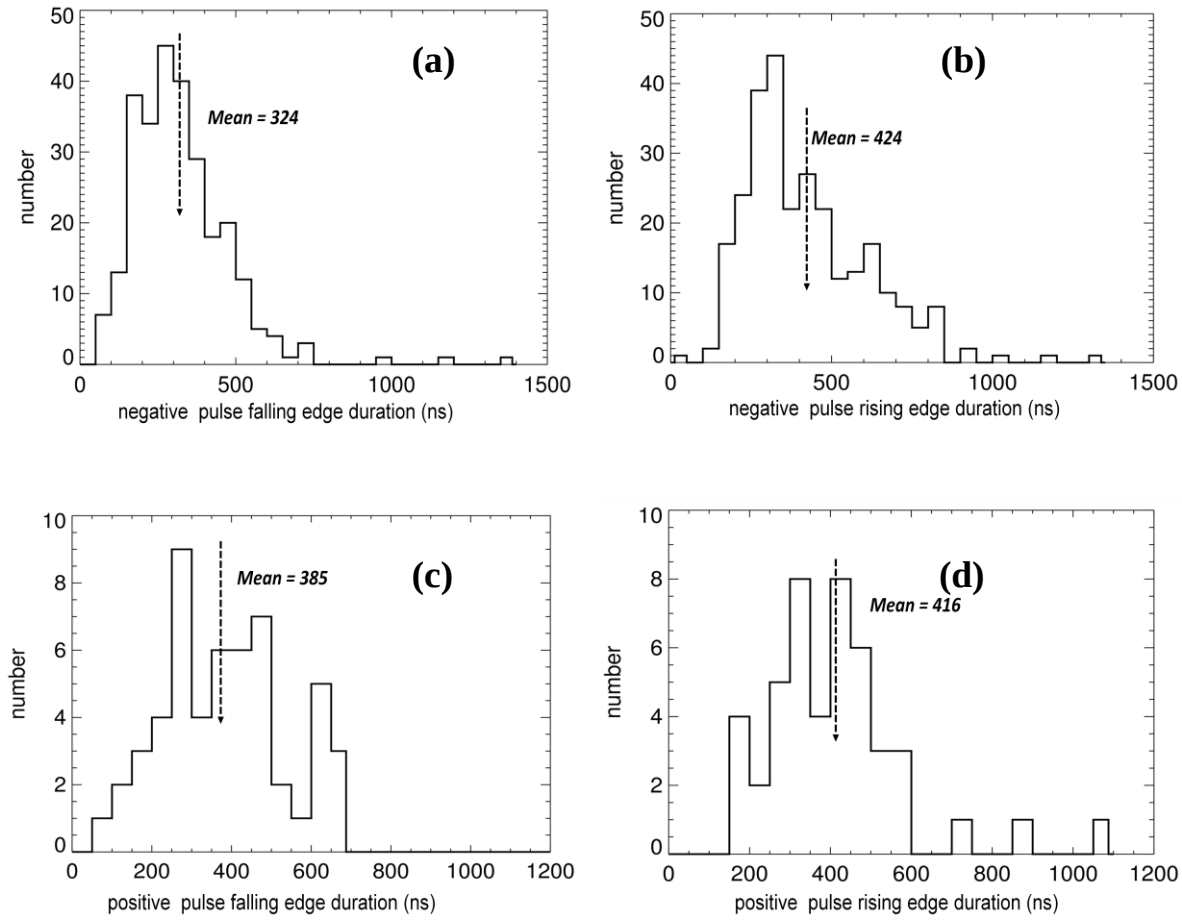

Fig. 37 Duration of (a) the falling edge and of (b) the rising edge for negative pulses; duration of (c) the falling edge and of (d) the rising edge for positive pulses

To examine a possible relation between the durations of the edges of positive and negative pulses, we use Student's t-test. The definition of the Student's *t* is given in the equations 14 and 15, where $\bar{x}$ and $\bar{y}$ are the mean values of tested datasets X and Y, S_D is the significance of differences, and N_x and N_y are the numbers of samples in the tested datasets.

$$t = \frac{\bar{x} - \bar{y}}{S_D} \tag{14}$$

$$S_D = \sqrt{\frac{\sum(x_i-\bar{x})^2+\sum(y_i-\bar{y})^2}{N_x+N_y-2}\left(\frac{1}{N_x}+\frac{1}{N_y}\right)} \quad (15)$$

Date set	Pulse polarity	Edge type	Mean value (ns)	Standard deviation (ns)	Number of samples
a	negative	falling (leading)	324	161	272
b	negative	rising (trailing)	424	193	276
c	positive	falling (trailing)	416	178	46
d	positive	rising (leading)	385	157	53

Table 1 Summary of the properties of the pulses

The results are summarized in Table 2. In the first column we show the tested pair of data sets (the letter assignments are the same as in Figure 37), $|t|$ is in the second column. In the third column we show the probability p, that the difference of average values could be this large or larger just by chance.

tested pair	$\|t\|$	p
a-b	6.60	0.0001
a-c	2.55	0.011
a-d	3.51	0.005
b-c	1.38	0.17
b-d	0.29	0.77
c-d	0.89	0.37

Table 2 Results of the t-test for different pairs of datasets

Note that the results are probably influenced by big differences in the sizes of the

datasets of the pulses with opposite polarities (the number of the analyzed negative pulses is five times larger than the number of the analyzed positive pulses). The table shows that the pair a-b (leading and trailing edges of negative pulses) has significantly different mean values. The mean value of their ratio is 0.84. The relation of leading and trailing edges of positive pulses (pair c-d) is opposite; with an average ratio of 1.25. However the statistical significance is much lower here, mainly due to the lower number of analyzed pulses. This asymmetry in the shapes of pulses will be discussed in section 5.3.3.

5.3.2 Verification of instrumental effects

Typical individual pulses were followed by a small overshoot. This overshoot of opposite polarity can be caused by an instrumental effect. Using a signal generator we generated an artificial signal with a shape similar to the observed pulses (Fig. 38). This signal was applied to one differential input of the analyzer. The second input was terminated by the 50 Ω terminator. Small signals (the amplitude of 125 mVp-p) as well as a large signal (the amplitude of 4 Vp-p) were used for the test in order to see a possible difference in the response of the analyzer.

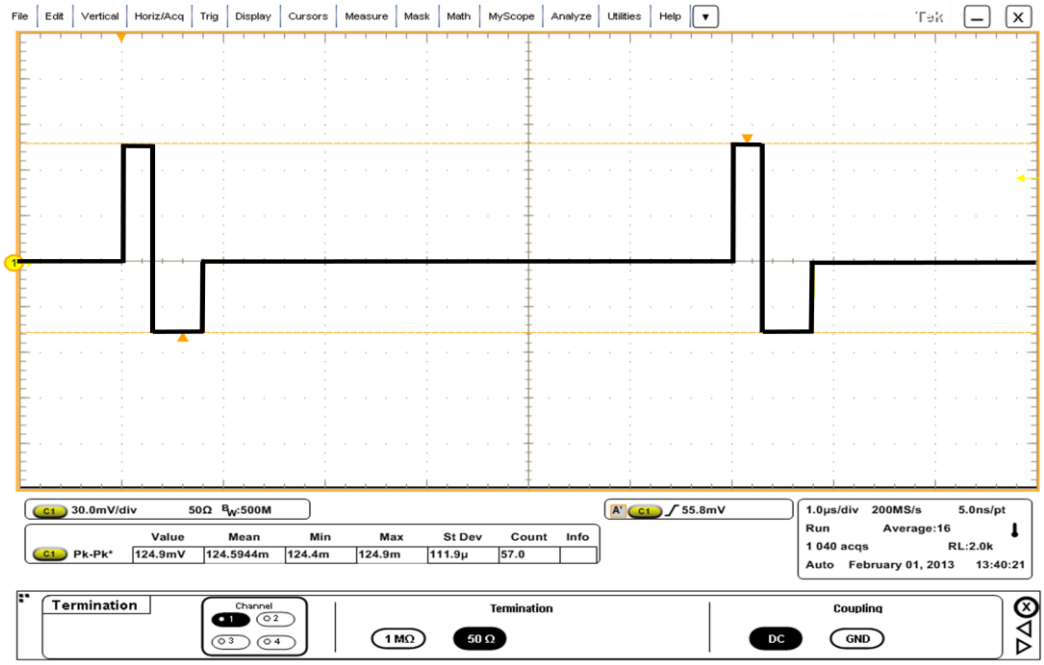

Fig. 38 Screenshot of the artificial signal applied to the analyzer

The waveforms recorded by the analyzer and the numerically integrated waveforms are plotted in Figure 39. The top panels correspond to the response of the analyzer to a small signal, the bottom panels correspond to the response of the analyzer to a large signal. The left panels show the recorded waveforms and the right panels the numerically integrated waveforms.

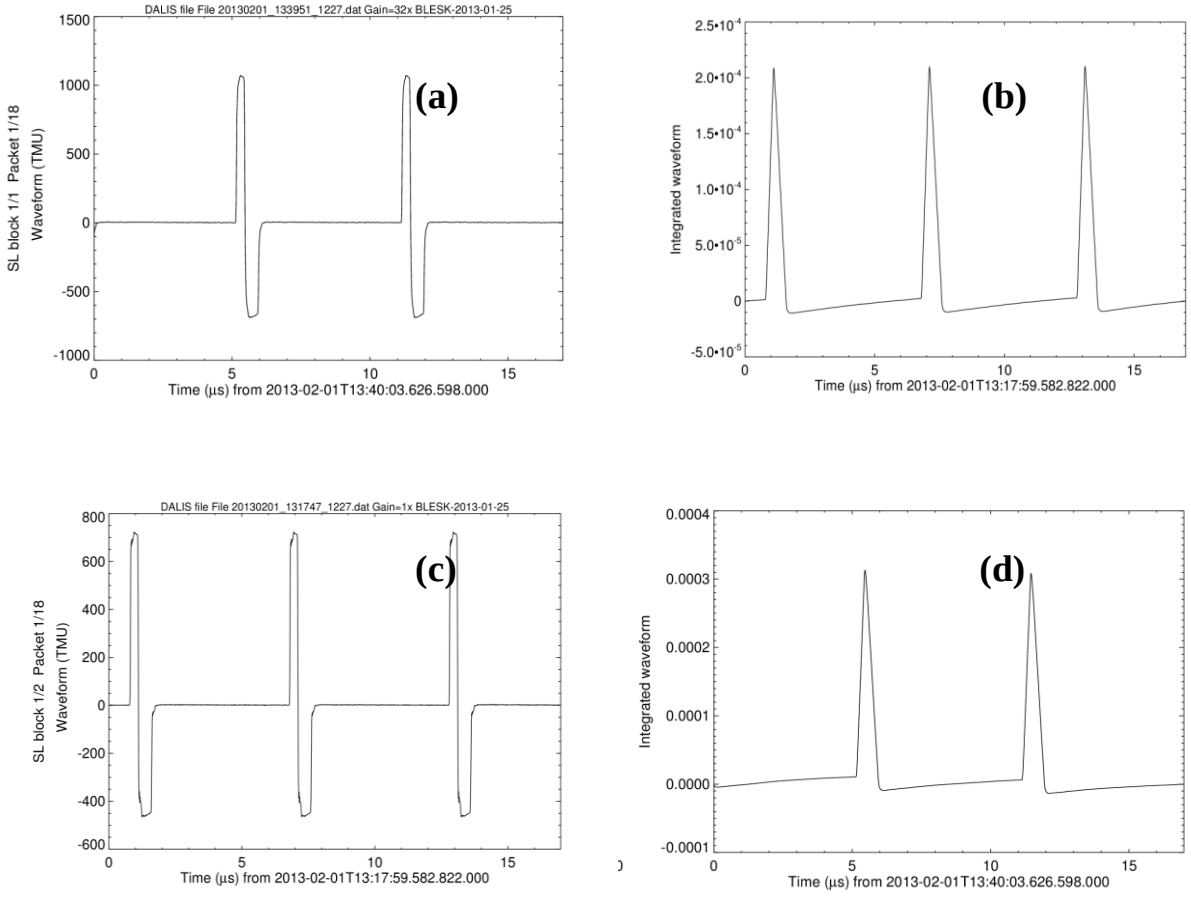

Fig. 39 The response of the analyzer to (a) small and (c) large artificial impulsive signal; the numerical integration of the recorded (b) small and (d) large artificial impulsive signal

As we consider each individual pulse to be unipolar, the immediately following overshoot of the opposite polarity should need to exceed one half of the peak amplitude of the original pulse, otherwise it is not significant. Based on the figures 39b and 39d we can conclude that the instrumental effect doesn't dominate, because an overshoot of only 8% caused by the instrument is seen in the numerically integrated waveform.

Similar overshoot was also observed in records of other lightning phenomena

and wasn't explained yet. For example *Haddad et al.* [2012] observed the overshoots of opposite polarity in 96% of 178 recorded return strokes in E-field waveforms, and interpreted the overshoots as a "ground wave" of radiated E.

5.3.3 Discussion

Rakov et al [1996] reported that the occurrence of the trains with the pulses of positive and negative polarities was nearly equal in their electric-fields records. A vertical electric dipole was used as an antenna for their measurements. Since we have used a magnetic loop for the measurements of the derivative of the magnetic field, the polarity of the signals recorded by our analyzer was dependent not only on the polarity of the source currents, but also on the relative position of the antenna with respect to these currents. We have verified this change of the polarity of our signals by comparison of the recorded return stroke waveforms with the data (position and the current direction) from the CELDN (Central European Lightning Detection Network.

Our dataset contains 68 % of the trains with the negative pulses and 32 % of the trains with positive pulses. The polarity of pulses in the trains recorded during a 120-ms long "event" would depend on the direction of the current in the discharge only if we assumed that the relative position of the antenna and the discharge remained substantially unchanged during each individual record.

We have compared our measurements of the FWHM of individual pulses with previous studies. The FWHM of the pulses in our dataset was two times shorter than the values reported by *Krider et al.* [1975] (Fig. 15) and by *Rakov et al.* [1996]. This difference could be probably explained by the effect of propagation losses. *Cooray et al.* [2009] reported that the peak amplitude of the time derivative of the magnetic field decreased by about 50%, 65% and 85% while propagating 100 m, 200 m, and 1000 m, over finitely conducting ground. The attenuation is, moreover, dependent on the frequency. *Willet et al.* [1995] observed in the records of electric fields radiated by the lightning strokes in Florida that the first-stroke spectrum fell at about f^5. This significant attenuation probably resulted in the slowdown of the leading and trailing edges of the pulses, and also in shortening the pulse width.

The pulse rise time of individual pulses reported by *Krider et al.* [1975] and by *Rakov et al.* [1996] was estimated at a measuring system limit of 0.1μs. To our

knowledge, no more accurate measurements were reported in the lightning literature up to now. We measured separately the pulse rise and fall times of negative and positive pulses. The average durations of the rising and falling edges of the pulses from our data set are three to four times larger than the values reported by *Krider et al.* [1975] and by *Rakov et al.* [1996]. As mentioned above, this slowdown of the edges was probably caused by the propagation losses, while the attenuation increases nonlinearly with increasing frequency. A small contribution to the slowdown of the edges (at scales < 0.1 μs) can be also expected from the frequency response of our antenna (type CABLE) described in section 3.1.5.

We have also noticed a visible asymmetry in the durations of the rising and falling edges of the pulses. The rise time is about 30% longer for negative pulses and slightly longer for positive pulses. Thus the ratio between the leading and the trailing edges is smaller than 1 for the negative pulses and probably larger than 1 for the positive pulses. We can exclude that the asymmetry originates in the instrument design. The analog part of the analyzer is equipped with fully differential operational amplifiers and thus there is no difference in the processing of both the negative and the positive signals.

Our measurements indicate that the pulses of opposite polarity aren’t simply inverted in the records. A larger dataset of pulses is needed to verify this asymmetry. If the asymmetry of pulses is proven to be real, the following explanation can be proposed: The asymmetry of the pulses can simply originate in the asymmetry of the charge distribution in the charge "pockets" which can be caused by gravity effects. Then the upward propagating intra-cloud leader or an upward propagating branch of the leader meets first the denser parts of the charge "pockets" and the leading edges of the pulses will be steeper than the trailing edges. When the leader propagates downward, the pulses would have the inverted polarity and the leader tip will meet first the less dense parts of the "pockets" and the leading edges of the pulses will be less steep than the trailing edges. This is consistent with our observations if we assume that the relative position of the antenna and the discharge didn't substantially change during each individual record.

5.4 Fine structure of magnetic field waveforms from negative multiple-stroke lightning flashes

In this section we analyze and discuss a fine structure of the *B* waveforms from return strokes of two negative multiple-stroke lightning flashes near their dominant peak. The review of the lightning literature related to the properties of the return stroke and to the multiplicity of strokes was described in sections 2.6.3 and 2.6.5. A simple transmission line model, which we used for the estimation of the ratio of velocities of the current waves of return strokes, was described in section 2.6.6. Shapes of the *B* and *dB/dt* waveforms of the return stroke depend on the structure of the corresponding current lightning channel. The degree of the similarity of the *B* and *dB/dt* waveform shapes of the strokes in the same flash tells us if the subsequent stroke followed the first-stroke channel or if it created a separate channel with a new ground termination.

5.4.1 Measurements

Broadband waveforms of the magnetic-field derivative from lightning discharges were measured in inland (near Prague, Czech Republic). The analyzer, which was used for the measurements, is described in section 4.1. The high sampling frequency allows us to examine the timing properties of the onset and decay of the return stroke dominant peak. The measured waveforms are numerically integrated. Our data set for this study consists of seven return strokes of two negative multiple-stroke lightning flashes occurring on 20th of June 2012 in the vicinity of our receiving station. The first flash (Flash No 1, Table 3) consists of four strokes, the second flash consist of three strokes (Flash No 2, Table 4).

First, a 200 μs–long waveform of *B* was studied to obtain a general picture of the event, and then a time interval of 40 μs was chosen for a detailed study of the shape. We compare the shape, the amplitude (*B* waveforms) and the duration of the rising edge (*dB/dt* waveforms) of the dominant peak for the first and for all subsequent return strokes. We also use the information about the peak current and about the position of the strokes obtained from the lightning detection network CELDN [*Novak and*

Kyznarova, 2011].

FLASH No 1 : 4-STROKE CG- FLASH 20/June/2012		
	time	**peak current**
CG-	6:23:13.013	177 kA
CG-	6:23:13.035	35 kA
CG-	6:23:13.063	21 kA
CG-	6:23:13.086	21 kA

Table 3 Flash No 1: list of return strokes including the polarity, the times of the dominant *B* peak and the peak currents

FLASH No 2 : 3-STROKE CG- FLASH 20/June/2012		
	time	**peak current**
CG-	6:44:59.236	117 kA
CG-	6:44:59.260	40 kA
CG-	6:44:59.270	15 kA

Table 4 Flash No 2: list of return strokes including the polarity, the times of the dominant *B* peak and the peak currents

The 200 μs–long waveforms and the 40 μs–long waveforms of *B* are plotted in Figures 40 and 41. The figure 40 consists of eight plots, grouped in two columns and four rows. The 200 μs–long waveforms are plotted in the first column; the 40 μs–long waveforms are plotted in the second column. The first row is related to the first return stroke, the waveforms of the subsequent return strokes are shown sequentially in the following rows. The same organization of plots is used in Figure 41.

We estimated the peak-to-peak amplitudes of *B* of the dominant peaks and rise times of the *dB/dt* for all strokes. We calculated the ratio of the subsequent-to-first-return-stroke magnetic field peak for all subsequent strokes and both corresponding first

return strokes. We calculated also the ratio of the subsequent-to-first-return-stroke peak current and the ratio of the subsequent-to-first-return-stroke rise time of the *dB/dt* for all strokes. The results are summarized in Tables 5 and 6. The geometric mean of the ratio of the subsequent-to-first-return-stroke magnetic field peak for our data is 0.15.

	Bp_{SX}/Bp_F	I_{SX}/I_F	TR_{SX}/TR_F	*L (km)*
First subsequent stroke	0.18	0.20	0.67	1.7
Second subsequent stroke	0.10	0.12	0.26	2.0
Third subsequent stroke	0.15	0.12	0.33	2.0

Table 5 Flash No 1: Properties of the return strokes

	Bp_{SX}/Bp_F	I_{SX}/I_F	TR_{SX}/TR_F	*L (km)*
First subsequent stroke	0.31	0.34	0.24	0.1
Second subsequent stroke	0.11	0.13	0.24	0.2

Table 6 Flash No 2: Properties of the return strokes

The legend for Tables 5 and 6: Bp_F – dominant peak amplitude of the first stroke; Bp_{SX} – dominant peak amplitude of the x-subsequent stroke; I_F – peak current of the first stroke; I_{SX} – peak current of the x-subsequent stroke; TR_F – rise time of the *dB/dt* of the first stroke; TR_{SX} – rise time of the *dB/dt* of the x-subsequent stroke; *L* – the distance between the first stroke and the x-subsequent stroke

5.4.2 Discussion

To discuss our results, we can start by comparing the level of the similarity of the shapes of the *B* waveforms. We can speculate that the first subsequent stroke created a new channel; the second and third subsequent strokes followed the first subsequent

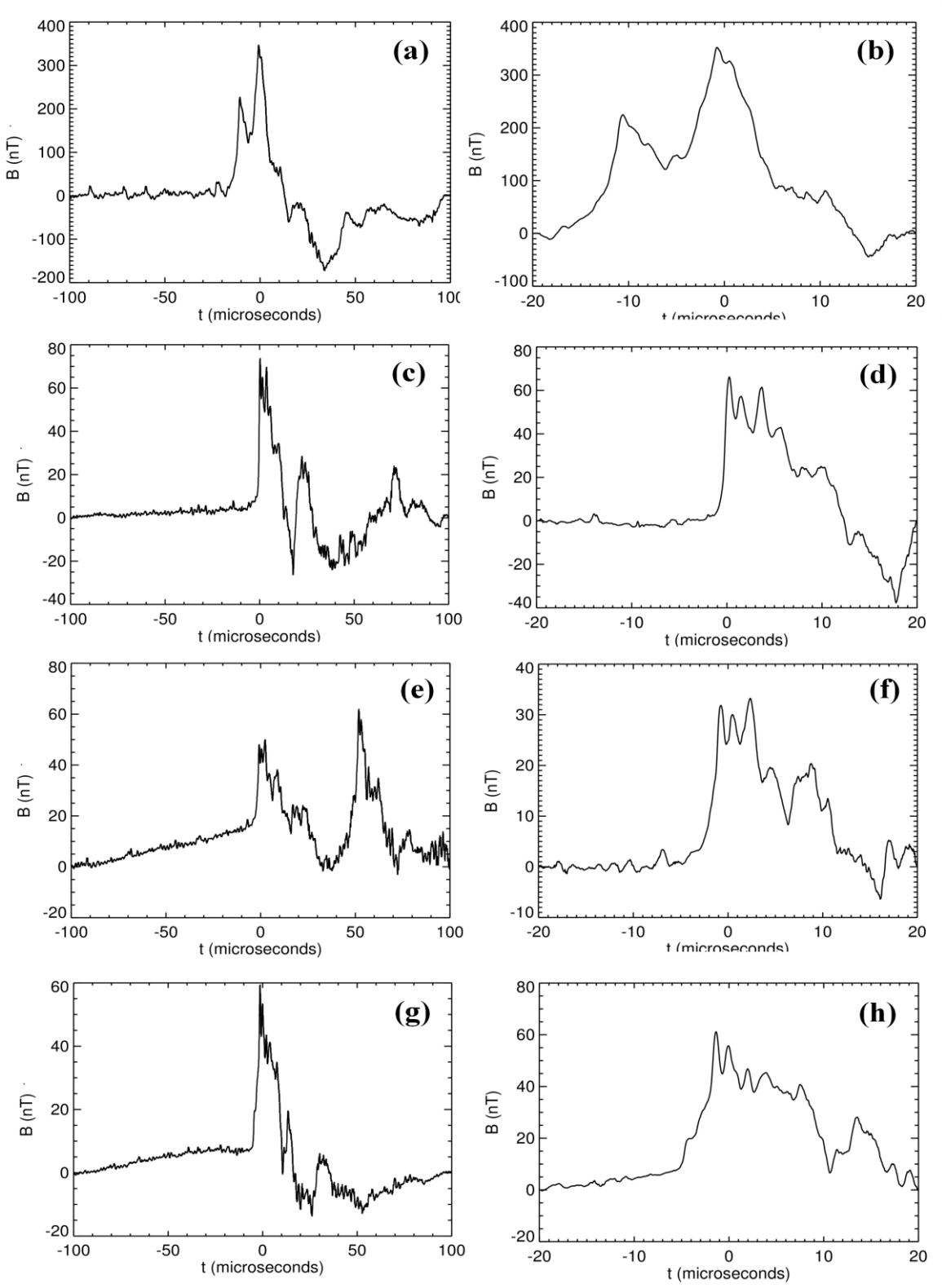

Fig. 40 Flash No 1: a, b) the *B* waveform of the first stroke; c, d) the *B* waveform of the first subsequent stroke; e, f) the *B* waveform of the second subsequent stroke; g, h) the *B* waveform of the third subsequent stroke

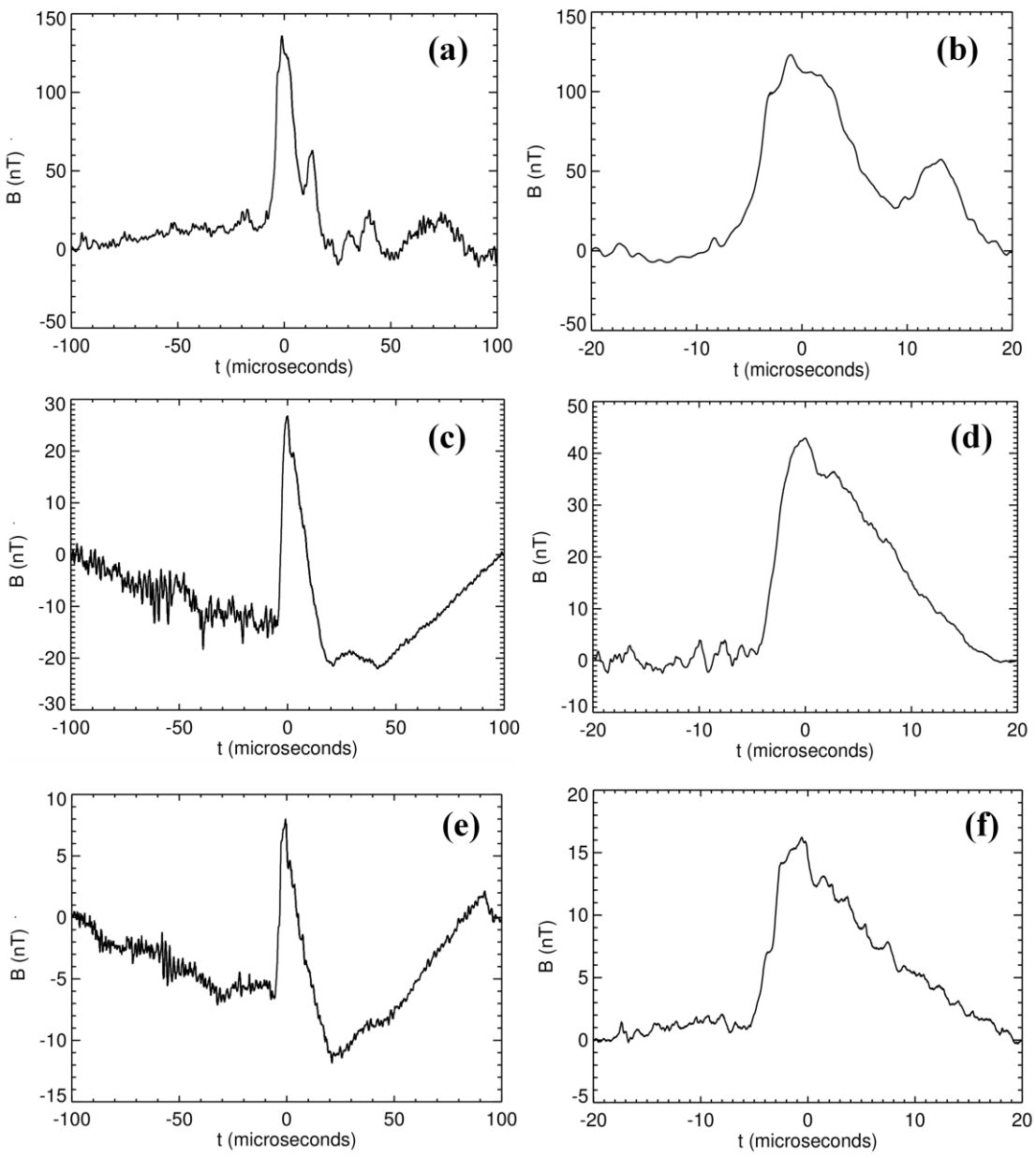

Fig. 41 Flash No 2: a, b) the *B* waveform of the first stroke; c, d) the *B* waveform of the first subsequent stroke; e, f) the *B* waveform of the second subsequent stroke

stroke in Flash No 1. Our observations are consistent with the optical observations made by *Valine et al.* [2002], who reported that 67% of the new strike points were produced by the second stroke in the channel, the chance of forming a new or an altered channel rapidly decreased with the stroke order. The subsequent strokes in Flash No 2 probably followed the channel of the first stroke.

Besides the somewhat subjective criterion of visual similarity of recorded

waveforms, we can support our hypothesis by two additional considerations. Firstly, the ratio of the subsequent-to-first-return-stroke rise time of the *dB/dt* for the first subsequent stroke in the Flash No 1 is 0.64; this ratio is more than twice larger than the same parameter for all other subsequent strokes. The larger rise time can indicate that the stroke propagates slower when creating a new channel in the virgin air. *Weidman et al.* [1978] reported that the initial front of the electric field dominant peak of the subsequent return stroke rises 2-8 times faster than the initial front of the dominant peak of the first stroke. The relatively large variance in the durations of the initial front of dominant peaks of the return strokes probably originate in the dataset of *Weidman et al.* [1978], which included all types of the first strokes (branched and smooth) and all types of the subsequent strokes (creating new channels or following the previous one). We still can conclude that the initial front of the dominant peak of the stroke propagating in the virgin air is slower than the same parameter for the stroke following the existing channel, which is consistent with our measurement.

Secondly, we can use the simple transmission line model of the current in the lightning channel introduced in section 2.6.6. We can very roughly estimate whether the current waves of different subsequent strokes belonging to the same flash propagate with the same velocity or not. Considering the equation (5), the velocity of the current wave is proportional to the ratio of the magnetic field peak value and the peak current of the return stroke. We calculated the ratio of Bp_{SX}/Bp_F and I_{SX}/I_F (tables 5 and 6) for all subsequent strokes in the flashes No 1 and No 2. We obtained the ratio of the velocity of each subsequent stroke and the velocity of the corresponding first return stroke. The results for the flash No 1 indicate that the first stroke and the first subsequent stroke have similar velocity; the third subsequent stroke was faster. It indicates that the first subsequent return stroke propagated in a new channel and the third subsequent stroke followed the existing one. Since the magnetic-field waveform of the second subsequent stroke exhibits two peaks, the lightning channel probably forked and had two ground terminations. In that case we probably cannot speak about the existing and the new channels. These results are consistent with the measurement of the duration of the rising edges discussed in the preceding paragraph. The calculation based on the simplified transmission line model didn't give us satisfactory results for flash No 2. The ratios of the magnetic field peak value and the peak current for the first return stroke and for the subsequent strokes do not differ significantly, even though the comparison of the rise

times of the *dB/dt* for the first and the subsequent strokes indicates that the subsequent strokes followed the existing channel. It is necessary to analyze more flashes with multiple strokes to verify if the transition line model could help us when considering the sharing of the lightning channel by the subsequent strokes belonging to the same flash.

The geometric mean of the ratio of the subsequent-to-first-return stroke magnetic field peak for our data is 0.15. This value is much smaller than the values reported by *Nag et al*. [2008], who compared the geometric means of this ratio for Florida, Austria, Brazil and Sweden multiple stroke flashes and obtained 0.58, 0.64, 0.53 and 0.52, respectively. Since we have analyzed only two multiple-stroke flashes, our data set is too small to derive any conclusions from the difference in these ratios of the subsequent-to-first-return stroke field peak compared to the results of *Nag et al*. [2008].

5.5 Properties of trains of preliminary breakdown pulses occurring prior to the first stroke of negative lightning flashes

In this section we analyze and discuss the properties of trains of preliminary breakdown pulses occurring prior to the first strokes of negative lightning flashes. The review of the lightning literature related to the properties of the preliminary breakdown pulses is given in section 2.6.1.

5.5.1 Measurements

The waveforms containing the first return strokes and the corresponding trains of preliminary breakdown pulses were measured during one thunderstorm occurred on 11th of October 2012 in the vicinity of our receiving station in Rustrel in Southern France. The analyzer which we were using for the measurements is described in detail in section 4.1. Altogether we recorded 37 return strokes during this particular thunderstorm.

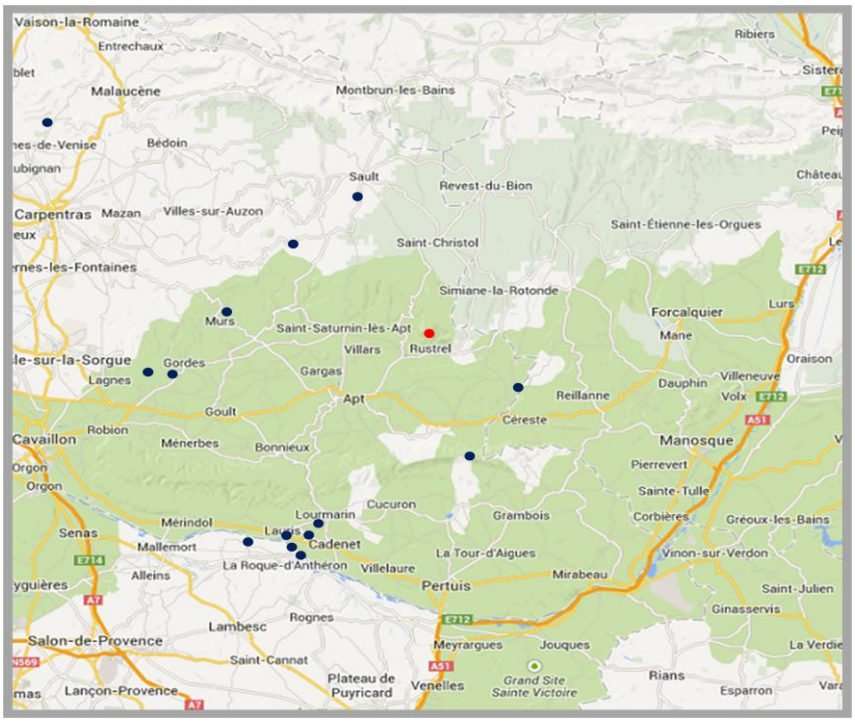

Fig. 42 Locations of the return strokes preceded by trains of pulses and reported by the METEORAGE service

We completed our records by the lightning data (the peak current, the polarity and the location) provided by the French meteorological service METEORAGE. Thus we are able to choose all negative cloud-to-ground discharges and look for the presence of the trains of preliminary breakdown pulses prior to the first stroke. We excluded all positive cloud-to ground discharges and all subsequent return strokes from our analysis. We excluded also the data recorded in the survey mode of our analyzer, as the 300 μs-long survey-mode waveforms are not long enough to contain both the return stroke and the corresponding train of preliminary breakdown pulses. Our data set consists of 14 CG- return strokes preceded by preliminary breakdown pulses and 2 return strokes with the pulses occurring prior to the stroke and not reported by the METEORAGE services. Thus we have altogether 16 cases, where the pulse activity prior to the first return stroke were present and could be analyzed. The locations of the return strokes reported by the METEORAGE service are plotted in the map (Fig.42). Each blue dot represents a stroke preceded by a train of pulses. The red dot shows the location of our receiving station on the top of the Grand Montaigne close to Rustrel. Table 7 shows, how we have selected our final data set consisting of 16 cases. We plotted the parts of the recorded waveforms starting with the first preliminary breakdown pulse and ending with the return stroke.

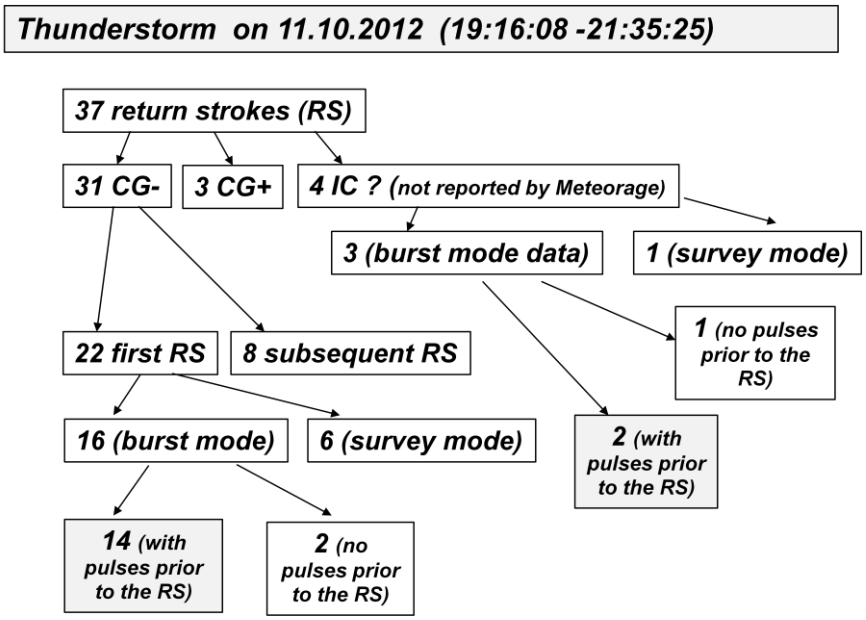

Table 7 Overview of return strokes recorded on the 11th of October 2012

The sequence of pulses occurring prior to the first return stroke is usually composed of three parts. It begins with an initial larger pulse train of preliminary

breakdown pulses, which is followed by a relatively low and irregular pulse activity. The sequence ends with another pulse train attributed to the last stages of the stepped leader. We can see two different patterns. We were able to separate the individual parts of the sequence in 8 cases. The parts were probably overlapping in remaining 8 cases and we were unable to divide the sequences into three parts. The examples of these two patterns of the sequences occurring prior to the first stroke are plotted in Figures 43a and 43b.The second pattern of the sequence with the highlighted detail showing the train of preliminary breakdown pulses is plotted in Figure 44.

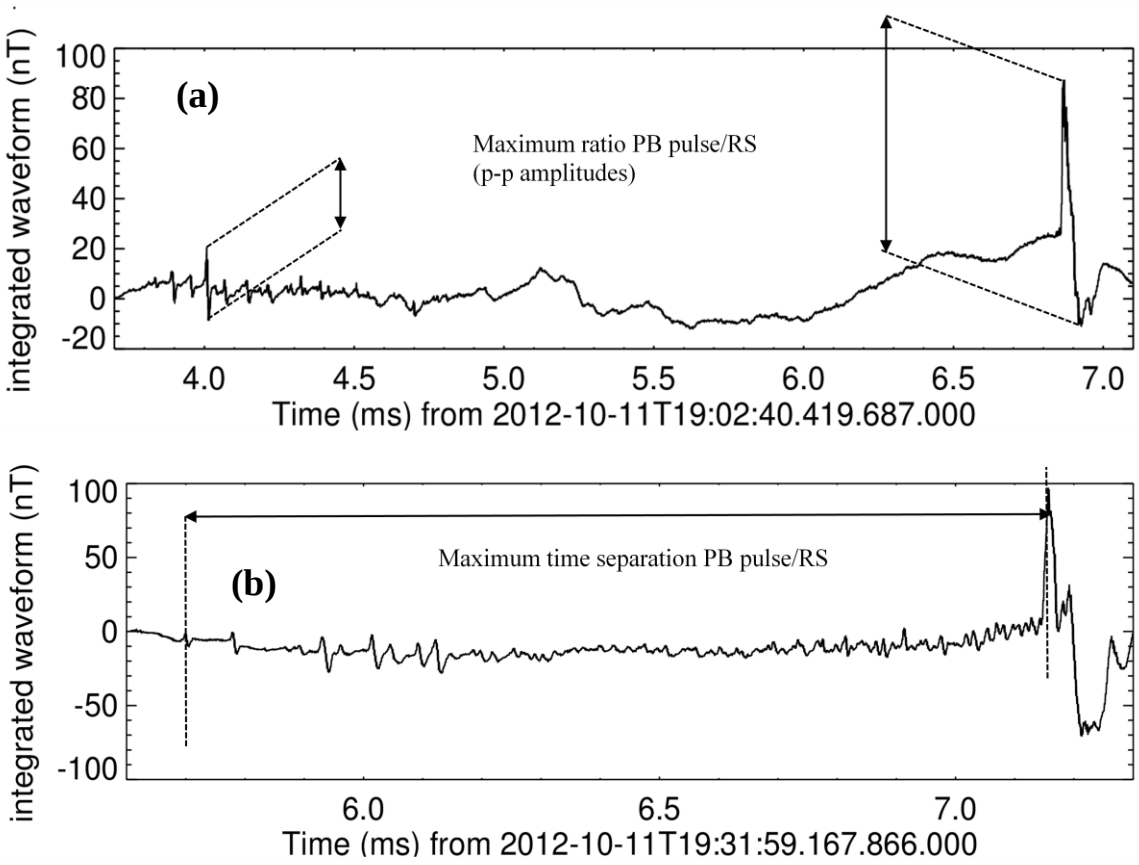

Fig. 43 Examples of sequences occurring prior to the first stroke with a) a separable train of preliminary breakdown pulses, b) an inseparable train of preliminary breakdown pulses

To estimate the properties of the trains of preliminary breakdown pulses we used the same procedure as in section 5.1. The amplitudes of all the pulses and the times of their peak values were estimated from the integrated *B* waveforms. To record a pulse we

have chosen a threshold of 1 nT for the peak amplitude. This threshold is several times larger than the noise level of the analyzer. Each individual pulse is considered to be unipolar, if the immediately following overshoot of the opposite polarity doesn't exceed one half of the peak amplitude of the original pulse.The maximum ratio of the peak-to-peak amplitudes of the preliminary breakdown pulses and of the return stroke and the maximum time separation of the first pulse and the dominant peak of the corresponding return stroke were estimated for all sequences. We calculated the number of pulses, the percentage of unipolar pulses in each individual train and the duration of the trains for sequences with a separable train of PB pulses. We also estimated the inter-pulse intervals between the pulses in the particular trains of PB pulses.

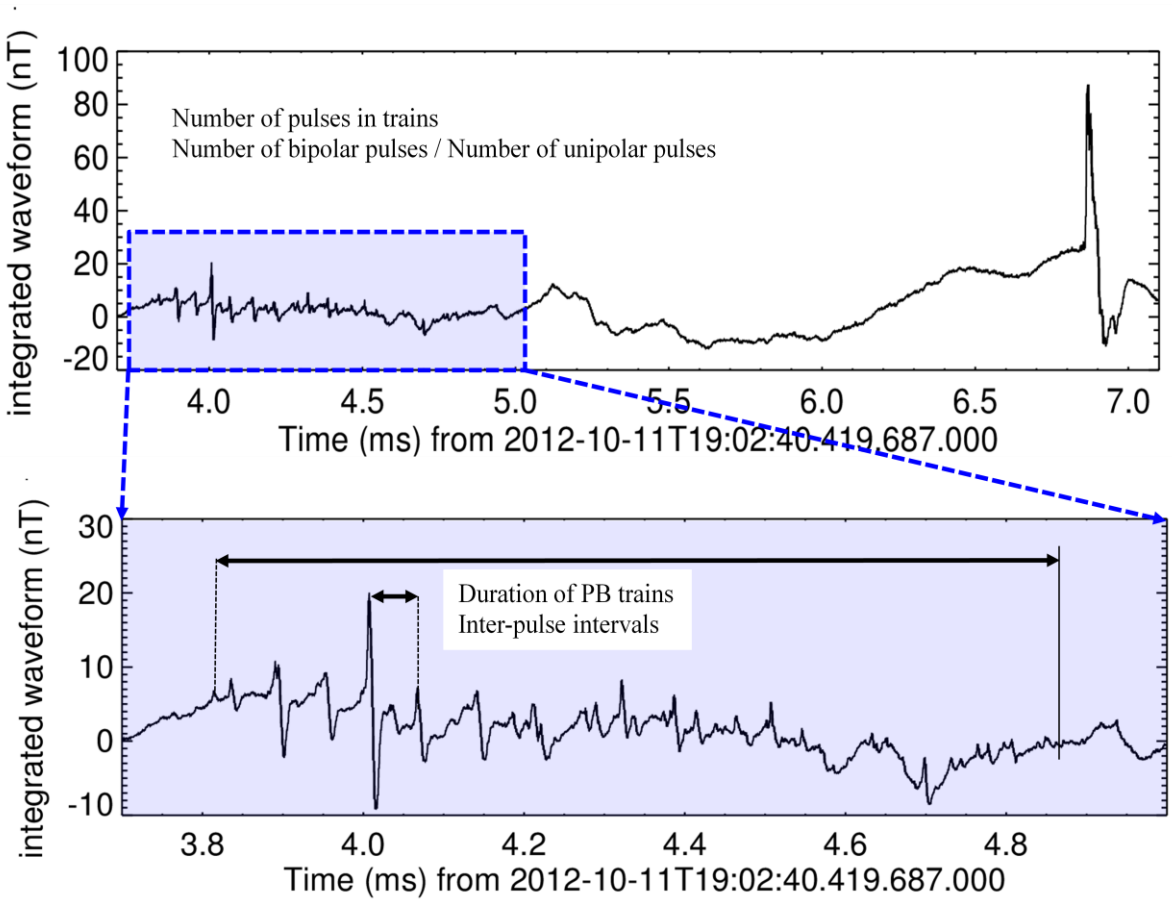

Fig. 44 Example of the second pattern of the sequence (the detail of the train of preliminary breakdown pulses is highlighted)

We found that both the first and the largest pulses are bipolar with the same initial polarity as the return stroke. The ratio of the peak-to-peak amplitudes of the largest preliminary breakdown pulse and the corresponding return stroke varies from

3.2 % to 46.1 % with a mean value of 21 %. The time separation of the first preliminary breakdown pulse and the corresponding return stroke varies from 0.9 ms to 7.1 ms with a mean value of 2.6 ms. The duration of the individual trains varies from 615 μs to 1768 μs with a mean value of 1294 μs. The number of pulses in the individual trains varies from 15 to 52 with a mean value of 32. The percentage of bipolar pulses in the individual trains varies from 7 % to 69 % with a mean value of 32 %. The inter-pulse interval varies from 8 μs to 253 μs with a mean value of 41 μs. The histogram of the obtained values of the inter-pulse intervals is plotted in Figure 45. The distribution clearly has a "heavy tail" and is far from being normal.

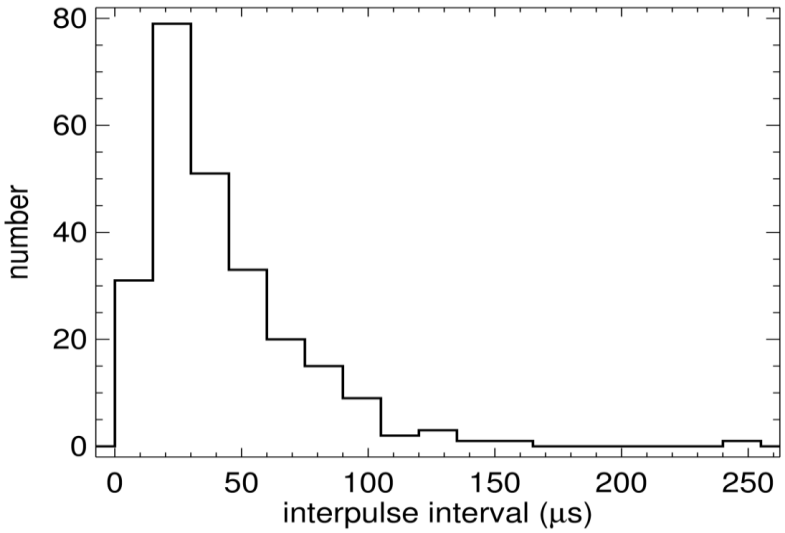

Fig. 45 Histogram of the obtained values of the inter-pulse intervals

5.5.2 Discussion

We start the discussion by comparing of our results with previously published studies. The properties of preliminary breakdown pulses were measured in five different locations (including our measurements). The ratios of the peak-to-peak amplitudes of the largest preliminary breakdown pulse and the corresponding return stroke measured in different locations are shown in Table 8. Our results are more similar to the results obtained in the tropical regions then to the results from the northern region.

Srí Lanka	16.5 %	*Gomes et al.* (1998)
Malaysia	27.8 %	*Baharudin et al.* (2010)
Florida	62 %	*Nag and Rakov* (2007)
France	21 %	*this study*
Sweden	101.4 %	*Gomes et al.* (1998)

Table 8 Comparison of different measurements of the largest PB pulse / RS ratio (peak-to-peak amplitudes)

Srí Lanka	11.9 ms	*Gomes et al.* (1998)
Malaysia	57.6 ms	*Baharudin et al.* (2010)
Florida	22.7 ms	*Baharudin et al.* (2010)
France	2.6 ms	*this study*
Sweden	13.8 ms	*Gomes et al.* (1998)

Table 9 Comparison of different measurements of the time separation of the first PB pulse and the corresponding RS

The time separation of the first preliminary breakdown pulse and the corresponding return stroke were measured in five locations with different geographic latitude. The average values of this time separation are summarized in Table 9. We obtained an extremely low value of the average time separation of the first preliminary breakdown pulses and the corresponding return strokes in comparison with the previously published studies. We can speculate that this low value can be linked to a low distance between the cloud base and the receiving station.

We can support our hypothesis using the LMA data (Lightning Mapping Array). The LMA is a deployable system that locates lightning radiation sources in three spatial dimensions and time. The Lightning Mapping Array measures the time of arrival of 60-

66 MHz RF radiation from a lightning discharge at multiple stations, and locates the sources of the radiation to produce a three-dimensional map of total lightning activity [*Rison et al.*, 1999]. The lightning phenomena as steps in the stepped leader, the K-changes, the preliminary breakdown pulses or the inter-stroke pulses can be seen in the LMA records, if they are strong enough to be detected. The LMA measuring system was deployed in autumn 2012 in France in frame of the HyMeX project (HYdrological cycle in Mediterranean EXperiment; http://www.hymex.org).

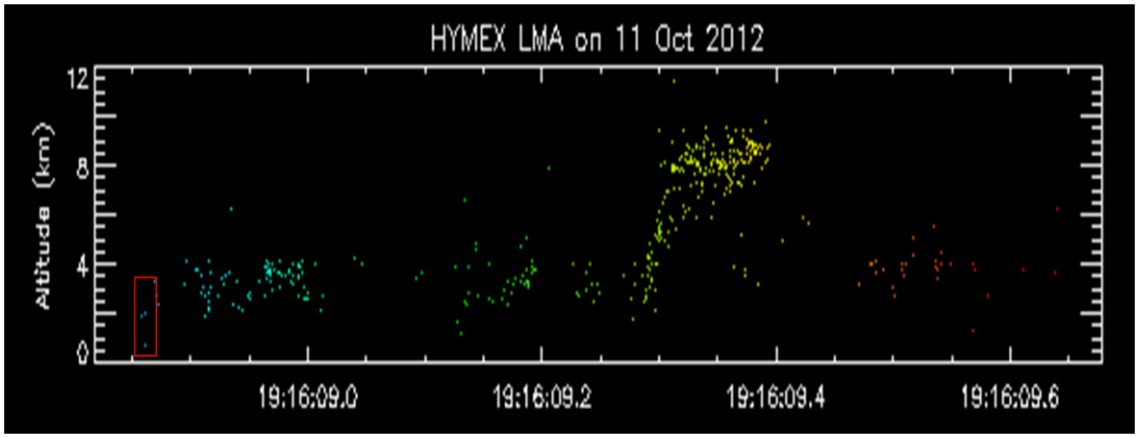

Fig. 46 LMA data from 11th of October 2012, (19:16:08,8 – 19:16:09,7), [*courtesy of T. Farges and W. Rison*]

Figure 46 shows one complete flash recorded by LMA during the thunderstorm on 11 October 2012. It lasts for ~ 900 ms. Each dot represents a source of the electromagnetic radiation in the LMA frequency range. The height of the irradiative source is given on the vertical axis; the horizontal axis represents the time. The first stroke of the flash is marked by a red box. Figure 46 clearly indicates that there was no activity recorded prior to the first stroke in this particular flash. The preliminary breakdown pulses are probably not strong enough to be detected. Knowing the height of the origin of the return stroke we can speculate that the combination of a relatively high altitude of the measuring site (1024 m) and a low height of the clouds (~ 2 km) probably results in the short duration of the pre-stroke sequence of pulses.

The inter-pulse intervals between the preliminary breakdown pulses were measured and reported only for the Florida seaside by *Nag and Rakov* [2009]. They obtained the average inter-pulse interval of 65 μs for their Florida measurements. The

mean value of the inter-pulse interval calculated from our dataset is 41 μs. Considering the large spread of obtained values in Figure 45, our results are consistent with the previously published data of *Nag and Rakov* [2009].

We can conclude that we observed a pulse activity prior to 84 % of the first RS recorded in the thunderstorm on 11th of October 2012. Our results are consistent with previously published studies with the exception of the duration of the pre-stroke pulse sequence. We didn't observe any significant difference in the properties of preliminary breakdown trains in flashes reported and not reported by the METEORAGE service. This means that we have most probably recorded CG flashes missed by the METEORAGE service, rather than IC flashes.

5.5.3 Comparison of the electric- and magnetic-field measurements: a case study

The flash shown in Figure 46 was selected for this comparative study. The first return stroke occurred at 9:16:08.854. The return stroke was identified by the METEORAGE service as a negative cloud-to-ground stroke having the peak current of 160 kA and located 14.6 km from our receiving station in Rustrel. We noticed the sequence of pulses prior to this return stroke in our magnetic-field data. This particular return stroke was recorded also by four CEA receivers equipped with the whip electric antennas. The 2-ms long parts of the electric- field waveforms measured by these receivers are plotted in Figure 47. The receivers are located in Rustrel, Humbligny, Bruyeres and Francourville in France. The distance between the receiver and the location of the analyzed lightning stroke was 14.6 km, 442 km, 497 km and 590 km for Rustrel, Humbligny, Bruyeres and Francourville, respectively. The pre-stroke pulse activity is not seen in the records of distant receivers (Fig. 47 b, c, d).

It is, however, well seen in the electric field data from Rustrel (Fig. 47a). Together with our magnetic field records, we have therefore measurements of the same phenomenon observed by different antennas and in different frequency bands at the same location in Rustrel. Now we can compare the waveform of the horizontal magnetic field (a sampling interval of 12.5 ns) with the waveform of the vertical electric field (a sampling interval of 80 ns). The parts of the waveforms showing the same sequence are plotted in Figure 48. The upper panels show the magnetic-field

waveforms; the bottom panels show the electric-field waveforms. The left-hand plots (Figs. 48a,c) give us the 2ms-long overview of the pre-stroke pulse activity including the return stroke. Waveforms showing only the pre-stroke pulse activity close to the return stroke dominant peak are given on the right (Figs. 48b, d). Red ovals show the corresponding time interval when the magnetic- and electric-field waveforms substantially differ. The initial part of the sequence is absent in the electric-field recordings. We can speculate that the absence of the part of pulses could be caused by their relative location with respect to the antenna radiation pattern. A whip antenna directed vertically is less sensitive to discharges which occur just above it. This hypothesis assumes the horizontal movement of the sources of the pre-stroke pulse activity, which was not reported in the lightning literature up to now.

.

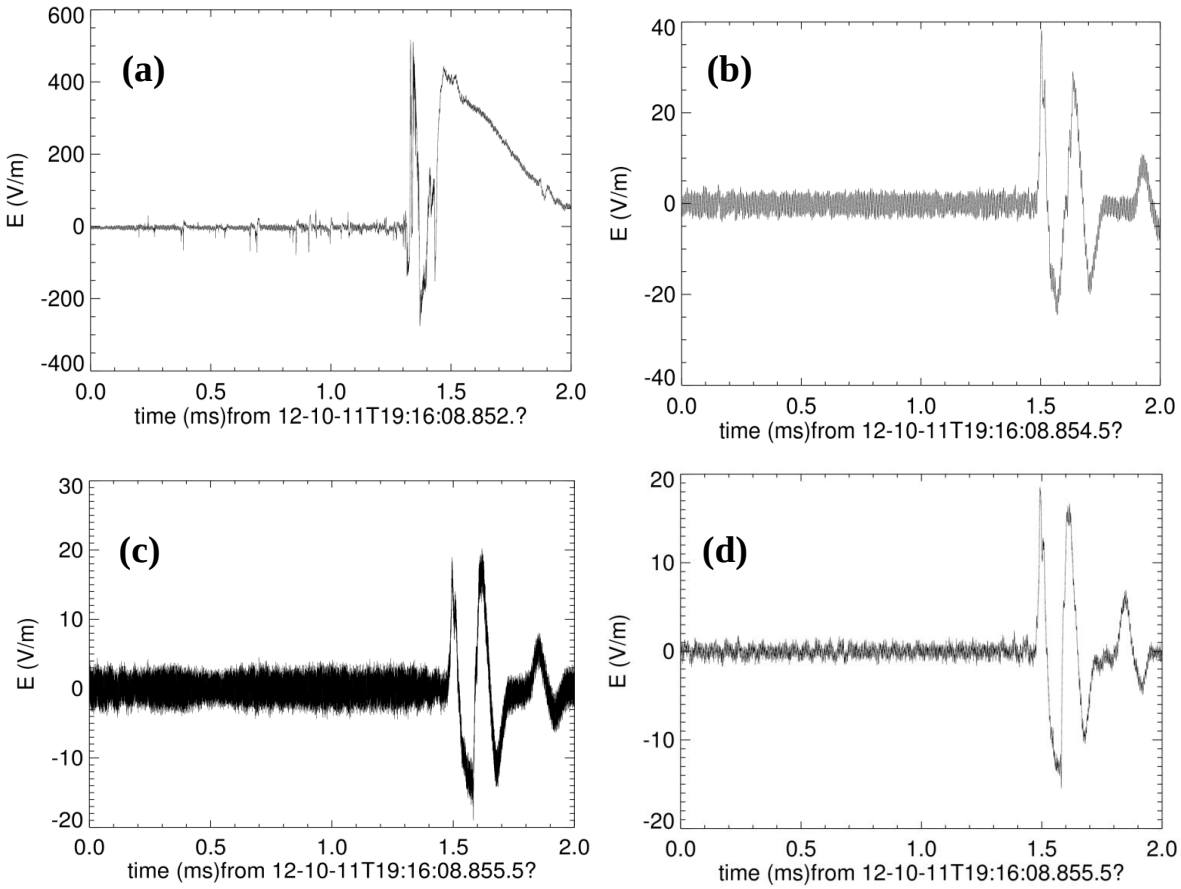

Fig. 47 2-ms long parts of the electric- field waveforms measured by CEA receivers in (a) Rustrel, (b) Humbligny, (c) Bruyeres and (d) Francourville (France)

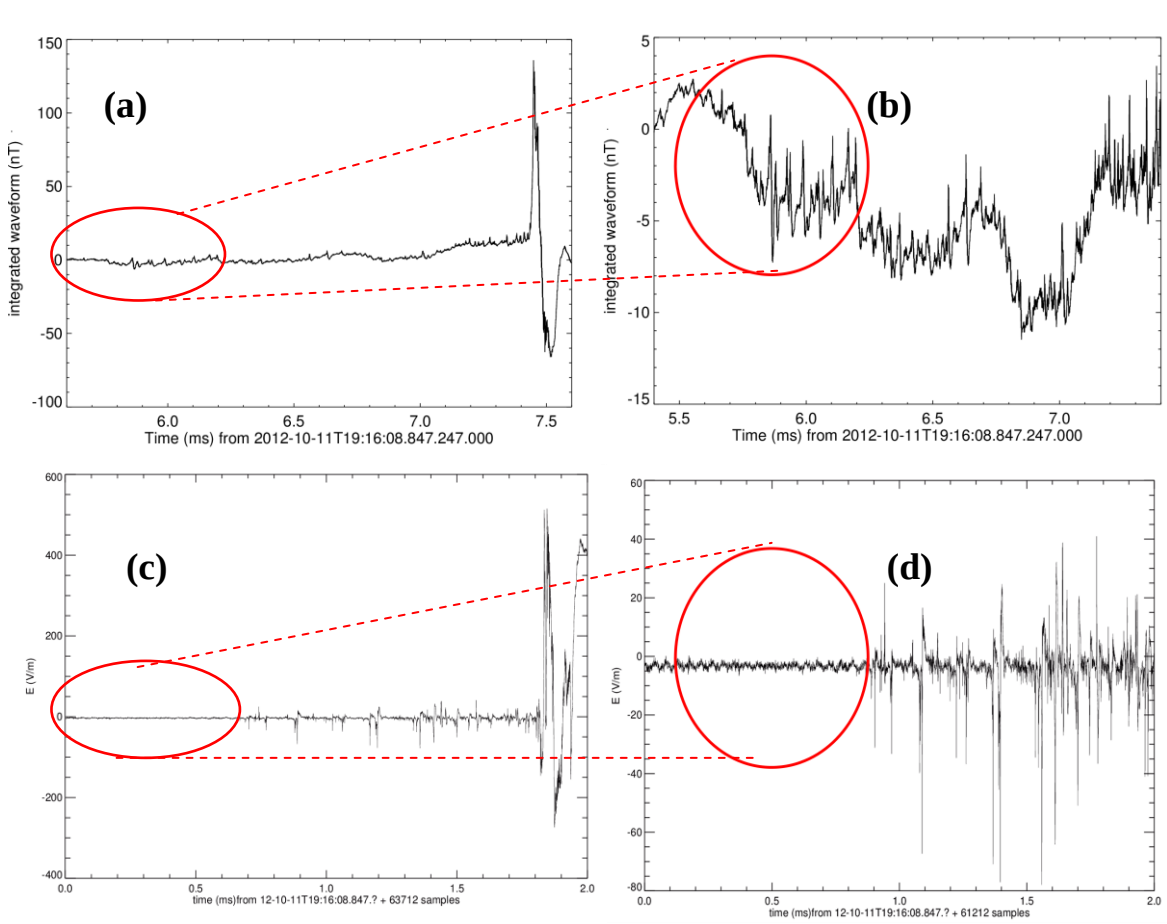

Fig. 48 2ms-long parts of the waveforms showing the same sequence of pulses. The upper panels (a, b) show the magnetic-field waveforms; the bottom panels (c, d) show the electric-field waveforms. The plots on the left (a, c) show the pre-stroke pulse activity including the RS; the plots on the right (b, d) show the pre-stroke pulse activity just before the RS on an expanded vertical scale.

5.6 Bouncing wave type discharge

The bouncing wave type discharge is a specific type of an intra-cloud discharge. It occurs quite rarely in comparison with cloud-to-ground discharges. We have recorded only a few cases of the bouncing wave type discharge during our summer campaigns. Analysis of one of these cases recorded by our analyzer initiated a case study of the electron acceleration above thunderclouds by *Fullekrug et al.* [2013]. This was the only high frequency event recorded during a passage of the thunderstorm overhead on 30 August 2012. The recorded magnetic-field waveform exhibits resonance type oscillations with a period of ~3.8 μs (corresponding to a frequency of ~260 kHz) lasting for about ~9 cycles (Fig. 49).

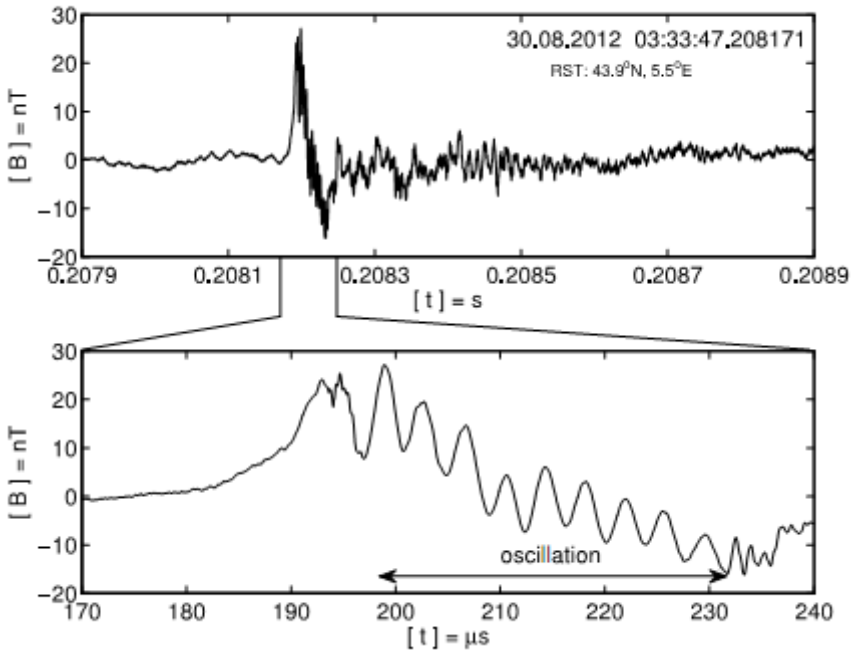

Fig. 49 Lightning discharge exhibiting resonant type oscillations with a period of ~3.8 μs (corresponding to a frequency of ~260 kHz) lasting for ~9 cycles over ~34.2 μs, and attributed to a bouncing wave type discharge

This type of oscillations was, to our best knowledge, observed and reported only in connection with compact intracloud discharges [*Nag and Rakov*, 2009]. However, in our case the observed lightning discharge lacks some features typical for compact intra-

cloud discharges. The bouncing wave can be explained by a travelling current pulse which is injected at one end of a conducting channel and reflected multiple times at both ends of the channel until the instability is attenuated and absorbed [*Nag and Rakov*, 2009]. The modeling results for the current propagation and reflection show that the pulse travels at a speed between $\sim 10^8$ m/s and the speed of light [*Nag et al.*, 2010]. In this case, the length of the lightning channel would be ~1 km resulting in the lower charge moment which is still consistent with a large peak current of the lightning discharge. We can exclude that the oscillations originate in the response of our instrument to the impulsive input signal.

The discovery of this particular bouncing wave type discharge in our data induced a wide search of unusual signatures in the data recorded by other instruments, which were doing their measurements in the same time and in the same region. The observed discharge was classified by the METEORAGE service as a positive cloud-to-ground discharge having the peak current of 124 kA. The discharge was strong enough to saturate all nearby ELF/VLF/LF receivers. The same discharge recorded in Orleans (France) and in Bath (UK) showed a trailing waveform ~9 ms later. The trailing waveform had relatively little spectral content in the VLF range. Such kind of flat spectra are characteristic for relativistic electron beams which have been described by *Fullekrug et al*. [2011]. In addition, this discharge produced an exceptional displacement current signature on a newly developed sensor network in southern England. The discharge caused a subsequent sprite, which was recorded with an astronomical color video camera in Ferrara, which is a part of the Italian Meteor and TLE network. The sprite producing lightning discharge was associated with a charge moment change as large as 1300 Ckm. The charge moment was calculated from an exponentially decreasing lightning current inferred from electric field measurements in the frequency range ~ 5–30 Hz at Nagycenk observatory in Hungary.

Even though it was only a single event, it was the first simultaneous detection of radio signatures from electrons accelerated to thermal and relativistic energies above thunderclouds. The multi-sensor aspect provided us with experimental criteria on how these events can be detected without relying on optical cameras.

5.7 Future plans

Recently (in August – September 2013), we have substantially upgraded our receiving station in Rustrel by installing of a new system of two perpendicular broadband magnetic antennas measuring the horizontal magnetic field up to 90 MHz. The separation distance between the antennas is now 89 m. With this system, we have started to calculate the azimuth and elevation of the lightning HF sources considering the difference in the times of arrival and in the amplitudes of a particular event recorded by both antennas. The new arrangement of the antennas is shown in Figure 50.

This new antenna system allows us to study different fast lightning phenomena (sequences of pulses preceding the first return stroke, the inter-stroke pulse trains, the stepped leader pulses and the dominant peaks of the return strokes) with a better resolution in time, frequency and space. We also plan to complete the measurements of radiated fields of lightning discharges with simultaneous high-speed optical observations.

Fig. 50 New antenna system installed in Rustrel (France); small red rectangles represent two antennas (1,2) and the main box (DELO) containing the power supply and the data processing unit.

5.7.1 New loop antenna: type SLAVIA

The magnetic loop antenna (type SLAVIA) has a rectangular shape and its mechanical structure consists of sewage plastic tubes. The inner conductor is formed by a copper wire, which is fixed in the middle axis of the tubes. A copper tape, which is wrapped around the tubes, forms the outer conductor. The shape of the antenna is shown in Figure 51.

Fig. 51 Antenna loop type SLAVIA (Shielded Loop Antenna with a Versatile Integrated Amplifier)

We have calculated the capacitance, the inductance and the resonant frequency of the antenna type SLAVIA. This antenna has a rectangular shape (the dimensions are a = 45 cm, b =55 cm; the distances between the centers of the tubes are considered).The inner conductor of this "tube coaxial cable" represents a wire with the radius r_1 = 0.89 mm, which is fixed in the middle of the tubes. The conductive surface of the tubes represents an outer conductor with the radius r_2 = 25 mm. The capacitance of one meter of the "tube cable" C_T/l calculated from the equation (10) is 16.7 pF/m.

$$\frac{C_T}{l} = \frac{2\pi\varepsilon_0}{\ln\frac{r_2}{r_1}} \qquad (10)$$

$$\frac{L_T}{l} = \frac{\mu_0 \ln \frac{r_2}{r_1}}{2\pi} \qquad (11)$$

Using the equation (11) we obtain the inductance of one meter of the "tube cable" L_T/l = 0.67 μH/m. Now we have the inductance and the capacitance of the "tube cable" and we are able to estimate its impedance, which we need for a proper matching of the antenna to the input of the preamplifier. Using the formula $Z = \sqrt{L_T/C_T}$ we find that the impedance of the "tube cable" is ~ 200 Ω. The inductance of the loop formed by the tubes can be calculated using the formula (12).

$$L_L = \frac{\mu_0}{\pi}\left[b \ln\left(\frac{2b}{r_1}\right) + a \ln\left(\frac{2a}{r_1}\right) - 2(a+b)\right] + \\ + \frac{\mu_0}{\pi}\left[2\sqrt{a^2 + b^2} - a \operatorname{arcsinh}\left(\frac{a}{b}\right) - b \operatorname{arcsinh}\left(\frac{b}{a}\right)\right] \qquad (12)$$

Having the inductance of the loop, the inductance and capacitance of the "tube cable" we can estimate the resonant frequency of the loop using formula (13).

$$f_r = \frac{1}{2\pi\sqrt{(L_T + L_L)C_T/2}} \qquad (13)$$

The resonant frequency of the antenna loop type SLAVIA is 29.9 MHz. The calculated parameters are used for the simulation of the antenna by a model with the distributed parameters shown in Figure 52.

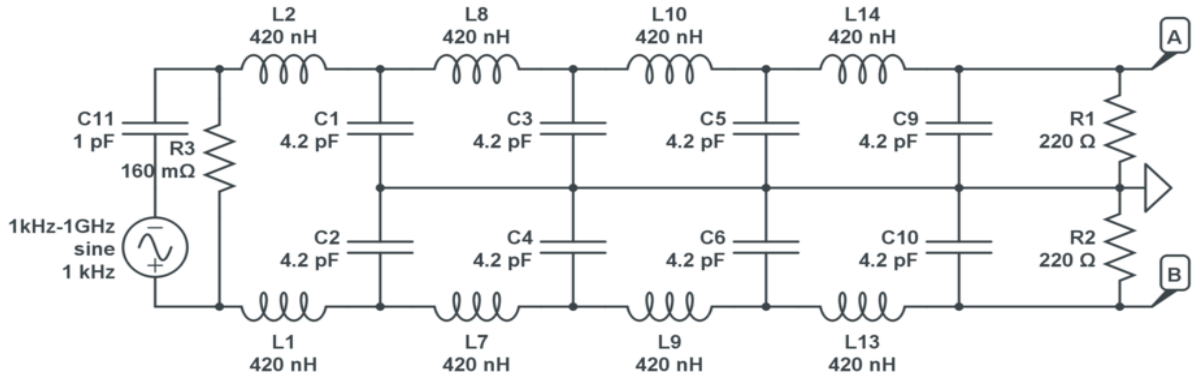

Fig. 52 Model of the antenna loop (type SLAVIA)

Now we can compare the frequency response of the model with the measurement of the frequency response of the real antenna loop (Figs. 53 and 54). The similarity of obtained curves indicates that the model represents quite accurately the properties of the loop. The antenna works well up to 50 MHz and thus it is suitable for observing the submicrosecond changes of the magnetic field, which are radiated by particular small-scale lightning discharges.

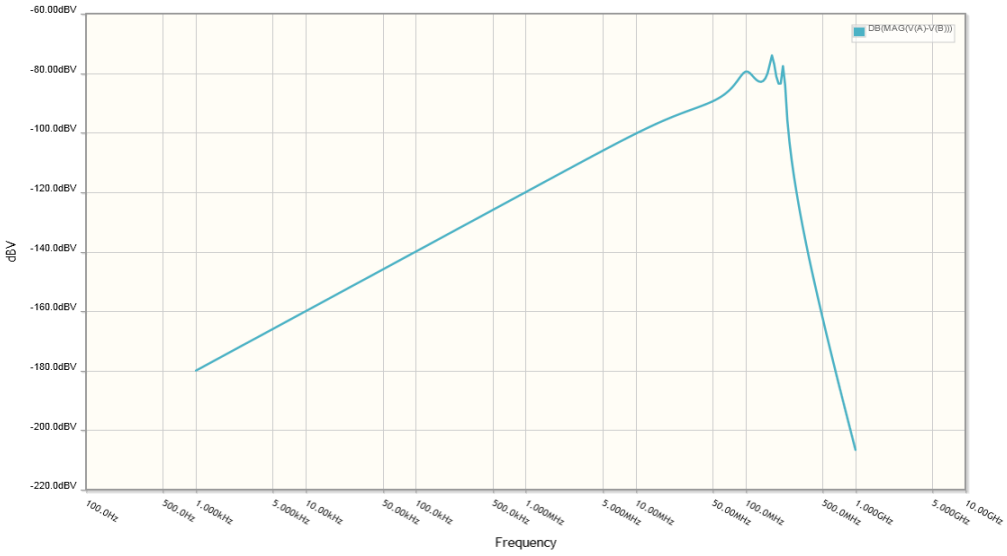

Fig. 53 The frequency response of the antenna model (type SLAVIA) with distributed parameters

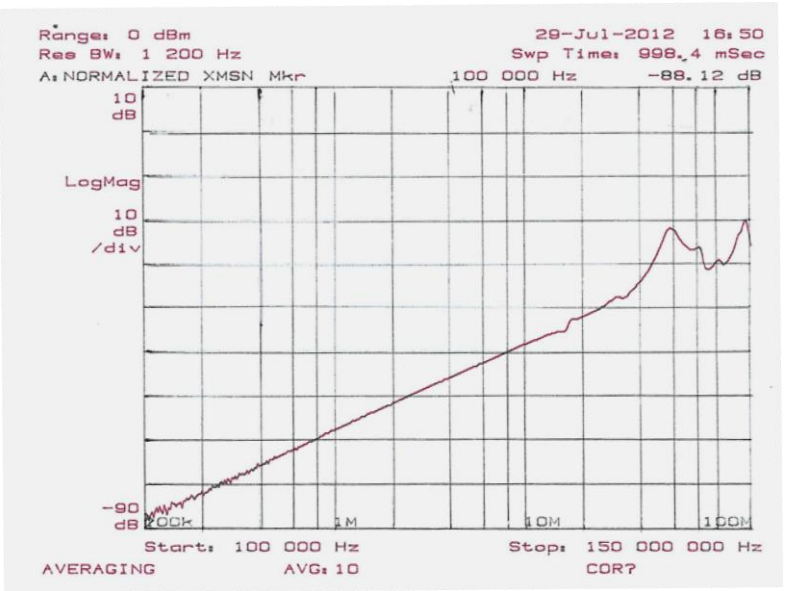

Fig. 54 The frequency response of the antenna loop (type SLAVIA)

The antenna was completed by an integrated preamplifier (Fig. 55). The digitally

controlled, variable gain amplifier AD8370 with a low noise figure, an excellent distortion performance and a wide bandwidth was used in the preamplifier design. High gain of the whole preamplifier (up to 47 dB) enables us to pre-amplify sufficiently the signals radiated by small-scale lightning discharges like the pulses described in sections 2.6.1 and 2.6.8. The gain is adjustable. The calibration curves for four preselected gains are plotted in Figure 56. The schematic drawing and the PCB design of the preamplifier are shown in Appendix B2.

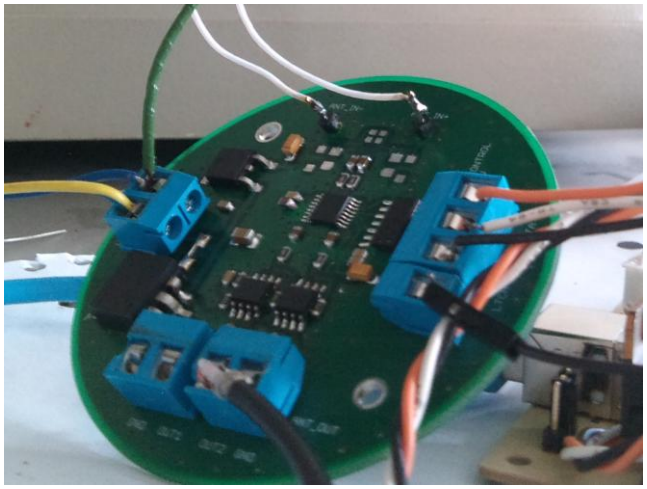

Fig. 55 Preamplifier before the integration into the antenna

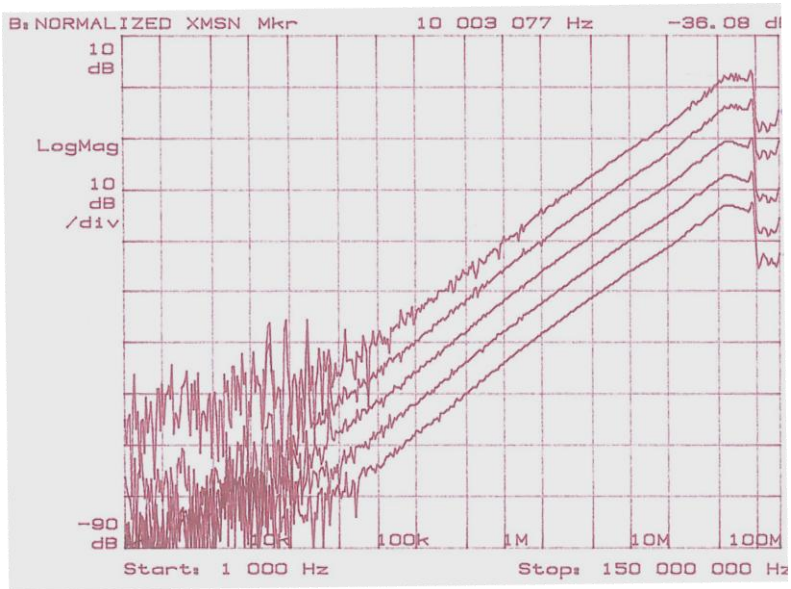

Fig. 53 Calibration curves of the preamplifier for four preselected gains

6. CONCLUSIONS

Electromagnetic signals radiated by different parts of lightning flashes were analyzed in this doctoral thesis. The signals were measured using a newly developed broad-band analyzer with a sampling interval of 12.5 ns. We studied the microsecond- and submicrosecond-scale variations of fields generated by the currents flowing in the lightning channels. We concentrated our attention on the electromagnetic pulses generated by the in-cloud currents because of their direct link to the charge distribution inside the thunderclouds. The conclusions of this thesis work are as follows:

(1) We analyzed trains of regular unipolar microsecond-scale magnetic-field pulses produced by intra-cloud lightning discharges between the return strokes. Our time resolution was more than four times better than the limit of measuring systems used in previously published studies [*Krider et al.*,1975; *Rakov et al*.,1996; and *Davis*, 1999]. A systematic analysis of variations of the inter-pulse intervals and of the peak amplitudes was done for the first time. We also analyzed properties of individual pulses and found visible asymmetries in their shapes. We proposed a possible generation mechanism of these trains of pulses based on a hypothesis that periodical charge structures were present in the thundercloud. This mechanism can explain the observed evolution of peak amplitudes and inter-pulse intervals and also the observed asymmetry in the shapes of pulses. The results were published in an international peer-reviewed journal [*Kolmasova and Santolik*, 2013] - see Appendix C1.

(2) We analyzed the pulse sequences occurring prior to the first return stroke. We observed an extremely short duration of the pre-stroke pulse activity in comparison with the previously published studies [*Gomes*, 1998; *Baharudin*, 2010]. We proposed a hypothesis that the duration of the pre-stroke pulse activity was dependent on the height of the thunderclouds. Our explanation was supported by the Lightning Mapping Array (LMA) data showing a very low localized origin of the return strokes. The results were presented at an international conference IAGA 2013 – see Appendix C.

(3) We tried to find a link between the properties of the lightning current channel and

the shapes of the dominant return stroke peaks in the magnetic-field waveform and in the waveforms of the time derivative of the magnetic field. These measurements combined with a simplified transition line model of the lightning current channel show that the lightning channel isn't necessarily shared by the subsequent strokes formally belonging to the same flash. This hypothesis needs to be verified by simultaneous electromagnetic and optical measurements of multiple stroke flashes. The results were presented at an international conference AGU 2012 – see Appendix C.

(4) We have recorded a case of the bouncing wave type discharge during our summer campaign in Rustrel, France. Analysis of this case initiated a case study of the electron acceleration above thunderclouds by *Fullekrug et al.* [2013] – see Appendix C2. The observed case lacks some features typical for compact intra-cloud discharges but other receivers in France, UK, and Hungary recorded signatures whish are consistent with a presence of a relativistic electron beam. A subsequent sprite was also observed by an optical camera from Italy.

This thesis work opens a clear perspective of our future work. We will continue to analyze the electromagnetic manifestations of fast in-cloud processes. The new arrangement of our receiving antennas will allow us to estimate the source locations of the pulses by considering the differences of the time of arrival and in the amplitudes of particular pulses recorded by different antennas. We expect that we will be able to recognize a possible movement of the sources. This will be done for the first time with high resolution data. We hope to have a new tool for the investigation of the small-scale properties of the charge distribution inside the thunderclouds.

.

APPENDIX A My personal contribution to common publications and to the development of the instrumentation

Publication C1:

- selection of the waveforms containing the trains of pulses
- estimation of the properties of the trains
- analysis of the properties of the trains
- comparison of obtained results with previously published studies

Publication C2:

- selection of the waveform containing the bouncing wave type discharge
- analysis of the properties of the particular bouncing wave type discharge

Development of the instrumentation:

- design of the analog part of the analyzer
- testing of the performance of the analyzer
- technical documentation
- design of the preamplifier
- installation of the ground-based measurements
- calibration of the antenna system

My work was supported by the international cooperation program of the ASCR grant M10042120 and by the GACR project 205-09-1253.

APPENDIX B Schematic drawings and PCB design

APPENDIX B1 Schematic drawing and PCB design of the analyzer

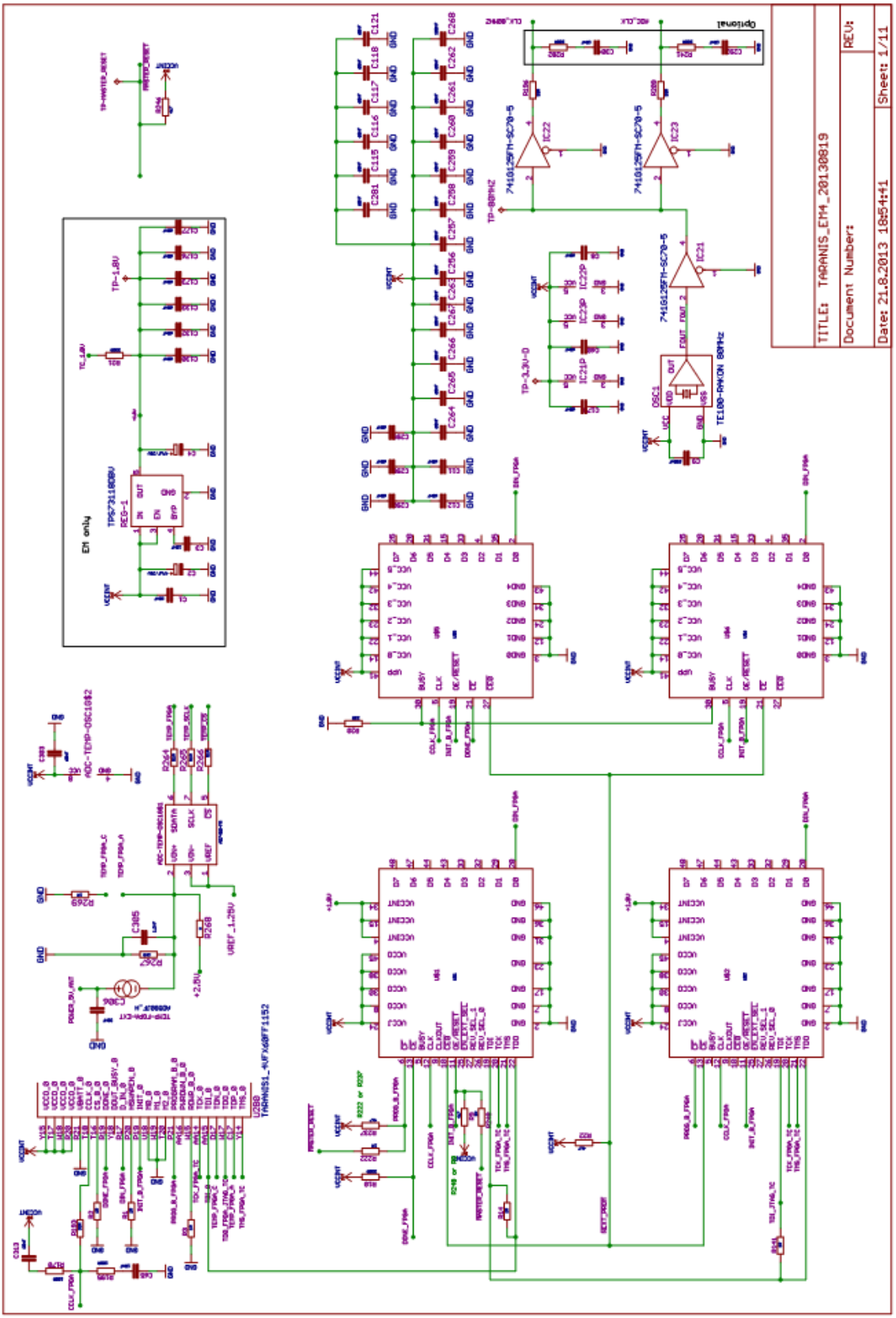

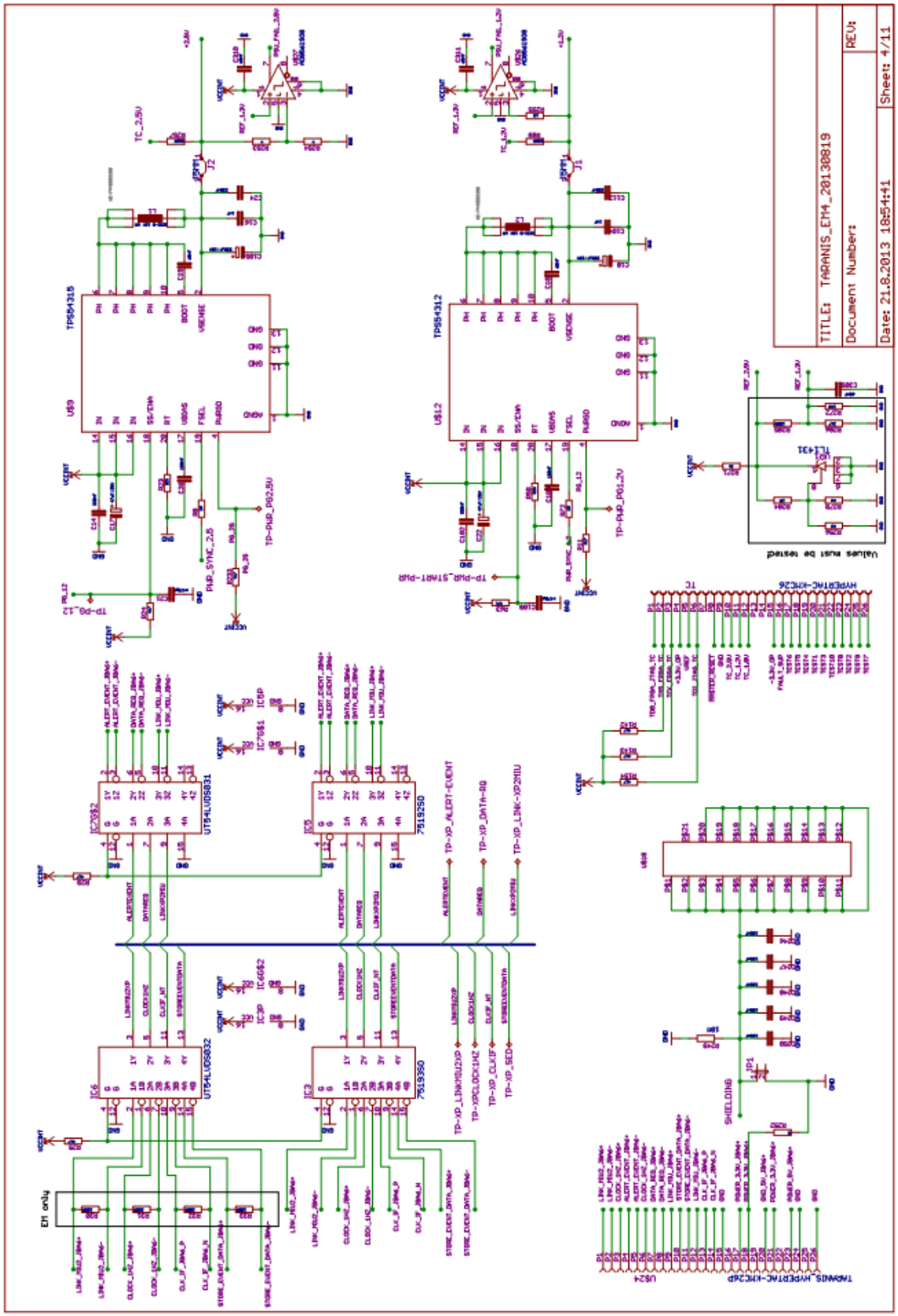
TITLE: TARANIS_EM4_20130819
Document Number:
REV:
Date: 21.8.2013 18:54:41
Sheet: 4/11
TARANIS_HYPERTAC-KHC24P
HYPERTAC-KHC24
SHIELDING
TP-XP_ALERT-EVENT
TP-XP_DATA-RQ
TP-XP_LINK-XP2MIU
TP-XP_LINKMIU2XP
TP-XPCLOCK1MZ
TP-XP_CLKIF
TP-XP_SED

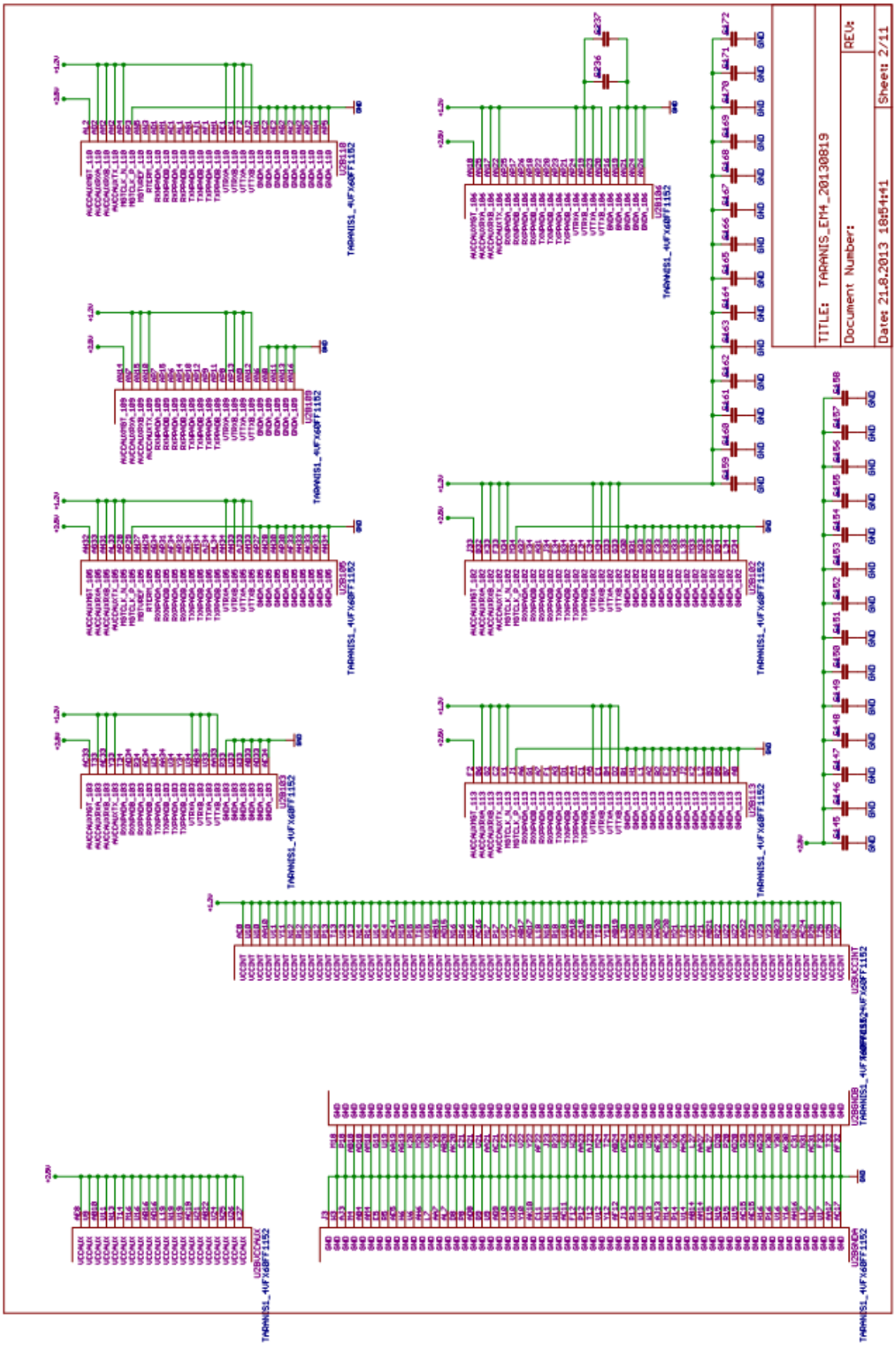
TITLE: TARANIS_EM4_20130819
Document Number:
REV:
Date: 21.8.2013 18:54:41
Sheet: 2/11

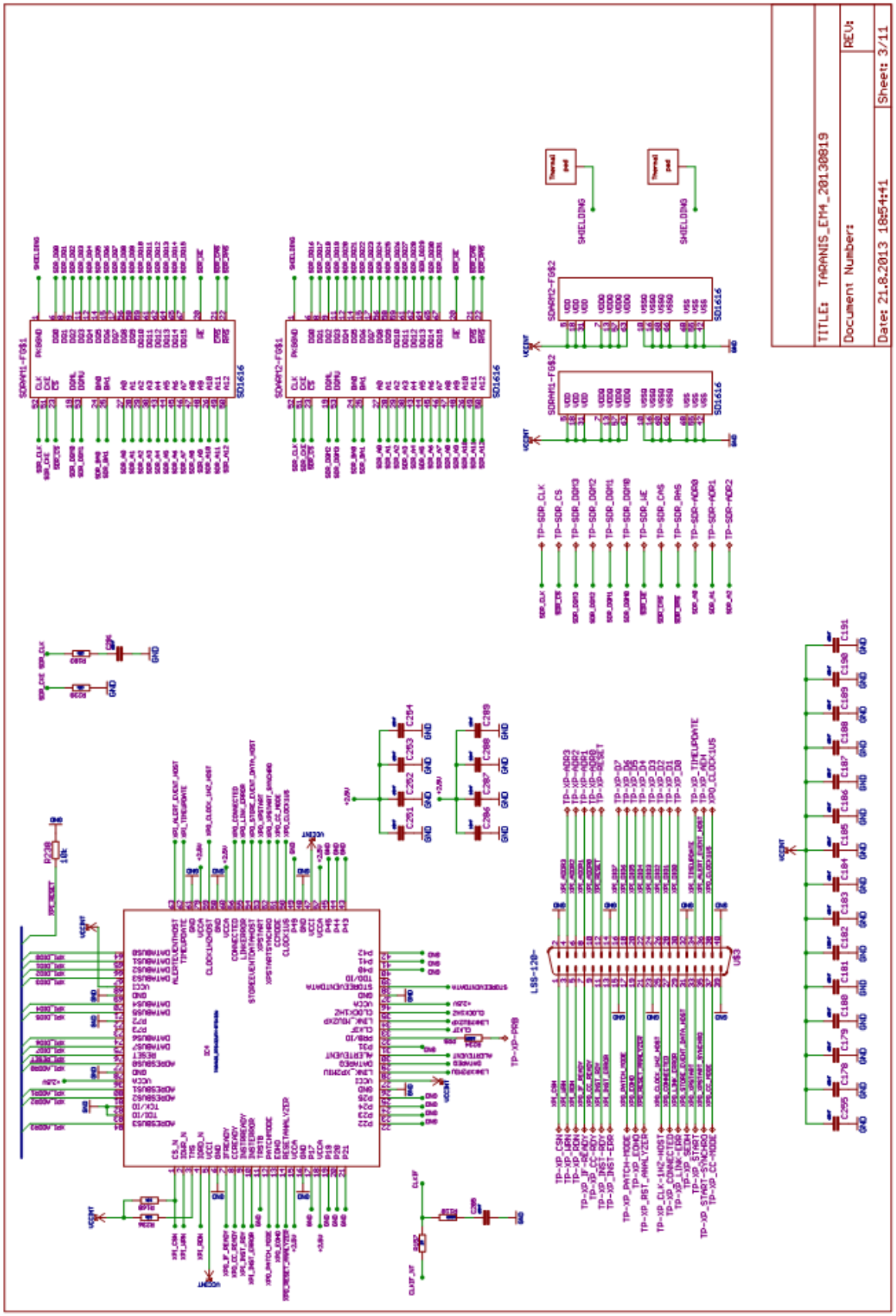
TITLE: TARANIS_EM4_20130819
Document Number:
REV:
Date: 21.8.2013 18:54:41
Sheet: 3/11

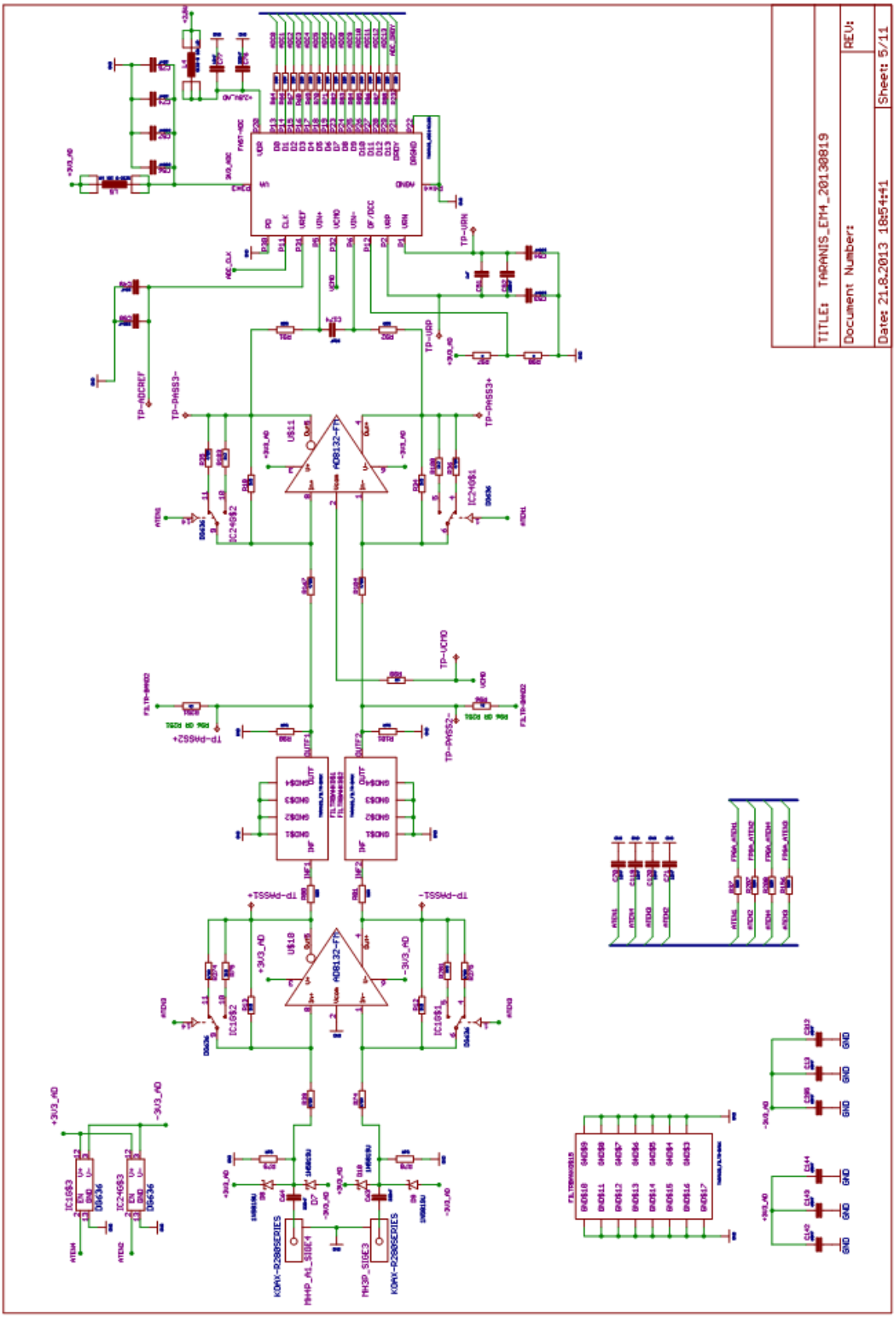
TITLE: TARANIS_EM4_20130819
Document Number:
REV:
Date: 21.8.2013 18:54:41
Sheet: 5/11

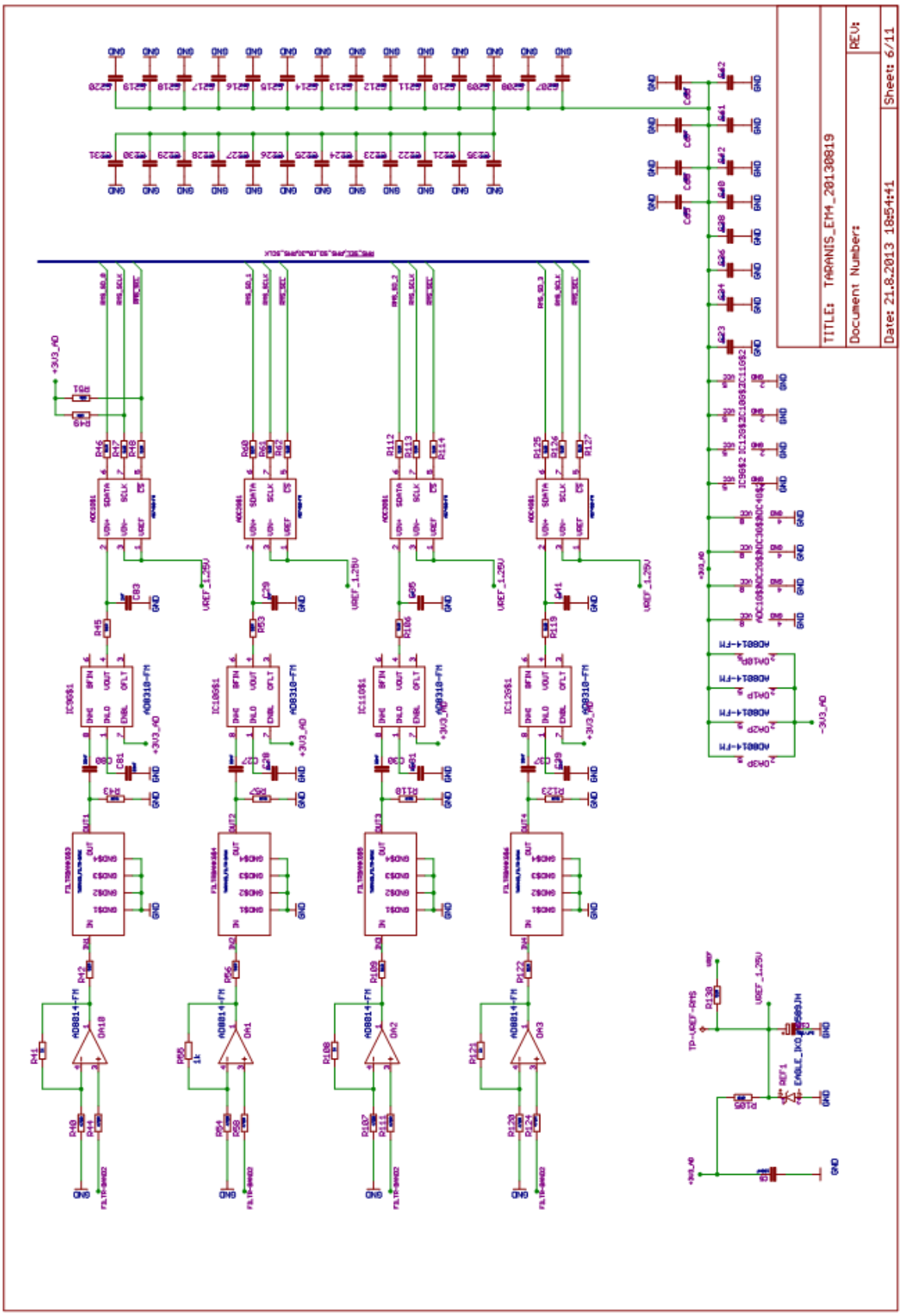
TITLE: TAPANIS_EM4_20130819
Document Number:
REV:
Date: 21.8.2013 18:54:41
Sheet: 6/11

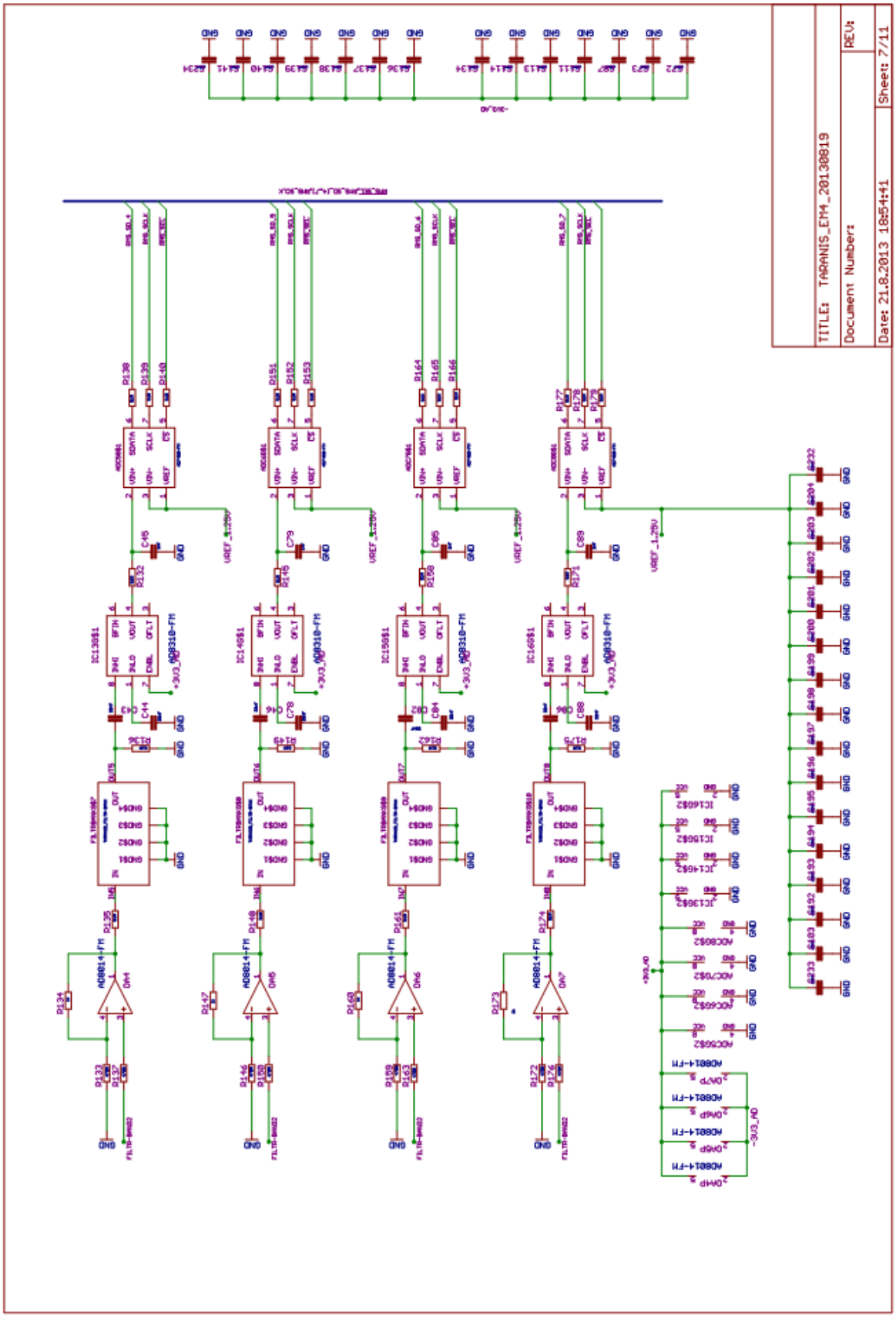
TITLE: TAPANIS_EM4_20130819
Document Number:
REV:
Date: 21.8.2013 18:54:41
Sheet: 7/11

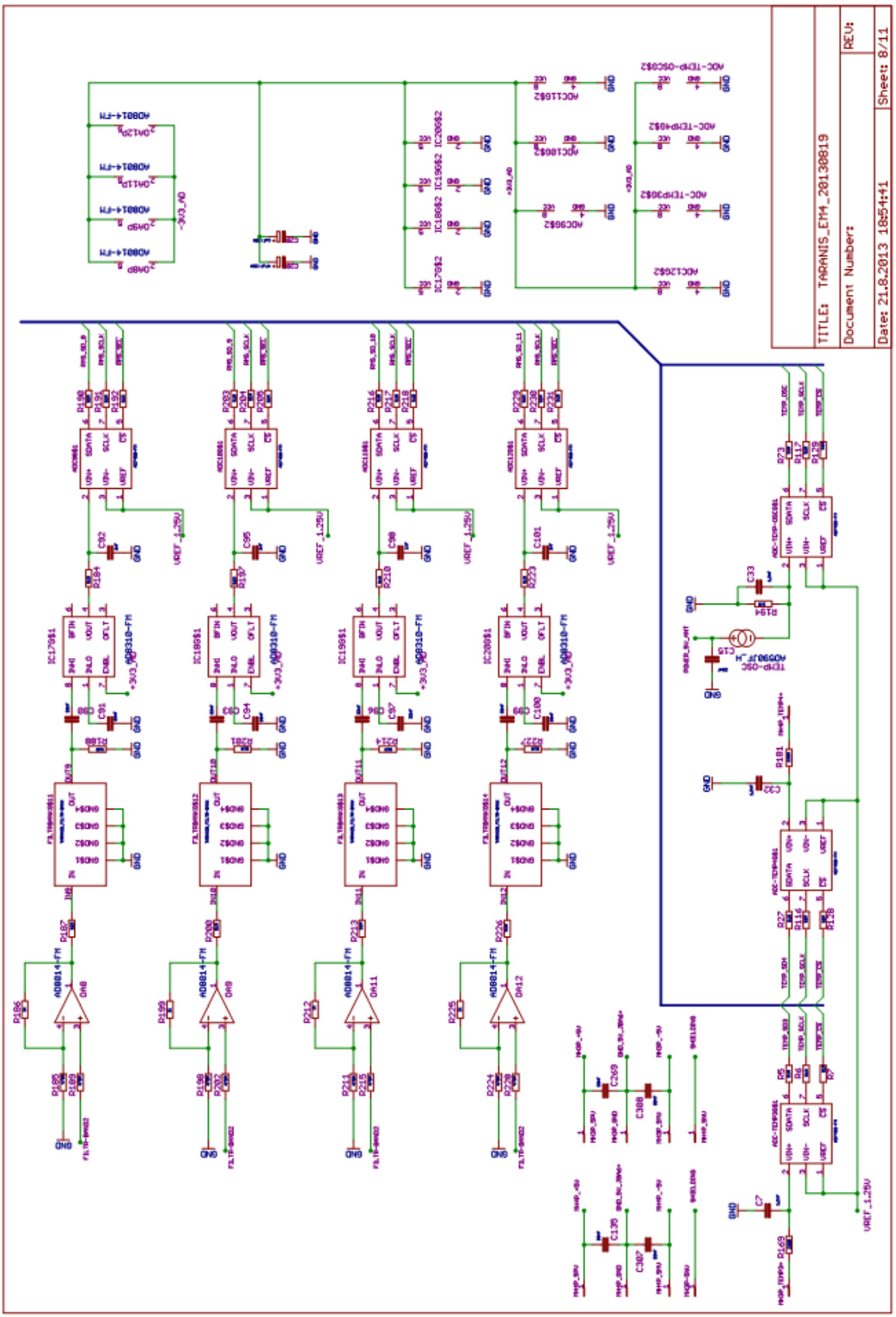
TITLE: TARANIS_EM4_20130819
Document Number:
REV:
Date: 21.8.2013 18:54:41
Sheet: 8/11

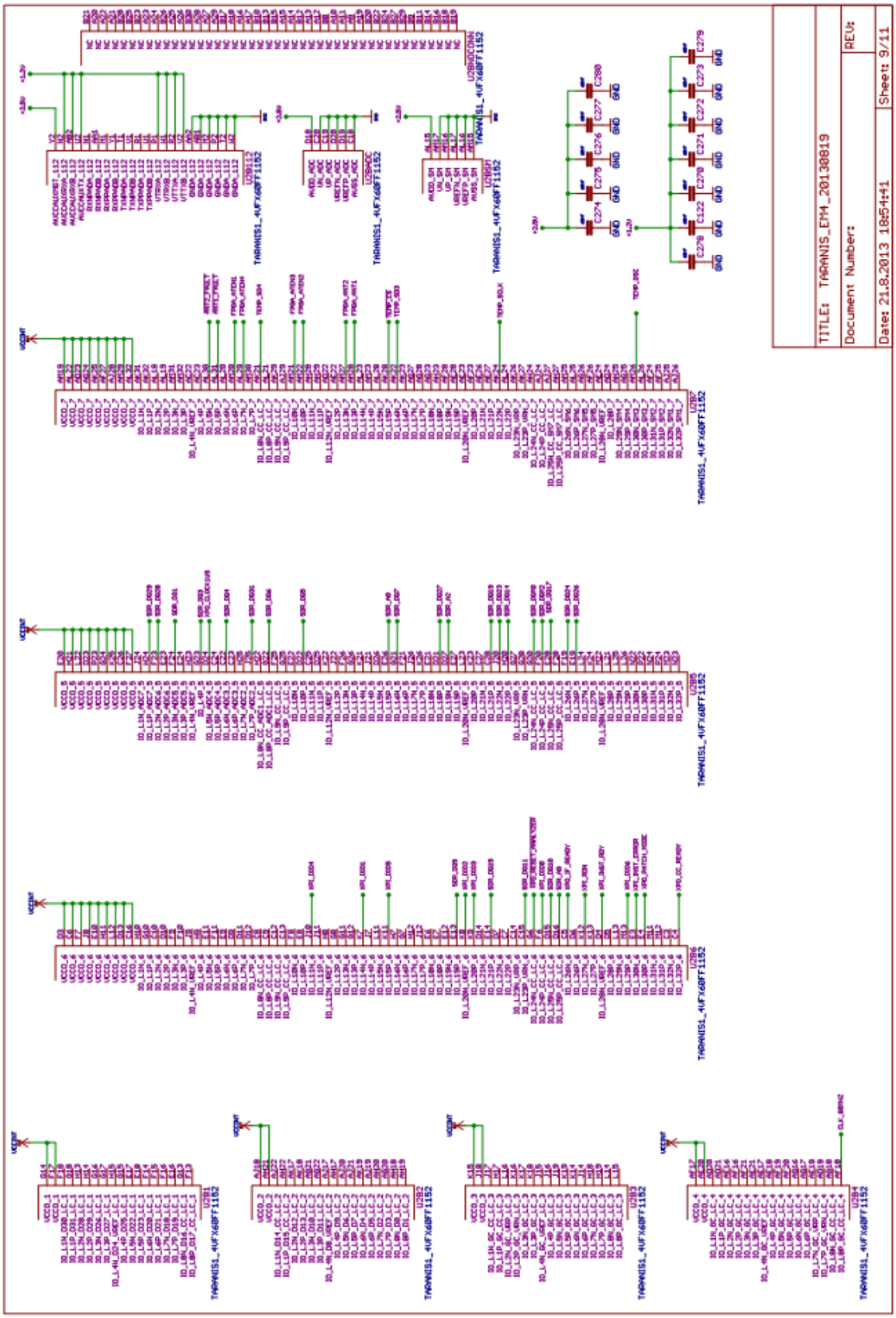
TITLE: TAMMIS_EM4_20130819
Document Number:
REV:
Date: 21.8.2013 18:54:41
Sheet: 9/11

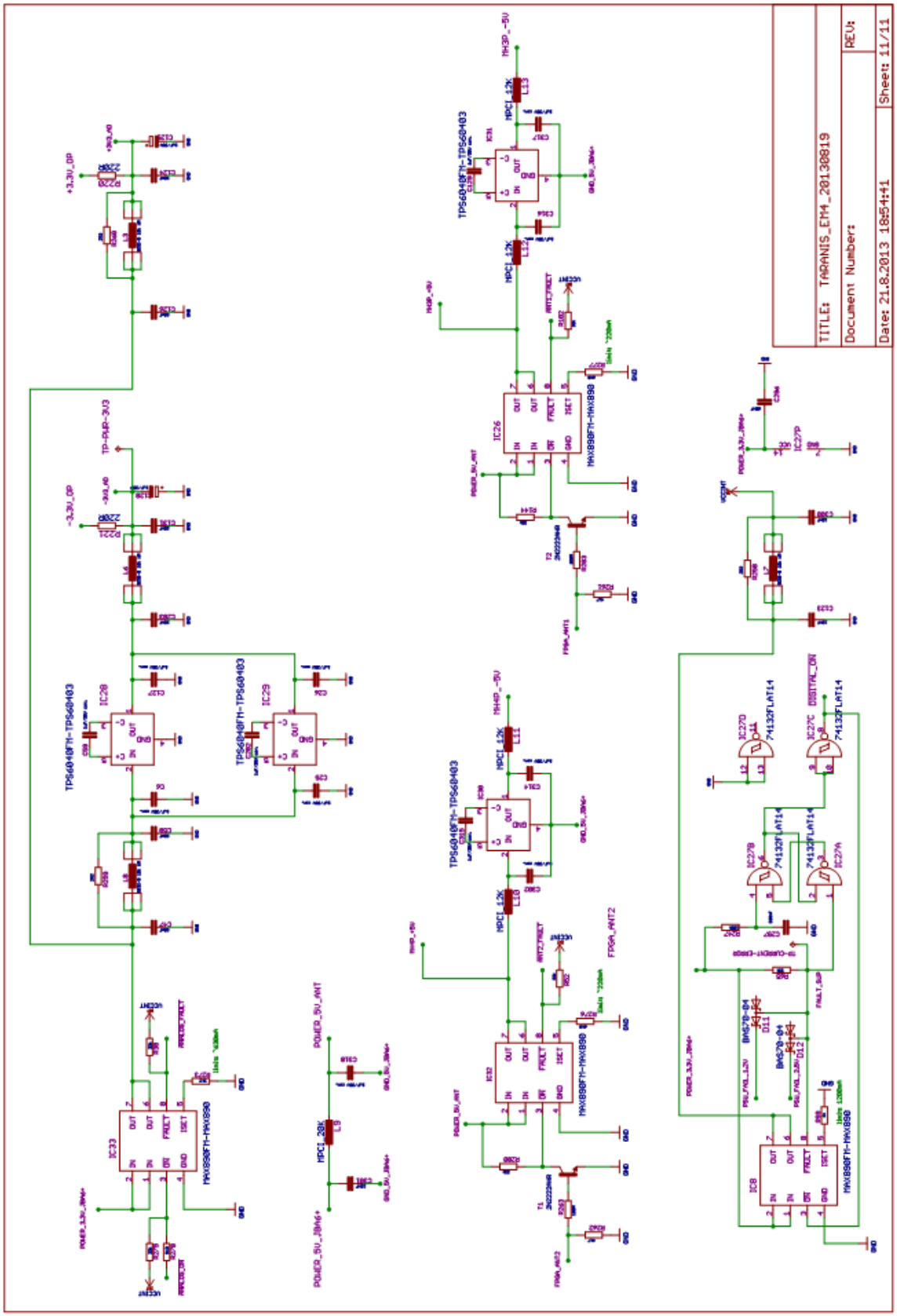
TITLE: TARANIS_EM4_20130819
Document Number:
REV:
Date: 21.8.2013 18:54:41
Sheet: 11/11

PCB design of the analyzer: component placement (TOP SIDE)

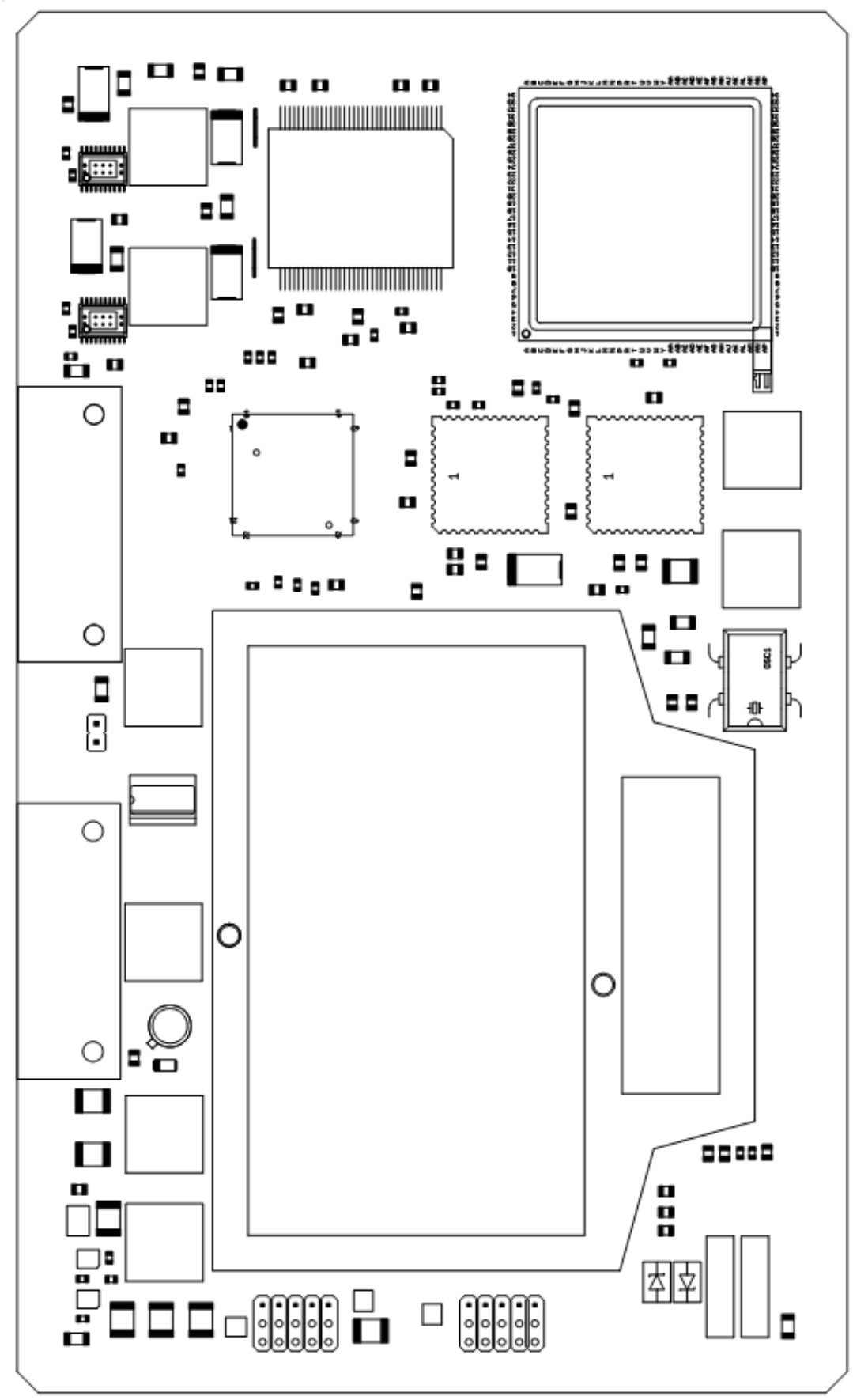

PCB design of the analyzer: component placement (BOTTOM SIDE)

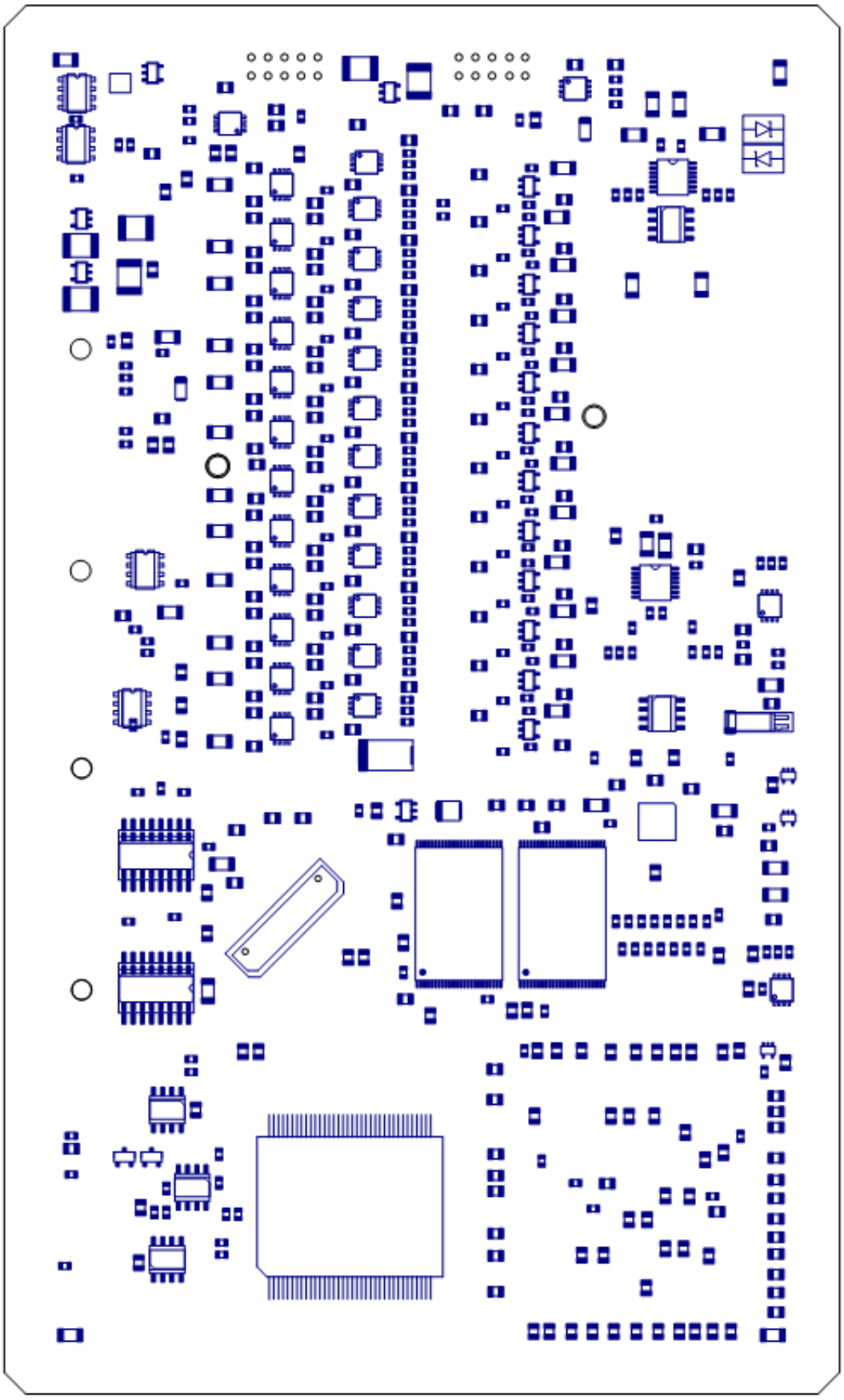

APPENDIX B2 Schematic drawing and PCB design of the preamplifier

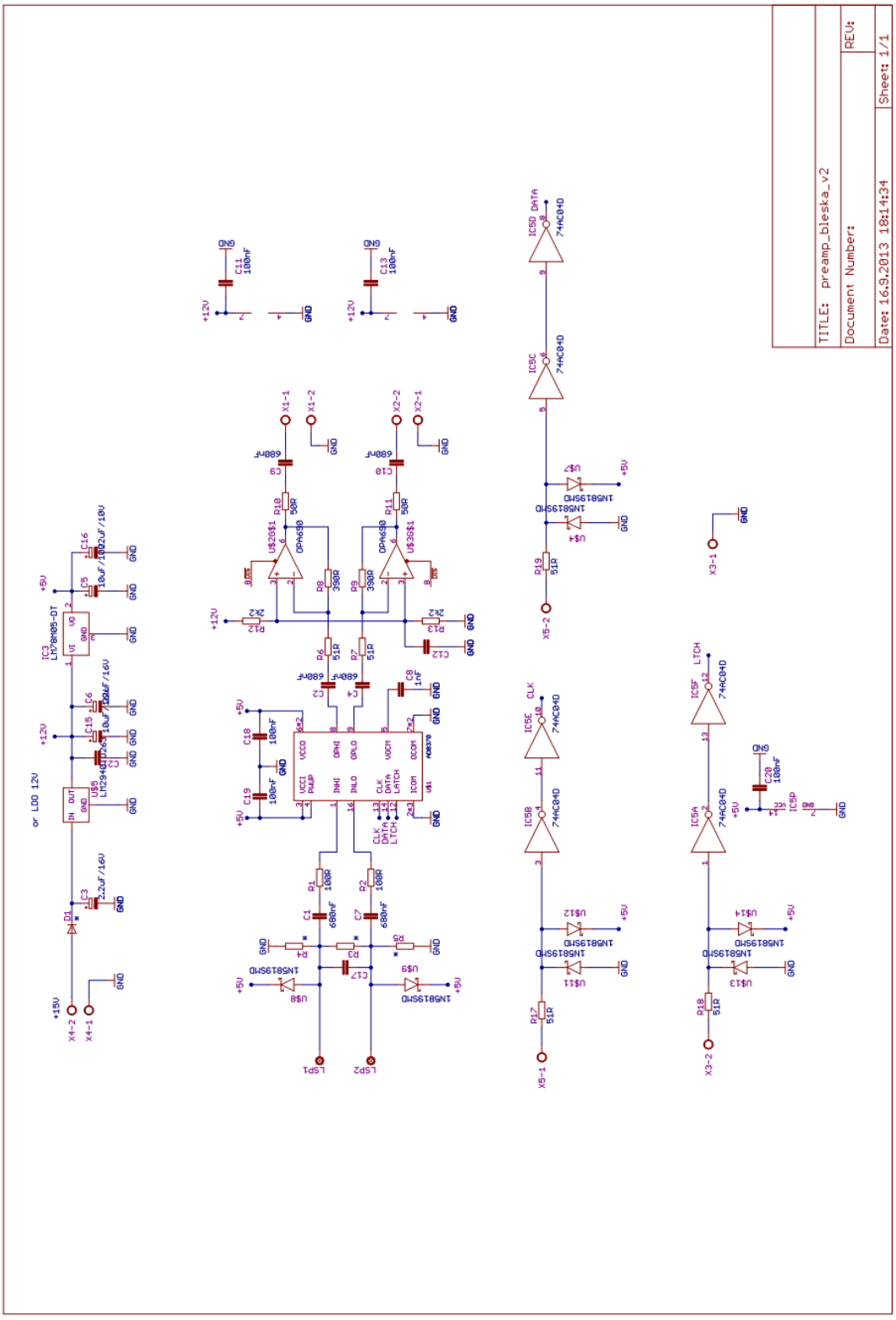

PCB design of the preamplifier: component placement (TOP SIDE)

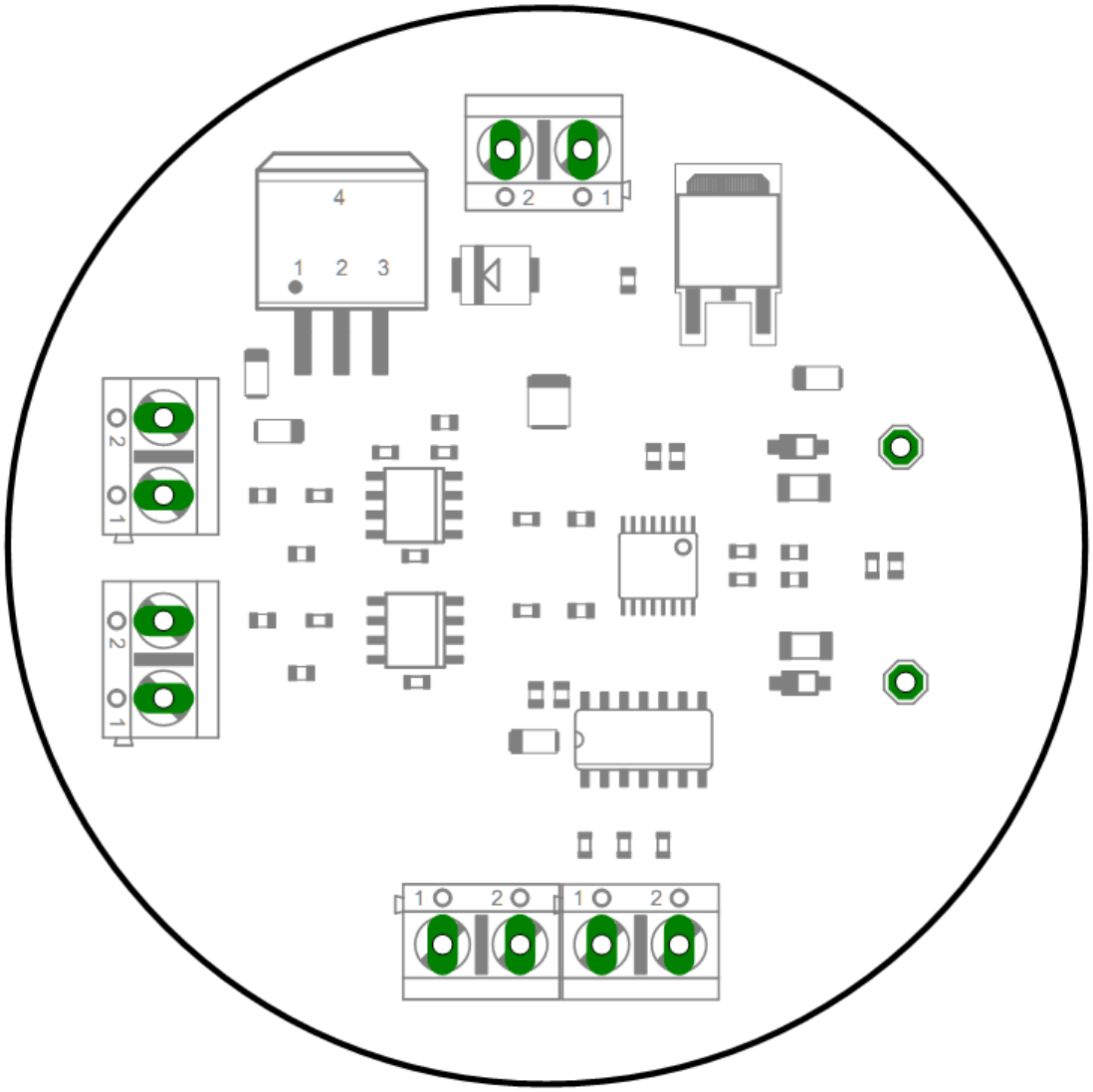

APPENDIX C List of publications

Publications in journals with impact factor:

(C1) Kolmasova, I. and O. Santolik (2013), Properties of unipolar magnetic field pulse trains generated by lightning discharges, *Geophys. Res. Lett., 40*, 1637–1641, doi:10.1002/grl.50366.

(C2) Fullekrug, M., I. Kolmasova, O.Santolik, T. Farges, J. Bor, A. Bennett, M. Parrot, W. Rison, F. Zanotti, E. Arnone, A.Mezentsev, R. Lan, L. Uhlir, G. Harrison, S. Soula, O. van der Velde, J.-L. Pincon, Ch. Helling, and D. Diver (2013), Electron acceleration above thunderclouds, *Environ. Res. Lett.* 8, doi:10.1088/1748-9326/8/3/035027.

The contributions of co-authors were equal in all cases.

Publications in refereed journals: (C1), (C2)

Publications excerpted in WOS: (C1)

Other:

(C3) Kolmasova, I., O. Santolik, L. Uhlir, and R. Lan (2013), Properties of trains of preliminary breakdown pulses occurring prior to the first stroke of negative cloud-to-ground lightning flashes, XII scientific Assembly IAGA 2013, Merida, Mexico.

(C4) Kolmasova, I., O. Santolik, L. Uhlir, R. Lan, J. Base, F. Hruska, and J. L. Rauch (2013), Broad band high frequency analyzers for measurements of lightning-induced signals on TARANIS satellite, COBRAT balloons and on the ground, AOGS 10th Annual Meeting, June 2013, Brisbane, Australia.

(C5) Kolmasova, I., O. Santolik, and P. Novak (2012), Fine structure of magnetic field waveforms from negative multiple stroke lightning flashes, Abstract AE13A-0364 presented at 2012 Fall Meeting, AGU, San Francisco.

(C6) Kolmasova, I., O. Santolik, L. Uhlir, R. Lan, J. Chum, J. Base, F. Hruska, and P. Novak (2012), Broadband analyzer for satellite, balloon and ground-based measurements of electromagnetic manifestations of thunderstorms, 5th VERSIM (VLF/ELF Remote Sensing

of the Ionosphere and Magnetosphere) Workshop September 2012, Sao Paulo, Brazil.

(C7) Kolmasova, I. and O. Santolik (2012), The submicrosecond structure of unipolar magnetic field pulse trains generated by lightning discharges, 1st TEA-IS (Thunderstorm Effects on the Atmosphere-Ionosphere System) Summer school June 2012, Malaga, Spain, published in the TEA-IS summer school abstract book.

(C8) Santolik, O., I. Kolmasova, and P. Novak (2012), Fine structure of magnetic field waveforms from the first return strokes of inland lightning, 1st TEA-IS (Thunderstorm Effects on the Atmosphere-Ionosphere System) Summer school, June 2012, Malaga, Spain published in the TEA-IS summer school abstract book.

(C9) Kolmasova, I., O. Santolik, and P. Novak (2012), Bursts of Regular Magnetic Field Pulses Produced by Lightning Discharges, EGU General Assembly 2012, held 22-27 April, 2012 in Vienna, Austria., p.1417, 2012EGUGA..14.1417K.

(C10) Kolmasova, I., O. Santolik, J. Chum, L. Uhlir, F. Hruska, J. Base, P. Novak, and J. L. Rauch (2011) , Electric and magnetic fields from lightning return strokes measured in Prague, Abstract AE33A-0279 presented at Fall Meeting AGU 2011, San Francisco, Calif., 8-13 Dec, 2011AGUFMAE33A0279K.

(C11) Kolmasova, I., O. Santolik, J. Chum, L. Uhlir, F. Hruska, J. Base, P. Novak, and J. L. Rauch (2011), Electric and magnetic fields from lightning return strokes measured by ground based version of the TARANIS IME-HF analyzer, TEA-IS, Thunderstorm Effects on the Atmosphere-Ionosphere System, November 2011, Leiden, Netherlands.

(C12) Kolmasova, I., O. Santolik, J. Chum, L. Uhlir, F. Hruska, J. Base, and J. L. Rauch (2011), First results of the ground-based measurements of the IME-HF analyzer XXXth URSI General Assembly and Scientific Symposium, July 2011, Istanbul, Turkey, Published in XXXth URSI General Assembly and Scientific Symposium Proceedings.

(C13) Kolmasova, I., J. Chum, O. Santolik, F. Hruska, and J. L. Rauch (2010), IME-HF Analyser for the TARANIS Satellite, American Geophysical Union, Fall Meeting 2010, abstract AE21B-0281, 2010AGUFMAE21B0281K.

APPENDIX C1 Kolmašová, I. and O. Santolík (2013)

Kolmašová, I. and O. Santolík (2013), Properties of unipolar magnetic field pulse trains generated by lightning discharges, *Geophys. Res. Lett.*, *40*, 1637–1641, doi:10.1002/grl.50366.

Properties of unipolar magnetic field pulse trains generated by lightning discharges

Ivana Kolmašová[1] and Ondřej Santolík[1,2]

Received 1 February 2013; revised 13 March 2013; accepted 13 March 2013.

[1] We analyze and describe trains of regular unipolar microsecond-scale magnetic field pulses produced by intracloud lightning discharges. Waveforms of the magnetic field are measured using a newly developed broadband analyzer with a sampling interval of 12.5 ns. The observed trains contained several tens of pulses, and the time interval between neighboring pulses typically varied between 1 and 10 μs. The amplitude of the pulses also varied by 1 order of magnitude. A systematic analysis of these variations is done for the first time. The interpulse interval is usually increasing (on average by 4.1 μs during a train), and the pulse amplitude is decreasing (on average by 15% of the maximum value within a given train). We propose a possible generation mechanism based on a hypothesis that periodical charge structures are present in the thundercloud. This mechanism can explain the observed evolution of peak amplitudes and interpulse intervals. **Citation:** Kolmašová, I., and O. Santolík (2013), Properties of unipolar magnetic field pulse trains generated by lightning discharges, *Geophys. Res. Lett.*, *40*, doi:10.1002/grl.50366.

1. Introduction

[2] Trains of electric field and magnetic field pulses were found to be connected with various lightning phenomena. Preliminary breakdown pulses [*Nag and Rakov*, 2008], stepped leader pulses [*Lee et al*., 2006], dart-stepped leader pulses [*Davis*, 1999], chaotic leader pulses [*Gomes et al*., 2004], pulses produced by bouncing-wave-type lightning discharges [*Nag and Rakov*, 2009], and bursts associated with either *K* changes or *M* components were observed [*Rakov et al*., 1992, 1996]. The shapes of individual types of pulses are generally similar, but the lengths of the rising and falling edges, the widths of the pulses, and the interpulse intervals vary from microsecond to millisecond scales. These transient events may play an important role in the complexity of the atmospheric electromagnetic fields [*Füllekrug and Fraser-Smith*, 2011].

[3] The trains of pulses occurring in cloud flashes were first studied by *Krider et al*. [1975], who compared the time intervals between neighboring pulses and the interval between bright steps in dart-stepped leader photographed, and reported by *Schonland* [1956]. Based on the similarity of these time intervals, *Krider et al*. [1975] suggested that a dart-like *K* change developing in a stepped manner could produce the observed uniform pulses. Similar trains in electric field waveforms of cloud-to-ground and intracloud lightning discharges were observed and reported by *Rakov et al*. [1992, 1996]. According to these studies, the movement of charge in the existing intracloud lightning channel between the strokes can give rise to the microsecond-scale electromagnetic pulses. The pulses occurring during the *K* step and *M* hook field changes differed in terms of amplitudes, regularity, and intervals between neighboring pulse trains. *Rakov et al*. [1992] found that 53% of the recorded *M* components and only 24% of the recorded *K* changes were accompanied by the microsecond-scale pulse activity.

[4] *Krider et al*. [1975] measured the time interval between successive pulses in both maritime (Florida) and continental (Arizona) conditions. The mean values of interpulse intervals were similar: 6.1 μs for the seaside and 5.1 μs for the inland, but the distribution of interpulse intervals for continental conditions was narrower than the distribution for maritime conditions. Thanks to to the multipoint measurement (five stations), *Davis* [1999] was able to estimate locations and speeds of the movement of the leaders from his measurements of the time derivative of the electric field. Due to a short length of the waveform records (205 μs only), he limited his study to the interpulse interval. The obtained averages of the interpulse intervals were 2.8, 7.6, and 5.1 μs for trains in dart-stepped leaders, in leaders preceding new ground termination, and for trains in intracloud (IC) discharges, respectively.

[5] The amplitude of the pulses and the spacing between successive pulses are changing with time within a given train. *Rakov et al*. [1992, 1996] reported that the amplitudes of the pulses and the pulse repetition rates tended to decrease with time. *Davis* [1999] not only showed cases of growing interpulse intervals in both dart-stepped leaders and IC leaders but also showed examples of leaders preceding new ground termination which did not exhibit any change of the interpulse interval. The growing intervals were consistent with his measurements of a decreasing speed of the leader movement assuming that the length of the steps in the propagation of the leaders remained unchanged. This assumption was based on optical observations of *Schonland* [1956], who reported approximately equidistant steps of about 10 m. *Wang et al*. [2010] classified four types of bursts according to the evolution of the interpulse interval and the polarity of the pulses and assigned them to different lightning phenomena. The pulses belonging to a given train usually have the same polarity. *Rakov et al*. [1996] reported that the trains with negative and positive pulses occurred with the same probability. They also noted occasional reversals of the polarity of pulses

[1]Institute of Atmospheric Physics, Academy of Sciences of the Czech Republic, Prague, Czech Republic.
[2]Faculty of Mathematics and Physics, Charles University, Prague, Czech Republic.

Corresponding author: I. Kolmašová, Institute of Atmospheric Physics, Academy of Sciences of the Czech Republic, Boční II 1401, 141 31 Prague 4, Czech Republic. (iko@ufa.cas.cz)

0094-8276/13/10.1002/grl.50366

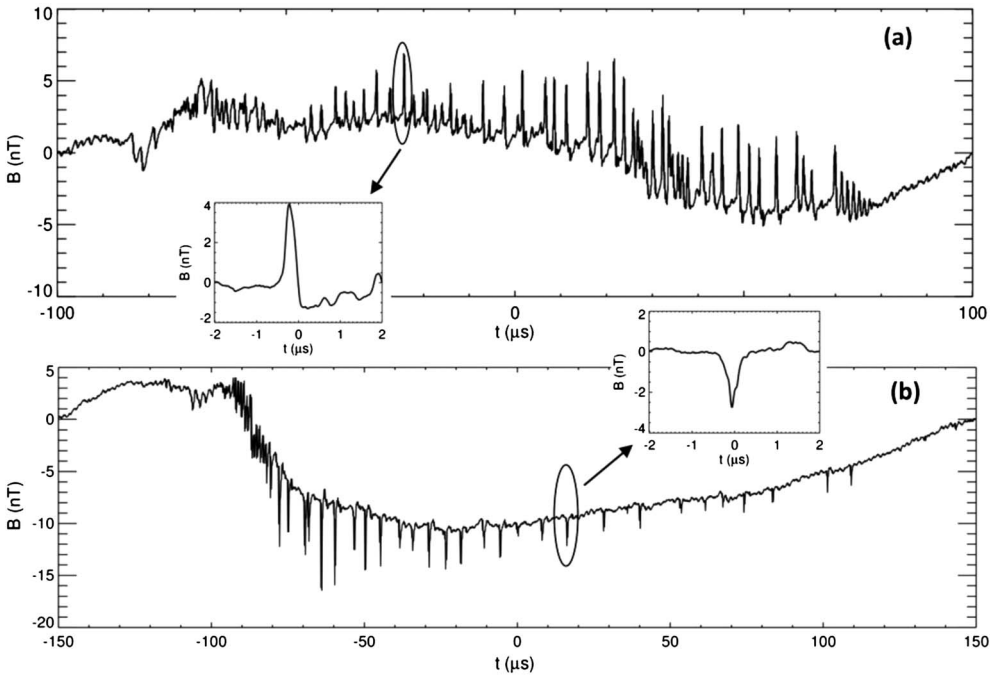

Figure 1. Examples of the trains with (a) positive and (b) negative pulse polarities. Detailed examples of individual pulses are shown in the insets.

within some of the observed trains. *Davis* [1999] found that for 66% of pulses, the polarity was consistent with the direction of the current flowing in the channel. The reversal in the polarity was attributed to changes of the channel geometry and to a possible development of branches.

[6] In the present study, we analyze properties of the trains of regular unipolar microsecond-scale magnetic field pulses produced by intracloud lightning phenomena in continental conditions (Prague, Czech Republic). We use a new broadband analyzer with a sampling interval of 12.5 ns. Our time resolution is by more than 1 order of magnitude better than the limit of measuring systems used in studies of *Krider et al*., 1975] and *Rakov et al*., 1996]. Our time resolution is also 4 times better than the resolution of *Davis* [1999], and the length of our recordings is about 3 orders of magnitude larger than in his data. Our measurements are therefore suitable for a clear identification of individual microsecond-scale pulses in the trains and, at the same time, for long recordings of multiple trains in a sequence.

[7] In section 2, we describe our experimental setup, and in section 3, we summarize our results concerning the time intervals between the trains, their lengths, the number of pulses in the individual trains, and the interpulse time intervals. In section 4, we present a systematic analysis of the evolution of interpulse intervals and pulse amplitudes within the trains, and, finally, in section 5, we discuss our results.

2. Instrumentation

[8] For our measurements, we use a magnetic field antenna coupled with a ground-based version of a broadband high-frequency analyzer which is being developed for the TARANIS spacecraft (http://babeta.ufa.cas.cz/TARANIS; http://smsc.cnes.fr/TARANIS). The analog part of the analyzer includes two fully differential amplifiers, two antialiasing filters, and a set of 12 band-pass filters with amplifiers and RMS detectors. The signals from these detectors are used as input data for a flexible event detection algorithm. The core of the digital part of the analyzer is a field-programmable gate array, where the sampled and digitized signals are processed. The analyzed frequency band goes from 5 kHz to 37 MHz. The signal is sampled at 80 MHz, and parts of the waveforms are recorded based on the results of the event detection algorithm. This procedure provides us with 120 ms long waveforms every 5 min. The time assignment is done by a GPS receiver connected to the analyzer. The magnetic field antenna is formed by a single loop of a 50 Ω coaxial cable with a loop diameter of 1 m (a similar antenna system was used by *Krider and Noggle* [1974]). We approximate the voltage induced in the antenna loop by the product of the loop area and the magnetic field time derivative dB/dt in the direction perpendicular to the loop. We numerically integrate the waveform records to estimate the B component in this direction. The integrated noise of the analyzer is about 0.14 nT in the frequency range from 1 MHz (the reciprocal value of the typical pulse time scale) to 37 MHz (upper frequency limit of our measurement).

3. Properties of the Pulse Trains

[9] Our original data set consisted of 1409 regular pulses in 33 trains recorded during two thunderstorms in summer 2011 in Prague, Czech Republic. We do not have reliable information about the distances to the lightning phenomena that generated the recorded pulses. However, based on the most distant return strokes recorded by the Central European Lightning Detection Network (P. Novák, private communication, 2011) and observed during the same campaign, we can estimate that the distances to the sources of the observed high-frequency signals were probably less than 20 km.

[10] The amplitudes of all the pulses and the times of their peak values were estimated from the integrated B waveforms. To record a pulse, we have chosen a threshold of

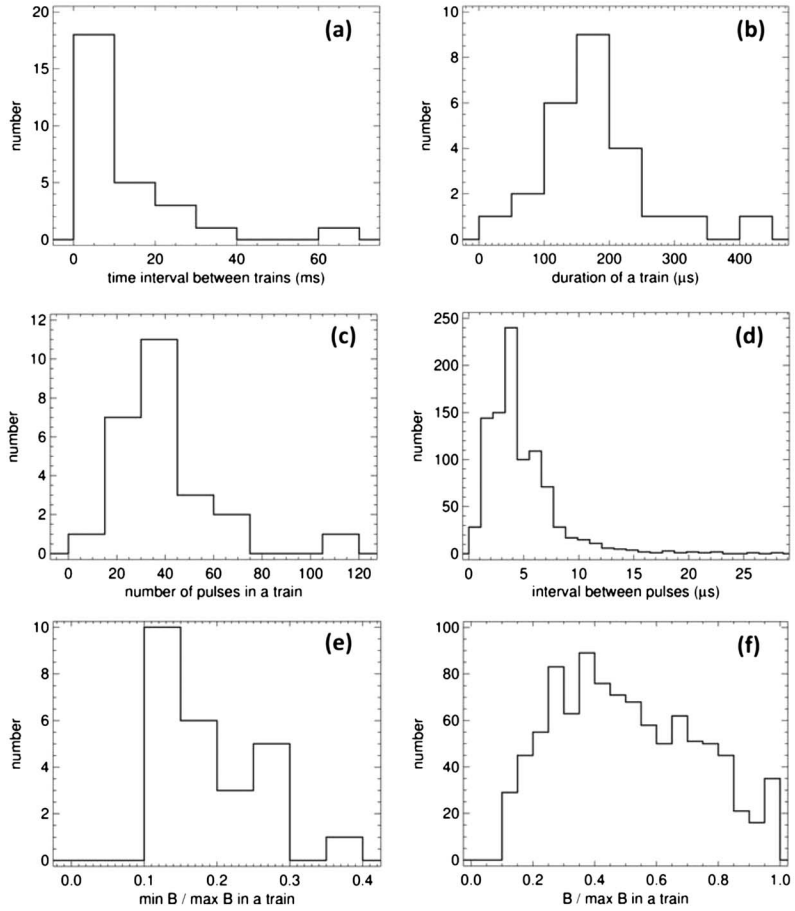

Figure 2. (a)Time interval between the neighboring trains. (b) Duration of the trains. (c) Number of pulses in the trains. (d) Time interval between neighboring pulses in each train. (e) Ratio of the largest to the smallest amplitude of pulses in each individual train. (f) Pulse amplitudes normalized by their maximum in each individual train.

1 nT for the peak amplitude. This threshold is several times larger than the noise level of the analyzer. Each individual pulse is considered to be unipolar if the immediately following overshoot of the opposite polarity does not exceed one half of the peak amplitude of the original pulse. A group of pulses is considered to form an individual train when the time interval between the last pulse of a train and the first pulse of the next train exceeds 80 μs. This threshold has been chosen to be more than 1 order of magnitude higher than the expected interpulse interval (several microseconds). Examples of waveforms of individual pulses and trains with positive and negative pulse polarities are shown in Figures 1a and 1b, respectively.

[11] Out of the original data set of 33 trains, we have observed 2 isolated trains, each in a separate 120 ms long recording, and 31 trains grouped in three separate sequences (with 12, 13, and 6 trains, respectively). We have measured the time interval between the beginnings (times of the first pulses) of the neighboring trains in these sequences. The histogram of these time intervals is plotted in Figure 2a. The distribution clearly has a "heavy tail" and is far from being normal. The geometrical average of the obtained values is 5.6 ms. The last train in the shortest sequence has a significantly longer time delay (68 ms).

[12] As the next step of our analysis, all trains which contained bipolar pulses and trains with both pulse polarities have been excluded from our statistics. Out of the 25 remaining trains, 8 trains contain pulses with positive polarities, and 17 trains have negative pulse polarities, corresponding to relations between directions of distant source currents and their unknown positions with respect to the orientation and position of the antenna. This analyzed data set contains the total number of 967 individual pulses. The duration of the individual trains varies from 48 to 448 μs with a mean value of 176 μs (Figure 2b). This is more than 30 times shorter than the typical time intervals between the trains. The total number of pulses in a train varies from 12 to 109 with a mean value of 39 (Figure 2c). The time interval between neighboring pulses within the trains ranges between 0.7 and 28 μs with a mean value of 4.7 μs (Figure 2d). The ratio between the smallest and the largest amplitude of pulses in each individual train varies from 0.1 to 0.4 with a mean value of about 0.2 (Figure 2e). The pulse amplitudes follow a wide distribution (Figure 2f), but on average, they reach approximately 0.5 of their maximum in a given train.

4. Evolution of the Pulse Amplitude and of the Interpulse Interval Within the Trains

[13] Figures 3a and 3b, respectively, show an example of evolution of the interpulse interval and the pulse amplitude

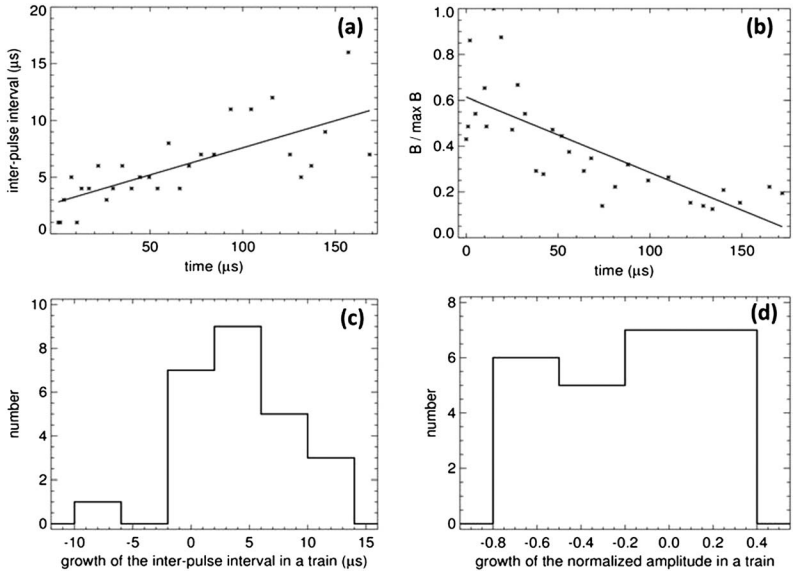

Figure 3. Evolution of (a) the interpulse interval and (b) the pulse amplitude normalized by its maximum value in a train from Figure 1b. Solid lines show linear fits. Histograms of linear trends for all analyzed trains: (c) The growth of the interpulse interval within each individual train. (d) The amplitude growth related to the maximum pulse amplitude in each train.

normalized by its maximum within the train from Figure 1b. The fluctuations of the obtained results are significant, but the general trend is that the interpulse interval is increasing and the pulse amplitude is decreasing within this train. To roughly characterize the evolution of the interpulse intervals and normalized pulse amplitudes, we have estimated linear trends in all trains. We have calculated coefficients of a linear least squares regression as a function of time. An example of the regression line is overplotted in Figures 3a and 3b. The histograms of the growth/decay rates in the separate pulse trains are plotted in Figures 3c and 3d, respectively, for the interpulse interval and the amplitude. The interpulse interval rises on average by 4.1 μs during the train duration, and, during the same time, the amplitude drops on average by 15% of its maximum. However, the spread of the obtained values is very large (from a decrease by 70% up to an increase by 37%) in the case of the normalized amplitudes.

[14] Although the approximation by a linear function is very crude, it suggests that the interpulse interval is typically increasing in our data set. To verify this result, we have calculated the rank correlation coefficients between time and interpulse intervals and the corresponding probabilities of random occurrence of a positive or a negative correlation. We have further selected only those trains where this probability is less than 5%, reducing the data set down to 16 trains. Out of these, 15 trains have a significantly positive correlation coefficient with an average value of 0.61, and only one train has a negative correlation coefficient of −0.51. For the normalized amplitude, the situation is less clear, with 6 significantly positive and 11 significantly negative correlation coefficients (average values of 0.42 and −0.66, respectively). This analysis therefore shows that the typical evolution pattern is represented by growing interpulse intervals and decreasing normalized amplitudes. However, cases with increasing amplitudes or uncertain evolution trends also occur.

5. Discussion

[15] In this study, we attempt to improve our experimental knowledge of the properties of the trains of unipolar pulses. The resolution of our instrumentation is about by more than 1 order of magnitude better than the limit of measuring systems used in previously published studies [*Krider et al*., 1975; *Rakov et al*., 1996], allowing us to fully resolve individual pulses and to also measure long sequences of pulse trains.

[16] To discuss our results, we can start by comparing the interval between the trains in our data set with the time properties of the *K* change and *M* component sequences reported by *Thottappillil et al*. [1990]. According to their measurements of close lightning flashes, the geometric-mean interval between neighboring *K* changes or *M* components, respectively, were 12.5 or 2.1 ms. The geometric-mean time interval between neighboring trains in our records is about 6 ms, which is 2 times shorter than the time interval between *K* changes and 3 times longer than the time interval between *M* components reported by *Thottappillil et al*. [1990]. However, our histogram of time intervals between neighboring trains (Figure 2a) is much closer to the histogram for *K* change intervals plotted by *Thottappillil et al*. [1990, Figure 4].

[17] *Shao et al*. [1995] reported that *K* changes are indistinguishable from dart leaders and attempted leaders in their radio interferometric observation. They concluded that, above the bottom of the thundercloud, these three lightning phenomena are identical. We can therefore also compare the time interval between neighboring trains in our records with the interstep intervals of dart-stepped leaders. *Krider et al*. [1977] reported that the mean interval between dart steps was 6–8 μs, which is in good agreement with our observations.

[18] The mean value of the interpulse interval in our data set is about 4 μs, which is consistent with the observations of *Krider et al*. [1975], who reported the mean value of 5.1 μs for the time interval between successive pulses measured in Arizona. The histogram plotted in Figure 2d is also

very close to the histogram of *Krider et al*. [1975, Figure 3b]. We can therefore conclude that we have measured the same phenomenon as *Krider et al*. [1975] and [*Rakov et al*., 1992, 1996] and that the observed pulse trains are most probably connected with *K* changes and dart-stepped leaders. Combining the occurrence rate (50%) of *K* changes in interstroke intervals reported by *Thottappillil et al*. [1990] with the 24% fraction of *K* changes accompanied by the microsecond-scale activity [*Rakov et al*., 1992], we obtain a relatively small probability of about 12% that a latter part of an interstroke interval contains *K*-related trains of pulses. Similar result can be obtained by combining the probability of occurrence of the dart-stepped leaders in the interstroke intervals [*Rakov and Uman*, 2003] with the probabilities of multiple stroke lightning.

[19] In spite of this relatively low occurrence, observations of the pulse trains can bring new information about the charge structure in the thunderclouds, based on the temporal evolution of pulse properties. According to our measurements, we can confirm that the most frequent evolution pattern of pulse train is characterized by an increasing interpulse interval and a decreasing pulse amplitude within an observed train, but we have less frequently observed all combinations of the evolution of the pulse amplitude and the interpulse interval. These different evolution patterns also occurred during a single 120 ms long record and probably belonged to the same type of lightning process. Our results therefore disagree with the assignment of different evolution patterns to particular lightning phenomena proposed by *Wang et al*. [2010]. Our measurements rather indicate that evolution patterns of the peak amplitudes and interpulse intervals reflect the movement of a dart-stepped leader inside the cloud.

[20] The observed variations of the pulse amplitudes can be also tentatively explained by the influence of a changing relative angle between the direction toward the source and the direction perpendicular to the antenna loop. Taking into account the typical speeds of dart stepped leaders on the order of 10^6 m/s [*Rakov and Uman*, 2003] and the typical duration of the pulse trains (~200 μs), the spatial dimension of the underlying lightning phenomena is on the order of a few hundreds of meters. This is by at least 1 order of magnitude lower than the typical distances between the antenna and the thundercloud, which correspond to possible amplitude variations of less than a few per cent within a given train, i.e., significantly lower than the observed variations.

[21] Assuming that the speed of the movement of the dart-stepped leader was decreasing with time, we can explain the observed increasing time interval between the neighboring pulses (96% trains in our data set) on the condition that the distance between the neighboring charge pockets in the thundercloud is nearly constant, forming a hypothetical periodic charge structure at spatial scales on the order of 10 m. We are then also able to explain the sequential decrease of the amplitude of the pulses by the decrease of the speed of the leader propagation, because the radiated magnetic field is proportional to the speed of the leader movement [*Uman and McLain*, 1970]. Different distances between neighboring charge pockets and/or an increase of the speed of the leader propagation could probably also explain the observed untypical evolution patterns of the trains of the pulses.

[22] Direct balloon measurements have shown that the charge distribution in the thunderclouds is rather complex at larger scales [*Stolzenburg and Marshall*, 1998]. Extended data set of trains recorded in different conditions is needed to verify the above-mentioned link of temporal properties of the trains to the small-scale properties of the charge structure. Future work using longer recording intervals and simultaneous optical measurements will contribute to the explanation of these fast processes and to their assignment to particular lightning phenomena.

[23] **Acknowledgments.** This work is an integral part of the cooperation of IAP Prague with LPC2E/CNRS Orleans, France, in the frame of the TARANIS project of CNES. It was supported in part by the international cooperation program of the ASCR (grant M10042120) and in part by GACR 205-09-1253. We are grateful to J. Chum, F. Hruška, J. Souček, J. Vojta, and J. H. Baše for their technical assistance and to P. Novák for comparison of return stroke data with CELDN.

References

Davis, S. M. (1999), Properties of lightning discharges from multiple-station wide band measurements, dissertation, Grad. Sch. of the Univ. of Fla., UMI Microform 9945961.

Füllekrug, M., and A. C. Fraser-Smith (2011), The Earth's electromagnetic environment, *Geophys. Res. Lett.*, *38*, L21807, doi:10.1029/2011GL049572.

Gomes, C., V. Cooray, M. Fernando, R. Montano, and U. Sonnadara (2004), Characteristics of chaotic pulse trains generated by lightning flashes, *J. Atmos. Sol. Terr. Phys.*, *66*, 1733–1743.

Krider, E. P., and R. C. Noggle (1974), Broadband antenna system for lightning magnetic fields, *J. Appl. Meteorol.*, *14*, 252–256.

Krider, E. P., G. J. Radda, and R. C. Noggle (1975), Regular radiation field pulses produced by intracloud lightning discharges, *J. Geophys. Res.*, *80*, 3801–3804.

Krider, E. P., C. D. Weidman, and R. C. Noggle (1977), The electric fields produced by lightning stepped leaders, *J. Geophys. Res.*, *82*, 951–960.

Lee, B.-H., D.-C. Jeong, D.-M. Lee, and T. Kawamura (2006), Characteristics of the lightning stepped-leader electromagnetic pulses, *Jpn. J. Appl. Phys.*, *45*, 933–939.

Nag, A., and V. A. Rakov (2008), Pulse trains that are characteristic of preliminary breakdown in cloud-to-ground lightning but are not followed by return stroke pulses, *J. Geophys. Res. 113*, D01102, doi:10.1029/2007JD008489.

Nag, A., and V. A. Rakov (2009), Electromagnetic pulses produced by bouncing-wave-type lightning discharges, *IEEE Trans. Electromagn. Compat.*, *51*, 466–470.

Rakov, V. A., and M. A. Uman (2003), Lightning—Physics and Effects, Cambridge Univ. Press, New York, ISBN:9780521583275.

Rakov, V. A., R. Thottappillil, and M. A. Uman (1992), Electric field pulses in *K* and *M* changes of lightning ground flashes, *J. Geophys. Res.*, *97*, 9935–9950.

Rakov, V. A., M. A. Uman, G. R. Hoffman, M. W. Masters, and M. Brook (1996), Burst of pulses in lightning electromagnetic radiation: Observations and implications for lightning test standards, IEEE Trans, *Electromagn. Compat.*, *38*, 156–164.

Schonland, B. F. J. (1956), The lightning discharge, Handbuch der Physik, Springer, Berlin, vol. *22*pp. 576–627 .

Shao, X. M., P. R. Krehbiel, R. J. Thomas, and W. Rison (1995), Radio interferometric observations of cloud-to-ground lightning phenomena in Florida, *J. Geophys. Res.*, *100*, 2749–2783.

Stolzenburg, M., and T. C. Marshall (1998), Charged precipitation and electric field in two thunderstorms, *J. Geophys. Res.*, *103*, 19777–19790.

Thottappillil, R., V. A. Rakov, and M. A. Uman (1990), *K* and *M* changes in close lightning ground flashes in Florida, *J. Geophys. Res.*, *95*, 18631–18640.

Uman, M. A., and D. K. McLain (1970), Radiation field and current of the lightning stepped leader, *J. Geophys. Res.*, *75*, 1058–1066.

Wang, Y., G. Zhang, T. Zhang, Y. Li, Y. Zhao, T. Zhang, X. Fan, and B. Wu (2010), The regular pulses bursts in electromagnetic radiation from lightning, *Asia-Pacific International Symposium on Electromagnetic Compatibility*, *Beijing*, *China*, doi:10.1109/APEMC.2010.5475814.

APPENDIX C2 Fullekrug et al. (2013)

Fullekrug, M., I. Kolmasova, O. Santolik, T. Farges, J. Bor, A. Bennett, M. Parrot, W. Rison, F. Zanotti, E. Arnone, A.Mezentsev, R. Lan, L. Uhlir, G. Harrison, S. Soula, O. van der Velde, J.-L. Pincon, Ch. Helling, and D. Diver (2013), Electron acceleration above thunderclouds, *Environ. Res. Lett.* 8, doi:10.1088/1748-9326/8/3/035027.

OPEN ACCESS
IOP PUBLISHING ENVIRONMENTAL RESEARCH LETTERS
Environ. Res. Lett. **8** (2013) 035027 (6pp) doi:10.1088/1748-9326/8/3/035027

Electron acceleration above thunderclouds

Martin Füllekrug[1], Ivana Kolmasova[2], Ondrej Santolik[2,3], Thomas Farges[4], József Bór[5], Alec Bennett[6], Michel Parrot[7], William Rison[8], Ferruccio Zanotti[9], Enrico Arnone[10], Andrew Mezentsev[1], Radek Lan[2], Ludek Uhlir[2], Giles Harrison[11], Serge Soula[12], Oscar van der Velde[13], Jean-Louis Pinçon[7], Christiane Helling[14] and Declan Diver[15]

[1] Centre for Space and Atmospheric Science, Department of Electronic and Electrical Engineering, University of Bath, Bath, UK
[2] Institute of Atmospheric Physics, Academy of Sciences of the Czech Republic, Prague, Czech Republic
[3] Faculty of Mathematics and Physics, Charles University in Prague, Czech Republic
[4] Commissariat à l'Energie Atomique et aux Energies Alternatives, DAM-DIF, Bruyères le Châtel, France
[5] Research Centre for Astronomy and Earth Sciences, Hungarian Academy of Sciences, Sopron, Hungary
[6] Bristol Industrial and Research Associates Ltd, Portishead, Bristol, UK
[7] Laboratoire de Physique et Chimie de l'Environnement et de l'Espace, CNRS, Orléans, France
[8] New Mexico Tech, Electrical Engineering Department, NM, USA
[9] Italian Meteor and TLE Network, Ferrara, Italy
[10] Istituto di Scienze dell'Atmosfera e del Clima, CNR, Bologna, Italy
[11] Department of Meteorology, University of Reading, Reading, UK
[12] Laboratoire d'Aérologie, Université de Toulouse, CNRS, Toulouse, France
[13] Department of Electrical Engineering, Technical University of Catalonia, Terrassa, Spain
[14] SUPA, School of Physics and Astronomy, University of St Andrews, St Andrews, UK
[15] School of Physics and Astronomy, University of Glasgow, Glasgow, UK

E-mail: eesmf@bath.ac.uk (Martin Füllekrug)

Received 12 May 2013
Accepted for publication 26 July 2013
Published 13 August 2013
Online at stacks.iop.org/ERL/8/035027

Abstract
The acceleration of electrons results in observable electromagnetic waves which can be used for remote sensing. Here, we make use of ~4 Hz–66 MHz radio waves emitted by two consecutive intense positive lightning discharges to investigate their impact on the atmosphere above a thundercloud. It is found that the first positive lightning discharge initiates a sprite where electrons are accelerated during the exponential growth and branching of the sprite streamers. This preconditioned plasma above the thundercloud is subsequently exposed to a second positive lightning discharge associated with a bouncing-wave discharge. This discharge process causes a re-brightening of the existing sprite streamers above the thundercloud and initiates a subsequent relativistic electron beam.

Keywords: atmospheric electricity, lightning, electromagnetic wave propagation, storms

1. Introduction

Transient energetic charged particle populations occur in association with thunderstorms where the lightning

electromagnetic field can release electrons from the radiation belts precipitating into the atmosphere (Voss *et al* 1998, 1984). These electrons have typical kinetic energies ∼100–250 keV in addition to their rest mass ∼511 keV and occur ∼0.1–1 s after the causative lightning discharge (Gemelos *et al* 2009). The electrons are decelerated when penetrating the neutral atmosphere and deposit their energy in ∼100–2000 km large ionization patches north/south of a lightning discharge in the northern/southern hemisphere (Inan *et al* 2007). Electrons are accelerated to very high energies ∼10–100 MeV inside thunderclouds, either in lightning leader tips (Celestin and Pasko 2011) and/or in large scale thunderstorm electric fields (Dwyer and Cummer 2013, Gurevich and Karashtin 2013, Dwyer 2012, Gurevich *et al* 1992). The acceleration of the electrons is accompanied by gamma rays emanating from thunderstorms (Østgaard *et al* 2013, Tavani *et al* 2011, Smith *et al* 2005, Fishman *et al* 1994) which can be used as a diagnostic tool. When the gamma rays interact with air molecules and exceed an energy of ∼1.022 MeV, i.e., two times the rest mass of an electron, the gamma rays can disintegrate into an electron–positron pair around ∼40–60 km height such that magnetized positrons and electrons are observed on board of satellites in near-Earth space (Briggs *et al* 2011, Carlson *et al* 2009, Dwyer *et al* 2008). Similarly, it was proposed that the lightning electromagnetic field can accelerate electrons above thunderclouds from the cosmic ray layer upwards to produce avalanching relativistic electron beams (Roussel-Dupré *et al* 1998, Roussel-Dupré and Gurevich 1996). Experimental evidence for such electron beams was reported by remote sensing with low frequency radio waves (Füllekrug *et al* 2011b, 2010). The lightning electromagnetic field also causes Joule heating above thunderclouds which results in electrical breakdown of air such that sprite streamers develop (Pasko 2010). The exponential growth and splitting of streamers results in an electron multiplication associated with the acceleration of electrons to a few eV. The accelerated electrons radiate a small amount of electromagnetic energy and the incoherent superposition of many streamers causes low frequency radio noise (Füllekrug *et al* 2013a, Qin *et al* 2012a). As a result, the remote sensing with radio waves can be used to investigate the acceleration of electrons above a thundercloud during a sprite followed by a consecutive electron beam which is the aim of this contribution.

2. Observations

Unstable air masses near the north-eastern coast of Spain developed into a thunderstorm in the evening of 29 August 2012. The storm propagated eastward along the Mediterranean coast of southern France and produced numerous lightning discharges in the early morning hours of August 30. The accumulated leader steps of one particular ∼1.7 s long lightning discharge were recorded with a lightning mapping array in 80 μs long time intervals as part of the HyMeX campaign (figure 1). Shortly after the beginning of the discharge process, one particularly intense positive lightning discharge (44.0°N, 5.6°E) with a peak

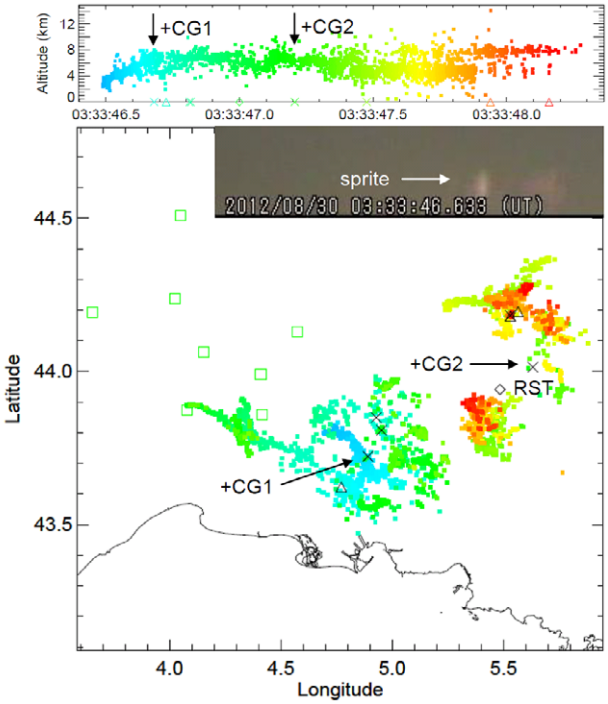

Figure 1. A lightning mapping array (green squares) records the leader steps of a ∼1.7 s long lightning discharge on 30 August 2012 (upper panel), which causes numerous positive (crosses) and negative (triangles) cloud to ground lightning discharges. A particularly intense positive cloud to ground lightning discharge at 03:33:46.680 (+CG1) causes a sprite (inset figure). The consecutive intense positive cloud to ground lightning discharge at 03:33:47.208 (+CG2) occurs ∼60 km north-eastward of the sprite and is recorded with a high frequency radio receiver near Rustrel (RST).

current of +124 kA occurred at 03:33:46.680 UTC and caused a subsequent sprite. The sprite was recorded with an astronomical color video camera in Ferrara (44.8°N, 11.6°E) as part of the Italian Meteor and TLE network. The sprite producing lightning discharge was associated with a charge moment change as large as ∼1300 C km. The charge moment was calculated from an exponentially decreasing lightning current inferred from electric field measurements in the frequency range ∼5–30 Hz (figure 2, left, upper panel) at Nagycenk observatory (47.6°N, 16.7°E) in Hungary (Sátori *et al* 2013, and references therein). This large charge moment change exceeded the charge moment change ∼600 C km which is typically required for sprite initiation (Qin *et al* 2012b, Cummer *et al* 2005). The lightning discharge was also intense enough to be picked up by a quasi-static current sensor operated in the frequency range of ∼1–50 Hz near Portishead (51.5°N, 2.8°W) in south-west England. Similar unusual quasi-static current signatures (figure 2, left, middle panel) have previously been used to successfully detect sprites with ∼30–50% detection efficiency because the detected sprites are almost certainly associated with halos (Bennett and Harrison 2013). Finally, the sprite streamers produced low frequency radio noise from ∼4–400 kHz (Füllekrug *et al* 2013a, Qin *et al* 2012a) lasting for ∼20 ms which was measured here with two independently recording radio receivers near Orléans (47.8°N, 1.9°E) in central France and

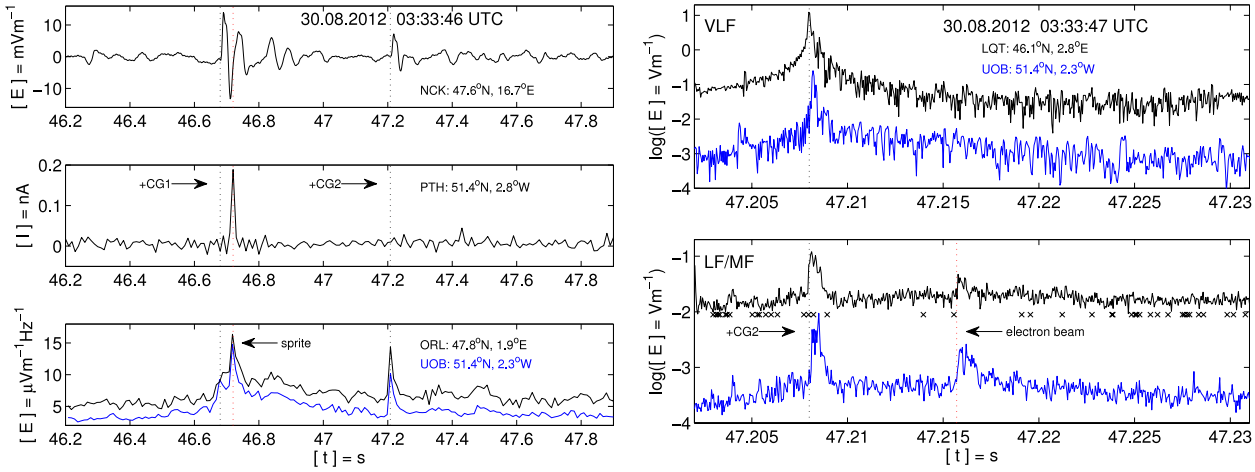

Figure 2. Left. Upper panel. Electric field measurements from ∼5–30 Hz at Nagycenk (NCK) are used to infer the charge moment change of the two consecutive lightning discharges (black dotted lines). The charge moment of the first positive lightning discharge exceeds the limit for sprite initiation. The second positive lightning discharge exhibits a much smaller charge moment. Middle panel. The recordings of the quasi-static current from ∼1–50 Hz near Portishead (PTH) indicate that the first lightning discharge initiated a sprite. Lower panel. The low frequency radio noise from ∼4–400 kHz near Orléans (ORL) and Bath (UOB) indicates radio emissions from sprite streamers (red dotted line) initiated by the first lightning discharge and a re-brightening of the remaining sprite streamers during the second lightning discharge. Right. Upper panel. The second lightning discharge exhibits the typical ∼0.1–1 ms long ∼5–15 kHz (VLF) electric field enhancement which is larger in LeQuartier (LQT) when compared to Bath as a result of the proximity to the lightning discharge. Lower panel. About ∼8–9 ms after the second lightning discharge, a ∼1 ms long ∼270–400 kHz (LF/MF) radio pulse indicates the acceleration of electrons associated with an electron beam which is recorded by both radio receivers. Note that the leader steps recorded with the lightning mapping array from ∼60–66 MHz (crosses in the lower panel) do not seem to be related to the VLF or LF/MF recordings.

Bath (51.4°N, 2.3°W) in south-west England (figure 2, left, lower panel). The remarkable coincidence of three entirely different proxy measures of sprite occurrence (figure 2, left) ensures that the luminosity patch observed with the video camera was indeed a sprite.

The low frequency radio noise from the sprite streamers is followed ∼528 ms later by a new intense positive lightning discharge (44.0°N, 5.6°E) with a peak current of ∼+121 kA which occurs at 03:33:47.208 UTC. The lightning discharge is located ∼60 km north-east of the preceding lightning discharge and it exhibits a ∼0.1–1 ms long 5–15 kHz electric field enhancement as recorded by the radio receiver near Bath and a vertical electric dipole antenna located near LeQuartier in central France (46.1°N, 2.8°E), ∼200 km north of the lightning discharge (figure 2, right, upper panel). The lightning discharge has a significantly smaller charge moment change of ∼570 C km than the preceding lightning discharge (figure 2, left, upper panel) and no quasi-static current is observed (figure 2, left, middle panel). The absence of a large charge moment change and a quasi-static current indicate that no full sprite developed such that the resurgence of the low frequency radio noise strongly suggests a weaker re-brightening of the existent sprite streamers (figure 2, left, lower panel). However, resonance type oscillations with a period of ∼3.8 μs (∼260 kHz) lasting for ∼9 cycles over ∼34.2 μs are superimposed on the radio signal from the cloud to ground lightning discharge (figure 3) as observed with high frequency magnetic field recordings from ∼5 kHz–40 MHz (Kolmasova and Santolik 2013) near Rustrel (43.9°N, 5.5°E) at a distance of ∼40 km north-east of the initial sprite and ∼16 km south-west of the second positive lightning discharge. The second positive lightning discharge with the resonance

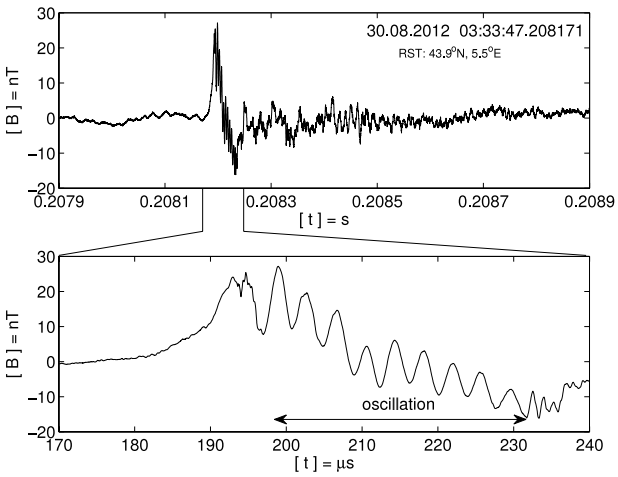

Figure 3. The high frequency magnetic field measurements from ∼5 kHz–40 MHz near Rustrel (RST) show that the second positive lightning discharge (upper panel) exhibits resonant type oscillations with a period of ∼3.8 μs (∼260 kHz) lasting for ∼9 cycles over ∼34.2 μs (lower panel) attributed to a bouncing-wave discharge.

type oscillations is followed ∼8–9 ms later by a characteristic ∼1 ms long ∼270–400 kHz radio pulse recorded by the radio receivers near Bath and LeQuartier (figure 2, right, lower panel). This radio pulse has a relatively featureless flat spectrum extending from ∼40–300 kHz when compared to the spectrum of ordinary lightning discharges (Füllekrug *et al* 2011b) which typically exhibit larger amplitudes at lower frequencies with a relative maximum near ∼10 kHz (figure 2, right, upper panel). A more detailed analysis of the electric field recordings in LeQuartier shows that the spectrum of the radio pulse extends up to ∼400–500 kHz,

but the presence of medium wave radio transmitters from ∼500–1600 kHz and the local electromagnetic environment inhibit an unambiguous assertion on the extent of the spectrum towards higher frequencies.

3. Interpretation

The first intense positive lightning discharge causes a sprite as evidenced by the optical observations and the radio recordings. The lightning discharge is followed ∼528 ms later by a second positive lightning discharge which exhibits ∼34.2 μs long resonance type oscillations at ∼260 kHz. This second lightning discharge is followed ∼8–9 ms later by a ∼1 ms long ∼270–400 kHz radio pulse.

This pulsed discharge event was initially discovered by high frequency magnetic field recordings with a ground based doublet of a high frequency receiver (Kolmasova and Santolik 2013) which is being developed for the TARANIS spacecraft (Blanc *et al* 2007). It was the only high frequency event recorded during the passage of the thunderstorm. The high frequency recordings of the second lightning discharge exhibit resonance type oscillations with a period of ∼3.8 μs lasting for about ∼34.2 μs. These oscillations are superimposed on the radio signal from the lightning discharge. To the best of our knowledge, these type of oscillations have been observed and reported only in connection with compact intracloud discharges (Nag and Rakov 2009). However, in our case the observed lightning discharge lacks some typical features of compact intracloud discharges. The bouncing wave can be explained by a traveling current pulse which is injected at one end of a conducting channel and reflected multiple times at both ends of the channel until the instability is attenuated and absorbed (Nag and Rakov 2009). The modeling results for the current propagation and reflection show that the pulse travels at a speed between $\sim 10^8$ m s^{-1} and the speed of light (Nag *et al* 2010). In this case, the length of the lightning channel would be ∼1 km resulting in the lower charge moment which is still consistent with a large peak current of the lightning discharge.

The bouncing-wave discharge is followed ∼8–9 ms later by a ∼1 ms long ∼270–400 kHz radio pulse without corresponding radio emissions near ∼10 kHz which are typical for ordinary lightning discharges (figure 2, right, upper panel). The radio pulse is also not associated with radio emissions near ∼60–66 MHz from intracloud lightning discharges (figure 2, right lower panel). The absence of ∼10 kHz radio emissions during the radio pulse also excludes an interpretation of the radio pulse as resurgent impulsive radio noise emanating from sprite streamers which exhibit a spectrum with amplitudes which increase towards lower frequencies (Füllekrug *et al* 2013a). On the other hand, the radio pulse was clearly observed by two entirely independent radio recordings, i.e., with the dipole antenna in LeQuartier and the flat plate antenna in Bath. Radio signatures with the observed characteristics have been predicted by numerical simulations of relativistic runaway breakdown above thunderclouds (Roussel-Dupré *et al* 1998, Roussel-Dupré and Gurevich 1996). These theoretical predictions

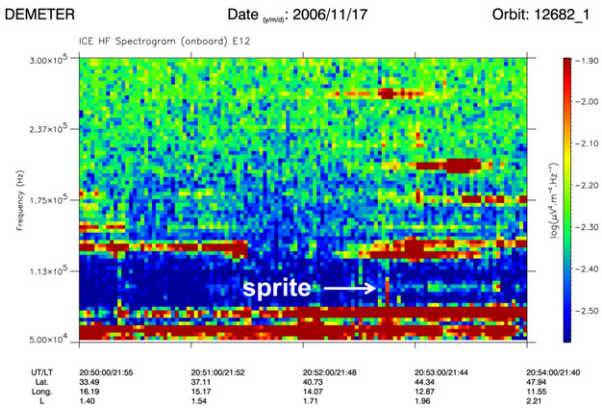

Figure 4. A sprite producing lightning discharge emits a particularly intense broadband radio signal up to ∼130 kHz which was recorded on board the DEMETER spacecraft on 17 November 2006.

have recently been confirmed by experimental measurements (Füllekrug *et al* 2011b, 2010). It is shown here for the first time that such experimental observations cannot easily be explained by currently known lightning discharge processes and that corresponding measurements can be obtained by another radio receiver with a sufficient sensitivity. As a result, the observed radio pulse is attributed to a relativistic electron beam following a sprite producing lightning discharge as predicted by numerical model simulations.

It is interesting to note that a recent detailed comparison of ground based optical sprite observations in southern France with electric field recordings on board the DEMETER satellite on 17 November 2006 (Parrot *et al* 2013), revealed low frequency radio signals up to ∼130 kHz associated with the sprite and/or the causative lightning discharge which have never been observed before in association with ordinary lightning discharges (figure 4). Given that the ionosphere attenuates ∼100 kHz radio signals by ∼2 orders of magnitude (Füllekrug *et al* 2011a), the signal intensity of the lightning and/or sprite was undoubtedly exceptionally large. This observation shows that powerful low frequency radio signals associated with sprite producing lightning, as reported here, can be observed in space with unprecedented temporal and spectral resolution which is the aim of the French TARANIS satellite due to be launched in 2015 (Blanc *et al* 2007).

4. Discussion

In plasma physics it is known that pulsed discharges can accelerate and beam electrons efficiently in the presence of a specific electrostatic field configuration defined by a hollow cathode (Becker *et al* 2006, Slevin and Harrison 1975). It is speculated that a similar physical mechanism might occur above thunderclouds in the presence of aerosols (Füllekrug *et al* 2013b, pp 8–9). In this picture, the first lightning discharge produces free electrons which attach to the aerosols and cause a quasi-static electric field. This electric field defines the geometric shape and the physical properties of any consecutive discharge process. For example, the leader

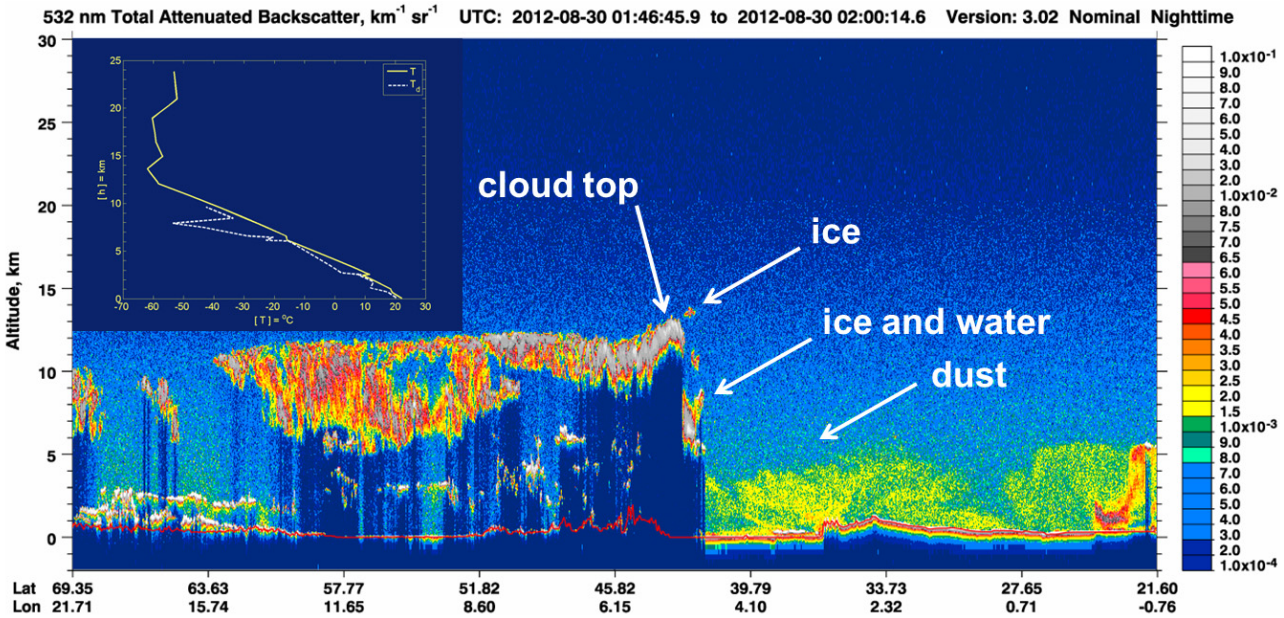

Figure 5. The thunderstorm cloud top height reaches up to ∼12–13 km as inferred from lidar measurements on board the CALIPSO spacecraft. Above the maximum cloud top height, an ensemble of stratospheric ice particles occurs at ∼13–14 km around the tropopause as inferred from temperature measurements during a preceding radiosonde ascent (inset figure). The mixed phase region of the thundercloud is found at ∼6–7 km height where ice and water coexist. The convective storm might have entrained dust which is confined to a layer from the ground up to ∼5–6 km.

stem of a gigantic jet defined the shape of a consecutive ring-formed column sprite (Neubert *et al* 2011, figure 1). The mechanism proposed here requires knowledge on the presence of charged aerosols above thunderclouds. The recent discovery of sporadic stratospheric aerosol layers (Renard *et al* 2010) which are possibly charged (Renard *et al* 2013) suggests that the presence of small quantities of stratospheric aerosols could assist the occasional formation of relativistic electron beams above thunderclouds caused by consecutive lightning discharges. In the absence of *in situ* measurements of charged aerosols above the thunderclouds investigated here, it is interesting to put the electromagnetic observations in the context of the surrounding atmospheric environment.

Air masses from a Saharan dust storm reached France around 17 August 2012, which might have helped to entrain silt into convective storms. The size of silt particles ranges from ∼2–4 μm to ∼62–64 μm and they tend to be larger than clay and smaller than sand. Silt can be carried over long distances in air, whereas sand particles settle down more quickly as a result of gravitational forces and clay particles attach more quickly to any larger particles. Interestingly, Saharan dust storms can be electrified (Nicoll *et al* 2011) such that dust particles are aligned by the electric field (Ulanowski *et al* 2007). In addition, smoke particles from ongoing forest fires in Spain might have been transported by the westerly trade winds towards air masses in France during the month of August and an unusual large number of sprites was observed in the second half of August 2012 as reported by numerous observers on the Eurosprite mailing list. It was previously speculated that the presence of smoke particles can increase the occurrence rate of positive lightning discharges inside thunderstorms and thereby increase the occurrence rate of sprites above thunderstorms (Lyons *et al* 1998).

The CALIPSO spacecraft (Cloud–Aerosol Lidar and Infrared Pathfinder Satellite Observation) passed over the investigated thunderstorm around ∼01:53 UTC and determined a thunderstorm cloud top height of ∼12–13 km (figure 5). These large heights are required for compact intracloud discharges to occur. In addition, CALIPSO reported the presence of a dust layer from the ground up to ∼5–6 km height (figure 5). It is very likely that this dust was entrained into the convective storm and transported upwards to the tropopause by convective updrafts. The tropopause was located around ∼13–14 km height as inferred from the radiosonde ascent from Nimes-Courbessac (43.9°N, 4.4°E) at 00:00 UTC (figure 5, inset). Finally, CALIPSO detected a disconnected ensemble of ice particles at ∼13–14 km height which might have been injected into the lower stratosphere by an overshooting cloud top where dust and smoke particles assisted ice nucleation. In any case, the unusual accumulation of ice particles above the thundercloud top might have helped to define a particular electrostatic charge configuration leading to the bouncing-wave discharge and/or the subsequent electron beam.

5. Summary

The impact of two consecutive positive lightning discharges on the area above a thundercloud is investigated in detail. It is found that the first positive lightning discharge initiates sprite streamers which discharge the lightning electromagnetic field above the thundercloud. The exponential growth and

splitting of the streamers results in an electron multiplication associated with the acceleration of electrons to a few eV. A consecutive positive lightning discharge occurs ∼528 ms later and is associated with a bouncing-wave discharge. About ∼8–9 ms after the bouncing-wave discharge an electron beam occurs associated with the acceleration of electrons to a few MeV. This is the first simultaneous detection of radio signatures from electrons accelerated to thermal and relativistic energies above thunderclouds. The environmental conditions leading to the bouncing-wave discharge and the subsequent electron beam remain to be investigated in more detailed future studies.

Acknowledgments

The work of MF and AM is sponsored by the Natural Environment Research Council (NERC) under grant NE/H024921/1. IK, OS, RL, and LU are supported by the international cooperation program of the ASCR grant M10042120 and by the GACR project 205-09-1253. JB is supported by the Earth-system project TAMOP-4.2.2.C-11/1/KONV-2012-0015 sponsored by the EU and European Social Foundation. OV is supported by the Spanish Ministry of Science and Innovation under project AYA2011-29936-C05-04. ChH acknowledges an ERC starting grant from the European Union. The authors wish to thank the team of the Laboratoire Souterrain à Bas Bruit for hosting the radio receivers. Special thanks to Julien Poupeney, Christophe Sudre, Alain Cavaillou, Daniel Boyer, and Stéphane Gaffet, whose assistance and hospitality were invaluable to conduct the experiments in south-eastern France. MF acknowledges enlightening discussions with Thorwald Stein and Robin Hogan. The CALIPSO data were made available by NASA through www-calipso.larc.nasa.gov. The communication between collaborators was facilitated by the scientific programmes EPHRAT/French Embassy, TEA-IS/European Science Foundation, HYMEX/European Commission, and IMTN/Eurosprite mailing list.

References

Becker K, Schoenbach K and Eden J 2006 *J. Phys. D: Appl. Phys* **39** R55–70
Bennett A and Harrison R 2013 *Phys. Rev. Lett.* **111** 045003
Blanc E, Lefeuvre F, Roussel-Dupré R and Sauvaud J 2007 *Adv. Space Res.* **40** 1268–75
Briggs M *et al* 2011 *Geophys. Res. Lett.* **38** L02808
Carlson B, Lehtinen N and Inan U 2009 *Coupling of Thunderstorms and Lightning Discharges to Near-Earth Space* ed N Crosby, T Huang and M Rycroft (Melville, NY: American Institute of Physics) pp 84–91
Celestin S and Pasko V 2011 *J. Geophys. Res.* **116** A03315
Cummer S, Zhai Y, Hu W, Smith D, Lopez L and Stanley M 2005 *Geophys. Res. Lett.* **32** L08811
Dwyer J 2012 *J. Geophys. Res.* **117** A02308
Dwyer J and Cummer S 2013 *J. Geophys. Res.* **118** 3769–90
Dwyer J, Grefenstette B and Smith D 2008 *Geophys. Res. Lett.* **35** L02815
Fishman G *et al* 1994 *Science* **264** 1313–6
Füllekrug M, Hanuise C and Parrot M 2011a *Atmos. Chem. Phys.* **11** 667–73
Füllekrug M, Mezentsev A, Soula S, van der Velde O and Farges T 2013a *Geophys. Res. Lett.* **40** 2395–9
Füllekrug M, Roussel-Dupré R, Symbalisty M, Chanrion O, Odzimek A, van der Velde O and Neubert T 2010 *J. Geophys. Res.* **115** A00E09
Füllekrug M *et al* 2011b *Atmos. Chem. Phys.* **11** 7747–54
Füllekrug M *et al* 2013b *Surv. Geophys.* **34** 1–41
Gemelos E, Inan U, Walt M, Parrot M and Sauvaud J 2009 *Geophys. Res. Lett.* **36** L21107
Gurevich A and Karashtin A 2013 *Phys. Rev. Lett.* **110** 185005
Gurevich A, Milikh G and Roussel-Dupré R 1992 *Phys. Lett.* A **165** 463–8
Inan U, Piddyachiy D, Peter W, Sauvaud J and Parrot M 2007 *Geophys. Res. Lett.* **34** L07103
Kolmasova I and Santolik O 2013 *Geophys. Res. Lett.* **40** 1637–41
Lyons W, Nelson T, Williams E, Cramer J and Turner T 1998 *Science* **282** 77
Nag A and Rakov V 2009 *IEEE Trans. Electromagn. Compat.* **51** 466–70
Nag A, Rakov V, Tsalikis D and Cramer J 2010 *J. Geophys. Res.* **115** D14115
Neubert T, Chanrion O, Arnone E, Zanotti F, Cummer S, Füllekrug M, Soula S and van der Velde O 2011 *J. Geophys. Res.* **116** A12329
Nicoll K, Harrison R and Ulanowski Z 2011 *Environ. Res. Lett.* **6** 014001
Østgaard N, Gjesteland T, Carlson B, Collier A, Cummer S, Lu G and Christian H 2013 *Geophys. Res. Lett.* **40** 2423–6
Parrot M, Sauvaud J, Soula S, Pincon J and van der Velde O 2013 *J. Geophys. Res.* at press
Pasko V 2010 *J. Geophys. Res.* **115** A00E09
Qin J, Celestin S and Pasko V 2012a *Geophys. Res. Lett.* **39** L22803
Qin J, Celestin S and Pasko V 2012b *Geophys. Res. Lett.* **39** L22801
Renard J, Berthet G, Salazar V, Catoire V, Tagger M, Gaubicher B and Claude R 2010 *Geophys. Res. Lett.* **37** L20803
Renard J, Tripathi S, Michael M, Rawal A, Berthet G, Füllekrug M, Harrison R, Robert C, Tagger M and Gaubicher B 2013 *Atmos. Chem. Phys. Discuss.* **13** 7061–79
Roussel-Dupré R and Gurevich A 1996 *J. Geophys. Res.* **101** 2297–311
Roussel-Dupré R, Symbalisty E, Taranenko Y and Yukhimuk V 1998 *J. Atmos. Sol.-Terr. Phys.* **60** 917–40
Sátori G, Rycroft M, Bencze P, Märcz F, Bór J, Barta V, Nagy T and Kovács K 2013 *Surv. Geophys.* **34** 255–92
Slevin P and Harrison W 1975 *Appl. Spectrosc. Rev.* **10** 201–55
Smith D, Lopez L, Lin R and Barrington-Leigh C 2005 *Science* **307** 1085–8
Tavani M *et al* 2011 *Phys. Rev. Lett.* **106** 018501
Ulanowski Z, Bailey J, Lucas P, Hough J and Hirst E 2007 *Atmos. Chem. Phys.* **7** 6161–73
Voss H, Walt M, Imhof W, Mobilia J and Inan U 1984 *Nature* **312** 740–2
Voss H, Walt M, Imhof W, Mobilia J and Inan U 1998 *J. Geophys. Res.* **103** 11725–44

REFERENCES

Ahmad, N. A., M. Fernando, Z. A. Baharudin, V. Cooray, H. Ahmad, and Z. A. Malek (2010), Characteristics of narrow bipolar pulses observed in Malaysia, *J.of Atm. and Solar-Ter. Phys.* 72, doi:10.1016/j.jastp.2010.02.006.

Baharudin, Z. A., N. A. Ahmad, M. Fernando, and V. Coorey (2010), Comparative study on preliminary breakdown pulse trains observed in Malaysia and Florida, *30th International Conference on Lightning Protection – ICLP2010.*

Bateman, M. G., W. D. Rust, B. F. Smull, and T.C. Marshall (1995), Precipitation charge and size measurements in the stratiform region of two mesoscale convective systems, *J. Geophys. Res. 100,* 16341-16356.

Byrne, G. J., A. A. Few, and M. E. Weber (1983), Altitude, thickness and charge concentration of charged regions of four thunderstorms during TRIP 1981 based upon in situ balloon electric field measurement, , *Geophys. Res. Lett. 10,* 39-42.

Coleman, L. M., M. Stolzenburg, T. C. Marshall, and M. Stanley (2007), Horizontal lightning propagation, preliminary breakdown, and electric potential in New Mexico thunderstorms, *J. Geophys. Res. 113,* D09208, doi: 10.1029/2007JD009459.

Cooray, V. and K.P.S.C. Jayratne (1994), Characteristics of lightning flashes observed in Sri Lanka in the tropics, *J. Geophys. Res. 99,* 21051-21056.

Cooray, V. (2009), Propagation effects on lightning electromagnetic fields, *Proceedings of the X International Symposium on Lightning Protection, 2009 – Curitiba, Brazil,* 19-41.

Cummer, S. A., N. Jaugey, J. Li, W. A. Lyons, T. E. Nelson, and E. A. Gerken (2006), Submillisecond imaging of sprite development and structure, *Geophys. Res. Lett., 33,* L04104, doi:10.1029/2005GL024969.

Davis, S. M. (1999), Properties of lightning discharges from multiple-station wide band measurements, *The dissertation presented to the Graduate school of the University of Florida, UMI Microform* 9945961.

Franz, R. C., R. J. Nemzek, and J. R. Winckler (1990), Television Image of a Large Upward Electrical Discharge Above a Thunderstorm Systém, *Science,*Vol. 249 no. 4964 pp. 48-51 DOI: 10.1126/science.249.4964.48

Fullekrug, M., R. Roussel-Dupre´, E. M. D. Symbalisty, J. J. Colman, O. Chanrion, S. Soula, O. van der Velde, A. Odzimek, A. J. Bennett, V. P. Pasko, and T. Neubert (2011), Relativistic electron beams above thunderclouds, *Atmos. Chem. Phys., 11*, 7747–7754, doi:10.5194/acp-11-7747-2011.

Fullekrug, M., I. Kolmasova, O. Santolik, T. Farges, J. Bor, A. Bennett, M. Parrot, W. Rison, F. Zanotti, E. Arnone, A. Mezentsev, R. Lan, L. Uhlir, G. Harrison, S. Soula, O. van der Velde, J.-L. Pincon, Ch. Helling, and D. Diver (2013), Electron acceleration above thunderclouds, *Environ. Res. Lett.* 8, doi:10.1088/1748-9326/8/3/035027.

Gomes, Ch., V. Cooray, and Ch. Jayaratne (1998), Comparison of preliminary breakdown pulses observed in Sweden and Sri Lanka, *J. Atmos. Sol.-Terr. Phys. 60*, 975-979.

Gomes, Ch., V. Cooray, M. Fernando, R. Montano, and U. Sonnadara (2004), Characteristics of chaotic pulse trains generated by lightning flash, *J. Atmos. Sol.-Terr. Phys. 66*, 1733–1743.

Haddad, M. A., V. A. Rakov, and S. A. Cummer (2012), New measurements of lightning electric fields in Florida: Waveform characteristics, interaction with the ionosphere, and peak current estimates, *J. Geophys. Res., 117*, D10101, doi:10.1029/2011JD017196.

Hamlin, T., T. E. Light, X. M. Shao, K. B. Eack, and J. D. Harlin (2007), Estimating lightning channel characteristics of positive narrow bipolar events using intrachannel current reflection signatures, *J. Geophys. Res., 112*, D14108, doi:10.1029/2007JD008471.

Heavner, M. J., D. A. Smoth, A. R. Jacobson, and R. J. Sheldon (2002), LF/VLF and VHF fast-stepped leader observations, *J. Geophys. Res. 107*, 4791, doi: 10.1029/2001JD001290.

Jacobson, A. R. and M. J. Heavner (2005), Comparison of narrow bipolar events with ordinary lightning as proxies for severe convection, *Mon. Weather Rev.*, 133, 1144–1154.

Karunarathne, S., T. C. Marshall, M. Stolzenburg, N. Karunarathna, L. E. Vickers, T. A. Warner, and R. E. Orville (2013), Locating initial breakdown pulses using electric field change network, *J. Geophys. Res. Atmos*., 118, 7129–7141, doi:10.1002/jgrd.50441.

Kigatawa, N. and K. Michimoto (1994), Meteorological and electrical aspects of winter thunderclouds, *J. Geophys. Res. 99*, 10713-10721.

Kolmašová, I. and O. Santolík (2013), Properties of unipolar magnetic field pulse trains generated by lightning discharges, *Geophys. Res. Lett., 40*, 1637–1641, doi:10.1002/grl.50366.

Krehbiel, P. R., J. A. Riousset, V. P. Pasko, R. J. Thomas, W. Rison, M. A. Stanley, and H. E. Edens (2008), Upward electrical discharges from thunderstorms, *Nat. Geosci., 1(4)*, 233–237, doi:10.1038/ngeo162.

Krider, E. P. and R. C. Noggle (1974), Broadband antenna system for lightning magnetic fields, *J. Appl. Meteorol. 14*, 252-256.

Krider, E. P., G. J. Radda, and R. C. Noggle (1975), Regular radiation field pulses produced by intracloud lightning discharges, *J. Geophys. Res. 80*, 3801-3804.

Krider, E. P., Ch. D. Weidman, and R. C. Noggle (1977), The electric fields produced by lightning stepped leaders, *J. Geophys. Res. 82*, 951-960.

Lee, B.-H., D.-Ch. Jeong, D.-M. Lee, and T. Kawamura (2006), Characteristics of the lightning stepped-leader electromagnetic pulses, *Jap. J. Appl. Phys. 45*, 933–939.

Maggio, Ch. R. , T. C. Marshall, and M. Stolzenburg (2008), Estimation of charge transferred and energy released by lightning flashes, *J.Geophys. Res. 114*, D14203, doi: 10.1029/2008JD011506.

Nag, A. and V. A. Rakov (2008), Pulse trains that are characteristic of preliminary breakdown in cloud-to-ground lightning but are not followed by return stroke pulses, *J. Geophys. Res. 113*, D01102.

Nag, A., B. A. DeCarlo, and V. A. Rakov (2008), Analysis of microsecond- and submicrosecond-scale electric field pulses produced by cloud and ground lightning discharges, *Atmospheric Res. 91*, 316-325.

Nag, A., V. A. Rakov, W. Schultz, M. F. Saba, R. Thottappillil, Ch. J. Biaggi, A. O. Filho, A. Kahmad, N. Theethayi, and T. Gotschl (2008), First versus subsequent return-stroke current and

field peaks in negative cloud-to-ground lightning discharges, *J. Geophys. Res. 113*, D19112, doi:10.1029/2007JD009729.

Nag, A. and V. A. Rakov (2009), Electromagnetic Pulses Produced by Bouncing-Wave-Type Lightning Discharges, *IEEE Trans. Electromagn. Compat. 51*, 466/470.

Nag, A., V. A. Rakov, D. Tsalikis, and J. A. Cramer (2010), On phenomenology of compact intracloud lightning discharges, *J. Geophys. Res., 115*, D14115, doi:10.1029/2009JD012957.

Nag, A. and V. A. Rakov (2010a), Compact intracloud lightning discharges: 1. Mechanism of electromagnetic radiation and modeling, *J. Geophys. Res.,115*, D20102, doi:10.1029/2010JD014235.

Nag, A. and V. A. Rakov (2010b), Compact intracloud lightning discharges: 2. Estimation of electrical parameters, *J. Geophys. Res., 115*, D20103, doi:10.1029/2010JD014237.

Nag, A. and V. Rakov (2012), Positive lightning: An overview, new observations, and inferences, *J. Geophys. Res. 117*, doi: 1029/2012JD017545.

Neubert, T. (2003), On sprites and their exotic kin, Science, 300, 747–749.

Novák, P. and H. Kyznarová (2011), Climatology of lightning in the Czech Republic, *Atmos. Res., 100*, 318-333.

Pasko, V. P. (2010), Recent advances in theory of transient luminous events, *J. Geophys. Res., 115*, A00E35, doi:10.1029/2009JA014860.

Qie, X., Y. Yu, G. Guo, P. Laroche, G. Zhang, and Q. Zhang (2002), Some features of stepped and dart-stepped leaders near the ground in natural negative cloud-to-ground lightning discharge, *Annales Geophysicae 20*, 863-870.

Rakov, V. A. and M. A. Uman (1990), Some properties of negative cloud-to-ground flashes versus stroke order, *J. Geophys. Res. 95*, 5447-5453.

Rakov, V. A., R. Thottappillil, and M. A. Uman (1992), Electric field pulses in K and M changes of lightning ground flashes, *J. Geophys. Res. 97*, 9935-9950.

Rakov, V. A. and M. A. Uman (1994), Origin of lightning electric field signatures showing two-return stroke waveform separated in time by millisecond or less, *J. Geophys. Res. 99*, 8157-8165.

Rakov, V. A., M. A. Uman, G. R. Hoffman, M. W. Masters, and M. Brook (1996), Burst of pulses in lightning electromagnetic radiation: Observations and implications for lightning test standards, *IEEE Trans. Electromagn. Compat. 38*, 156-164.

Rakov , V. A. and M. A. Uman (2003), Lightning – Physics and effects, *Cambridge University Press*, ISBN:9780521583275.

Rison, W., R.J. Thomas, P.R. Krehbiel, T. Hamlin, and J. Harlin (1999), A GPS-based Three-Dimensional Lightning Mapping System: Initial Observations in Central New Mexico, *Geophys. Res. Lett*., 26, No. 23, 3573-3576.

Rycroft, M. J., S. Israelsson, and C. Price (2000), The global atmospheric electric circuit, solar activity and climate change, *J.of Atm. and Solar-Ter. Phys.* 62, 1563-1576.

Rycroft, M. J., A. Odzimek, N. F. Arnoldb, M. Fullekrug, A. Kulak, and T. Neubert (2007), New model simulations of the global atmospheric electric circuit driven by thunderstorms and electrified shower clouds: The roles of lightning and sprites, *J.of Atm. and Solar-Ter. Phys.* 69, 2485–2509, doi:10.1016/j.jastp.2007.09.004.

Rycroft, M. J. , K. A. Nicoll, K. L. Aplin, and R. G. Harrison (2012), Recent advances in global electric circuit coupling between the space environment and the troposphere, *J.of Atm. and Solar-Ter. Phys.* 90–91, 198–211, http://dx.doi.org/10.1016/j.jastp.2012.03.015.

Schoene, J., M. A. Uman, V. A. Rakov, J. Jerauld, and G. H. Schnetzer (2003), Test of the transmission line model and the travelling current source model with triggered return strokes at very close range, *J. Geophys. Res. 108*, doi: 10.1029/2003JD003683.

Schonland, B. F. J., D. J. Malan, and H. Collens (1935), Progressive lightning, 2, *Proc. Roy. Soc. London. Ser. A, 152*, 595-625.

Shao, X. M., and P. R. Krehbiel (1996), The special and temporal development of intracloud lightning, *J. Geophys. Res. 101*, 26641-26668.

Sharma, S.R., M. Fernando, and V. Cooray (2008), Narrow positive bipolar radiation from lightning observed in Sri Lanka, *J.of Atm. and Solar-Ter. Phys.* 70, doi:10.1016/j.jastp.2008.03.002.

Soula, S., O. van der Velde, J. Montanya, P. Huet, C. Barthe, and J. Bór (2011), Gigantic jets produced by an isolated tropical thunderstorm near Réunion Island, *J. Geophys. Res., 116*, D19103, doi:10.1029/2010JD015581.

Stolzenburg, M., and T. C. Marshall (1998), Charged precipitation and electric field in two thunderstorms, *J. Geophys. Res. 103*, 19777-19790.

Stolzenburg , M., V. D. Rust, and T. C. Marshall (1998), Electrical structure in thunderstorm convective regions 3. Synthesis, *J. Geophys. Res. 103*, 14097-14108.

Stolzenburg M., T. C. Marshall, S. Karunarathne, N. Karunarathna, L. E. Vickers, T. A. Warner, R. E. Orville, and H.-D. Betz (2013a), Luminosity of initial breakdown in lightning, *J. Geophys. Res. Atmos., 118*, 2918–2937, doi:10.1002/jgrd.50276.

Stolzenburg, M., T. C. Marshall, S. Karunarathne, N. Karunarathna, T. A. Warner, and R. E. Orville (2013b), Stepped-to-dart leaders preceding lightning return strokes, *J. Geophys. Res. Atmos.,* 118, doi:10.1002/jgrd.50706.

Thottappillil, R., V. A. Rakov, and M. A. Uman (1990), K and M changes in close lightning ground flashes in Florida, *J. Geophys. Res. 95*, 18631-18640.

Thottappillil, R., V. A. Rakov, M. A. Uman, W. H. Beasly, M. J. Master, and D. V. Shelukhin (1992), Lightning subsequent- stroke electric filed peak greater than the first stroke peak and multiple ground termination, *J. Geophys. Res. 97*, 7503-7509.

Uman, M. A. and D. K. McLain (1969), Magnetic field of lightning return stroke, *J. Geophys. Res. 74*, 6899-6910.

Uman, M. A. and D. K. McLain (1970), Radiation field and current of the lightning stepped leader, *J. Geophys. Res. 75*, 1058-1066.

Uman, M. A., C. Swanberg, J. A. Tiller, Y. T. Lin, and E. P. Krider (1976), Effects of 200 km propagation on Florida lightning return stroke electric fields, *Radio Sci. 11*, 985-990.

Valine, W. C. and E. P. Krider (2002), Statistics and characteristics of cloud-to-ground lightning with multiple ground contacts, *J. Geophys. Res. 107*, 4441, doi:10.1029/2001JD001360.

Wang, Y., G. Zhang, T. Zhang, Y. Li, Y. Zhao, T. Zhang, X. Fan, and B. Wu (2010), The regular pulses bursts in electromagnetic radiation from lightning, *Asia-Pacific International Symposium on electromagnetic compatibility, Beijing, China*, doi: 10.1109/APEMC.2010.5475814.

Weidmann, Ch. D. and E. P. Krider (1978), The fine structure of lightning return stroke waveforms, *J. Geophys. Res. 83*, 6239-6247.

Weidmann, Ch. D. and E. P. Krider (1980), Submicrosecond rise times in lightning return-stroke fields, *Geophys. Res. Lett.* 7, 955-958.

Weinhammer, A. J., J. E. Dye, D. W. Breed, M. P. Spowart, J. L. Parrish, and T. L. Hoglin (1991), Simultaneous measurements of the charge, size and shape of hydrometeors in an electrified cloud, *J. Geophys. Res. 96*, 20809-20829.

Willet, J. C., D. M. Le Vine, and V. P. Idone (1995), Lightning-channel morphology revealed by return-stroke radiation field waveforms, *J. Geophys. Res. 100*, 2727-2738.

Williams, E. R. (1989), The tripole structure of thunderstorms, *J. Geophys. Res. 94*, 13151-13167.

Williams, E. R. (2009), The global electrical circuit: A review, *Atm. Res. 91*, 140–152, doi:10.1016/j.atmosres.2008.05.018.